Technische Universiteit Delft

Uncontrolled Motion for Asteroid Missions

An Application to the Binary Asteroid 1999 KW4

Paul Torrente

TU Delft

Uncontrolled Motion for Asteroid Missions

An Application to the Binary Asteroid 1999 KW4

by

Paul Torrente

to obtain the degree of Master of Science at Delft University of Technology, to be defended publicly on September 20, 2021.

Student number:	4905261	
Project duration:	September 01, 2020 – July 07, 2021	
Thesis committee:	Ir. R. Noomen,	TU Delft, supervisor
	Dr.ir. E. Mooij,	TU Delft, chair
	Dr.ir. A. Cervone,	TU Delft, external examiner

An electronic version of this thesis is available at `http://repository.tudelft.nl/`.

Front cover: Artist illustration of the (66391) 1999 KW4 binary asteroid. Credits: ESO/M. Kornmesser

TU Delft

List of Abbreviations

AIDA	Asteroid Impact Deflection Assessment	5
AIM	Asteroid Impact Mission	5
BIBO	Bounded Input, Bounded Output	9
COPINS	CubeSat Opportunity Payloads Independent Nano-Sensors	5
DART	Double Asteroid Redirection Test	5
DCP	Detailed Characterisation Phase	70
DRO	Direct Retrograde Orbit	5
GEO	Geostationary Orbit	5
GNC	Guidance, Navigation and Control	3
IMU	Inertial Measurement Unit	4
InSight	Interior Exploration using Seismic Investigations, Geodesy and Heat Transport	8
JPL	Jet Propulsion Laboratory	34
LIDAR	Light Detection and Ranging	4
MarCO	Mars Cube One	8
NEA	Near-Earth Asteroid	9
ODCS	Orbit Determination and Control System	69
PDP	Payload Deployment Phase	70
SPK	Spacecraft and Planet Kernel	34
SRP	Solar Radiation Pressure	10
SSB	Solar-System Barycenter	34
TCM	Trajectory Correction Manoeuvres	9
TUDAT	TU Delft Astrodynamics Tool	
USM	Unified State Model	28
YORP	Yarkowski-O'Keefe-Radzievskii-Paddack effect	13

List of Symbols

Roman Symbol	Parameter	Unit
a	Semi-major axis	m
$\vec{a}$	Acceleration vector	m/s^2
A	Reference area	m^2
B	Area-to-mass ratio	m^2/kg
$\vec{C}$	Transformation matrix	n.a.
$C_{n,m}$	Cosine spherical harmonics coefficient of degree n and order m	-
e	Eccentricity	-
$\vec{f}$	Acceleration vector	m/s^2
G	Universal gravitational parameter	$m^3/kg \cdot s^2$
i	Inclination	rad
$J_{n,m}$	Spherical harmonic scaling factor of degree n and order m	-
M	Mass	kg
P_n	Legendre function of the first kind of degree n and order n	-
$P_{n,m}$	Associated Legendre polynomial of degree n and order m	-
$\vec{q}$	Coordinate vector	m
r	Radial distance	m
$\vec{r}$	Radial distance vector	m
R	Radial dimension	m
s	Fraction of specularly reflected photons among reflected ones	-
$S_{n,m}$	Sine spherical harmonics coefficient of degree n and order m	-
t	Time	s
T	Period	s
U	Gravity potential	m^2/s^2
$\vec{v}$	Velocity vector	m/s
$\vec{x}$	State vector	m, m/s

Greek Symbol	Parameter	Unit
α	Longitude	rad
γ	Flight-path angle	rad
δ	Latitude	rad
Λ	Longitude	rad
μ	Gravitational parameter	m^3/s^2
θ	Time of pericenter passage	s
Φ	Latitude	rad
Ψ	Flight-path azimuth	rad
ω	Argument of pericenter	rad
Ω	Right-ascension of ascending node	rad

Preface

In your hands lies the thesis *Uncontrolled Motion for Asteroid Missions: An application to the 1999 KW4 Binary Asteroid*. This thesis has been written in order to obtain the degree of Master of Science in Aerospace Engineering at Delft University of Technology (TU Delft). Its contents may interest anyone in the field of spacecraft trajectories in small-body environments, with a particular focus on cubesats and binary asteroids.

This work was carried out entirely in France during a difficult time for everyone. On a personal note, working remotely has become morally very challenging in the past few months. 'Slow but steady' has become a motto I kept over time. Much more had been envisioned at first for this thesis, but everything needs an end at some point. The liberating point for me was the reopening of my home town library: the change of setting was all the fresh air I needed to finally make things done. For anyone struggling with similar issues, fighting isolation is crucial, please keep safe and remember that brighter days are coming for sure.

The road to completion of this thesis has been a challenging one, which could not have been possible without the support and guidance of several people.

I would like to first thank my supervisor Ir. Ron Noomen for the weekly Skype support over this whole period. His guidance on this thesis has been invaluable to help me focus in the right direction, while his availability and cheering during these past months have been determining. I will miss the weekly side discussions about how life is going.

I also thank the committee members that accepted to be part of this thesis.

I would like to particularly thank C. for her continuous support over the months, champagne is definitely on the way. My gratitude also goes to G. and Q. for their presence and friendship. To my friend Q. specifically, I will only state that I would be a perfect godfather. I wish to thank B., N. and V. for punctually helping me to escape these troubled times, may it be online. To other friends I have not seen in a long time, I can only hope that things will change soon.

Finally, I would like to thank my parents for encouraging me and, let's be honest, bearing with me this whole period.

Paul Torrente
Saint-Maur-des-fossés, France, July 7th 2021

Abstract

A spacecraft is known to experience various perturbations in the Solar System which will affect its dynamics. Depending on the environment, such perturbations may even be so strong that the spacecraft becomes uncontrollable, with worst-case scenarios being an impact or an escape situation which could very well mean the end of the mission. Orbital manoeuvres are in that sense commonly used to correct any deviation from a nominal path, as a given space application may be of too high a risk not to rely on a propulsion system. Such control methods may even simply be a necessity in order to achieve specific mission goals such as repeat orbits. On-board payloads and propellant however represent a significant cost in any mission, while orbital manoeuvres also tend to affect the orbit determination process. The entire focus of this thesis is therefore to investigate whether a relevant mission without any means of orbit control could be designed in a perturbed environment.

Small satellites and especially cubesats have quickly appeared to be the most promising concept for a mission without orbital control due to their inherent cost and mass-efficient design which enable taking higher risks to test out new promising applications in space. While being originally created for educational purposes, cubesats have now entered the realm of space agency missions, with famous examples like MarCO A & B during the landing and descent of InSight, or in the upcoming cubesats to be deployed in the future Hera mission around the binary asteroid 1999 KW4. It is this particular last mission that drove the interest in a cubesat mission around an asteroid, as a mission in a highly perturbed environment is believed to benefit most from a concept without orbit control. The specific case of binary asteroids like Didymos was outlined as an even more interesting subject, as such systems inherently show additional stable zones in the orbital plane due to the presence of the secondary asteroid. This thesis thus focused on the uncontrolled orbital behaviour of a cubesat in a binary asteroid environment, with an emphasis on the representative Near-Earth Asteroid (66391) 1999 KW4 and using the TU Delft Astrodynamics Tool (TUDAT) for numerical computations.

The first finding of this thesis is that the tuning of the integration/propagation settings is not an easy task in such a perturbed environment. It was found that flybys closer than 400 meters to either the primary Alpha or the secondary Beta could introduce sufficient sensitivity for a large build-up of integration differences between two integrators/propagators, so a choice was made to choose this distance as an impact criterion for both bodies. This enabled to find smoother, less sensitive results but came at the expense of filtering close approaches to the asteroids. An extensive tuning of the integration/propagation methods led to the conclusion that a requirement in accuracy of ten meters for the cubesat's position can be reached for integrations over more than a hundred days targeting pseudo-periodic orbits in the interior part of the binary system, while this time interval drops to 60 days in the exterior part due to higher sensitivities.

Entire regions of space were investigated to identify stable zones from which an uncontrolled cubesat mission could benefit. The best orbits found in the interior ring of the binary system are all pseudo-periodic orbits around Alpha almost starting in the initial orbital plane of Beta. They lie in a stable band zone for initial semi-major axes of the cubesat between 1200 and 1500 m, with propagation times greater than a hundred days w.r.t. our termination conditions. Some of these orbits are found to remain stable after the introduction of various uncertainties, where the orbit determination error on velocity in particular appears to be dominant. This proves that an uncontrolled cubesat mission could in theory be flown for more than a hundred days targeting such orbits around Alpha. Early impacts on either Alpha or Beta may appear due to the very constraining distance requirements, but tend to disappear if the uncertainties in the initial velocity of the cubesat can be lowered to 5 mm/s using a 1-σ normal distribution, by either a better injection mechanism or smaller OD errors at injection. Orbits found in the exterior ring are very sensitive to the introduction of uncertainties, in particular the orbit determination error on velocity again, and generally cannot be ensured to last for at least 60 days without taking high risks. This assessment can however be mitigated if the initial velocity uncertainties of the cubesat can be once again be lowered.

Contents

1 Introduction

A spacecraft will almost always experience numerous perturbations in the vicinity of Solar System bodies which will affect its dynamics. Such perturbations may even lead to an uncontrollable situation, with an impact or an escape as a worst-case scenario that could mean the end of the entire mission. To avoid such fatal scenarios, it is common that a spacecraft relies on a guidance, control and navigation system, with propulsion as a crucial element. Orbital manoeuvres are used to correct any deviation from a desired nominal path to ensure the success of the mission, and it is the usual way of dealing with perturbations. With high risks at stake in space missions, relying on control methods is usually deemed a pure necessity. Even without talking about escape or impact, control methods are simply needed to achieve specific mission goals such as repeat orbits. A downside is however that on-board subsystems always represent a significant cost for the mission, with orbit manoeuvring also needing propellant. As an indication, the propulsion system usually represents about 5% of the total mass for a big spacecraft of 300 kg, and about 20 % for a smaller one around 1 kg, using cold gas propulsion [Sanders et al., 2007]. Orbit manoeuvres also may deteriorate the orbit determination process as it creates a break in the velocity (and position) profile. The question therefore arises whether a relevant spacecraft mission could be designed in a perturbed environment without the use of propulsion system. While this question could in essence be investigated for a mission around any Solar System body, it has been chosen to focus on one of the most challenging applications: asteroids, and more particularly binary asteroids. Their environment allegedly has more favourable stable regions in comparison to standard asteroids, and they are in the line of sight of future space missions such as Hera. The research question of this thesis work can thus be formulated as:

- Can we identify attractive trajectories around binary asteroids that can be used by cubesat missions without any means of orbit control?

with subquestions:

- What is their relevance? What is their level of stability?

Chapter 2 first highlights how space missions usually rely on orbital maintenance to ensure the success of a mission, while briefly discussing the budget cost at stake for different applications. The example of cubesats is then outlined as they represent promising applications regarding an uncontrolled space mission, while it is also shown that asteroid missions could greatly benefit from such a concept. Chapter 3 then focuses on the orbital dynamics in binary asteroid environments, with the introduction of the 1999 KW4 binary system that was investigated in this thesis. Chapter 4 is all about how to assess stability or instability in the general sense in such a perturbed environment, with a focus on the more practical and implementation that was preferred in this thesis. Chapter 5 presents the numerical tools used in this thesis, with an emphasis on the TU Delft Astrodynamics Toolbox (TUDAT). An environment model was implemented using this software, and is described in Chapter 6. The extensive tuning of the propagation and integration methods to be used in this thesis work is presented in Chapter 7. This enabled to compute the first nominal results of this thesis in Chapter 8 for a first assessment of the feasibility of an uncontrolled cubesat mission in a binary environment. Chapter 9 introduces uncertainties in the model and presents whether nominal results are still attractive. Chapter 10 is finally about the validation of the implemented model and of some results, while Chapter 11 concludes on the main findings of this research and provides some recommendations for future related work.

2

Heritage

2.1. Introduction

During the mission analysis and design phase of a space mission, a nominal trajectory is computed by taking into account numerous constraints as well as the chosen end conditions [Mooij, 2017-2018]. It is the next step that brings the problem into the real physical world, as it is crucial to prove that the vehicle is actually able to fly this nominal trajectory without violating the constraints. Another fundamental aspect is the fact that the vehicle will experience unforeseen perturbations, making it deviate from its nominal path. It is then critical to ensure that the vehicle is still able to fulfil its mission goal and that it does not meet a premature end of the mission.

To cope with this issue, the usual way of doing is to equip the vehicle with a so-called Guidance, Navigation and Control (GNC) system. GNC is a whole branch of engineering per se from cars to spacecraft including ships and aircraft, that aims to control the movement of a vehicle. While this function could in essence be performed manually, the applications at stake are often of high risk needing both high accuracy and reactivity as it is the case in the space industry. It is however common knowledge that any additional subsystem on a spacecraft has an impact on the mission mass and cost, and an on-board GNC system is no exception to the rule. GNC and propulsion systems are however always deemed necessary to ensure the mission's objectives and limit the risks, while their contributions to the mass and cost budgets could have maybe be used for more science instrumentation. Could it be possible to answer this concern in a different way? Could it be possible to remove such systems for relevant space applications, and be able to prove that the mission could still be a success?

The intent of this chapter is not to be very exhaustive on the subjects at stake and is thus written with that logic. GNC is not the primary focus of the thesis research and should only be seen as an informative addition that serves as base argumentation for a mission concept with control-free motion. The main objective of this chapter is to highlight how space missions usually rely on GNC to ensure the success of the mission, and quantify their impact on budgets. Also, background information on asteroid missions is given.

A general overview of GNC systems is presented in Section 2.2 in order to understand their role and importance in various engineering domains, focusing on space engineering. Section 2.3 then highlights the budget of the Orbit Maintenance and Control segment in some space missions, in an attempt to present the kind of saving that could be gained in an orbit control-free mission. Section 2.4 finally aims at presenting some applications that seem promising in the direction of an orbit-control free concept, while also highlighting some missions that already do without.

2.2. Guidance, Navigation and Control

The first step towards the control-free orbit concept of this thesis is to first briefly understand the system that is aimed to be removed and discuss GNC. This section is divided into two different sections that cover the topics as one could expect: Guidance, Navigation, and Control respectively.

2.2.1. Navigation

On a simple note, the navigation aspect of GNC answers for the vehicle the question of "Where am I?". The aim is to estimate the state vector and the attitude of the vehicle with the required accuracy.

To that end, one needs a particular reference, and this is why three navigation strategies can be distinguished[1]:

- **Navigation w.r.t. a fixed point of reference**
  Mention can be made here of star trackers that can measure the position of surrounding stars using a star catalogue, photo-sensitive cells or a camera [Mooij, 2017-2018].
- **Navigation w.r.t. the relative position to a target**
  One example is Light Detection and Ranging (Light Detection and Ranging (LIDAR)). This remote-sensing technology enables to measure the distance to a target using light, often laser pulses [Mooij, 2017-2018]. The underlying principle of LIDAR is simple: it is based on the measurement of the time of flight for a light pulse to reach a target and come back to determine the relative distance.
- **Navigation w.r.t. an initial known position**
  One example in this group is an Inertial Measurement Unit (Inertial Measurement Unit (IMU)) [2], usually consisting of a combination of one collinear accelerometer, gyroscope and sometimes magnetometer for all three axes of the vehicle covering all three dimensions. While the accelerometers measure the acceleration, gyroscopes are able to measure the angular velocity [Mooij, 2017-2018]. The vehicle can then be tracked by pairing the computed data.

Multiple input sensors are usually used in a navigation system for accuracy and redundancy, and the state of the vehicle is estimated by combining the data. From there, if the estimation does not need to be performed in real time, the Least-Squares Method can be used, while real-time applications will need recursive filtering techniques such as the well-known Kalman filters [Kalman, 1960].

2.2.2. Guidance and Control

The guidance function of GNC also answers a simple question for the vehicle: "Where should I go?". The information from the navigation system serves as input to the guidance system to generate steering commands taking into account constraints and a desired end state [Mooij, 2017-2018].

The control aspect of GNC finally answers the straightforward "How do I get there?" for the vehicle. It ensures that the steering commands generated by the guidance system are well carried. [Mooij, 2017-2018] mentions that many control theories exist, the most common one being by integration of feedback by either the output or state of a process, but other more advanced techniques do exist like adaptative control.

These two aspects of GNC are grouped because they are the ones that are aimed to be removed for specific applications. It is emphasized once again that the study does not have the intent to be exhaustive on guidance and control theory as it is not the main focus of the research that was led. For a more in-depth analysis, the reader can refer to literature, for instance [Mooij, 2017-2018].

2.3. Orbit Maintenance and Control

After a spacecraft is placed into its nominal orbit, it is often required to use orbit manoeuvres to compensate for unforeseen perturbations so that the trajectory remains between mission tolerances. The orbit maintenance and control mission segment of a space mission is the one coping with this issue from orbit injection to end of life. While such manoeuvres typically require a small ΔV, they are often performed many times during the mission depending on the degree of perturbations, and thus represent a non-negligible portion of the mission budget. Its inherent and affiliate components are also of significance due their mass and power consumption. What if it could be possible to remove them without endangering the mission? This whole section aims at getting a sense of the budget involved in this particular mission element, with the ultimate purpose of providing sound argumentation in favour of a mission concept with control-free motion. It is however

[1] https://en.wikipedia.org/wiki/Guidance_system
[2] https://en.wikipedia.org/wiki/Inertial_measurement_unit

emphasized that such budgets are very scarce in literature, but the few examples provided below give some grip on the subject.

Orbit maintenance is traditionally performed via ground operations, but it can also be performed autonomously on-board, which is something to consider w.r.t. the mission requirements [Larson and Wertz, 2005]. It is also interesting to point out that the vast majority of spacecraft without a propulsion system are small satellites in orbit around Earth, which saves in design complexity, mass and cost [Wertz et al., 2011]. This however comes at the expense of not being able to do anything with the spacecraft after injection, and its orbital parameters will inevitably drift away over time due to accumulated secular gravitational field perturbations.

For LEO satellites, [Wertz et al., 2011] highlights that a commonly performed maintenance manoeuvre is orbit raising, which aims at compensating for the spacecraft altitude decay due to atmospheric drag by using its thrusters at the desired orbit point to provide an in-plane ΔV. The lower the nominal altitude of the mission, the more frequent these manoeuvres are usually required, but it is also a matter of tolerances from the mission requirements. On average, the required ΔV for such LEO maintenance is however quite small: a one-time 1 km adjustment at 1000 km altitude requires for example a maintenance ΔV of approximately 0.5 m/s. LEO manoeuvres are also often performed on a frequency basis of a few weeks, as it was the case for the Earth observation satellite Envisat which had an average maintenance frequency of 15 weeks at 800 km altitude [Wertz et al., 2011].

[Wertz et al., 2011] also addresses Geostationary Orbit (GEO) satellites regarding orbit maintenance. Such satellites come with some demanding requirements: they need to keep a given spot in space to both avoid radio interferences and keeping a required distance between each other (2 degree longitude along the equator, or about 220 km). This requires a station-keeping in all directions of space of approximately $\pm$75 km. Such considerations arise in a context where available slots for GEO satellites are becoming very scarce. The largest perturbation that a GEO satellite can experience is an inclination drift coming from perturbations from the Sun and the Moon, which leads in the worst-case scenario to required velocity changes of about 36.93 m/s per year and 14.45 m/s respectively, with a drift in inclination of about 0.9° per year. Another important contribution is due to the oblateness of the Earth, needing a station-keeping of about 10% of the above contribution.

When it comes to the on-board propulsion system used for orbit control, it can also represent a non-negligible portion of the satellite mass depending on the mission, as explained by [Wertz et al., 2011]. The mission requirements drive the type of thrusters to be used. A small thruster with a mass of 0.1 kg can for example provide a propulsive force of 0.1 N, while bigger thrusters of about 10 kg can provide almost 3000 N with a typical specific impulse for thrusters between 200 and 300. As an example, [Wertz et al., 2011] highlights a few numbers regarding the orbit control of Landsat 7 launched in 1999 which aimed at refreshing the database of Earth satellite imagery. It was performed using a mono-propellant hydrazine control system with 12 jets each producing a propulsive thrust of 4.4 N. Each tank in the spacecraft could contain up to 122.5 kg of hydrazine which would represent 6% of the total mass of the spacecraft.

Regarding smaller spacecraft, [Manghi and al., 2017] focused on a preliminary analysis for a small satellite mission to the Didymos binary asteroid system, in the context of the Asteroid Impact Deflection Assessment (AIDA). This plan aims at demonstrating the so-called kinetic impactor concept, which consists in modifying the orbit of the smaller of the pair by impacting. The Asteroid Impact Mission (AIM) spacecraft (now replaced by the Hera spacecraft) is supposed to characterize the impact of the Double Asteroid Redirection Test (DART) probe as it hits the smaller asteroid with a speed of approximately 6 km/s. The study led by [Manghi and al., 2017] aimed at selecting promising orbits for two or more small satellites called CubeSat Opportunity Payloads Independent Nano-Sensors (COPINS) which will also be flown and whose goal is to demonstrate deep-space inter-satellite communication that is deemed too risky to perform by their AIM mothership. The authors explored three alternative scenarios for the cubesat concept, one where operations are performed while remaining at an L4 parking orbit, one where the cubesat is injected in a high Direct Retrograde Orbit (DRO) from the secondary (300 m from the surface), and one where it is injected in a low DRO (100 m from the surface). The study highlighted that these three scenarios would require a station-keeping ΔV of about 5 mm/s per day in their nominal case. In their worst case (when introducing larger state errors in the model), this ΔV goes up to 12 mm/s per day for parking at L4, while the two other scenarios did not

converge, which would indicate that even more frequent correction manoeuvres would be required in comparison to one per revolution as in the study.

On a final note, [Sanders et al., 2007] performed a scaling exercise of a 300 kg spacecraft with a standard gold gaz propulsion using commercially off the shelf components, down to 10 kg and then 1 kg, which is characteristic of a cubesat. Although a bit dated, such exercise is helpful to quantify what can be gained for an uncontrolled spacecraft, in particular for a big spacecraft and for a cubesat. The propulsion system mass percentages of the total spacecraft mass can be seen in Figure 2.1 for different types of spacecraft, along with the repartition between the propulsion system components, the propellant itself, and its storage. While the propulsion system represents about 5% of the total mass of a big conventional spacecraft, the pure scaling using off the shelf components showed that a typical 1 kg cubesat could have a propulsion system of about 40 % of the total mass. Using different techniques for weight and volume reduction, the authors showed that this number could be reduced to about 20 % of the total mass.

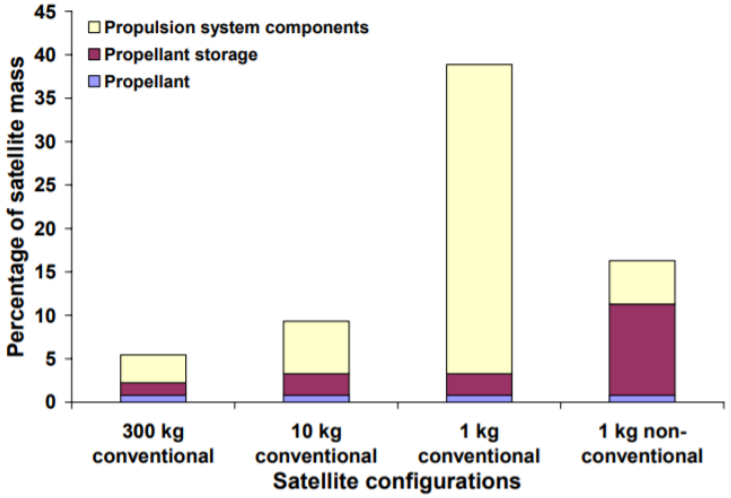

Figure 2.1: Mass percentages of the propulsion system w.r.t. to the total mass of different types of spacecraft, using cold gas propulsion. From [Sanders et al., 2007].

A conclusion that can be drawn at this point is that orbit maintenance manoeuvrers are usually performed most frequently in highly perturbed environments. With that in mind, it seems that such highly perturbed environments seem to be the most challenging but scientifically interesting scenarios for an orbit control-free mission, and it is that logic that is kept all along the study.

2.4. Applications

This section aims at presenting, in a very general way, some space applications that are the most promising for an orbit control-free mission. The aim is also to show how challenging this idea is by mentioning the few existing examples launched with no orbital control whatsoever.

As mentioned previously, the very far majority of space applications do use orbit control to ensure the success of their mission. The point of this subsection is to highlight a few specific cases that could potentially benefit the most by removing their orbit control segment without endangering the goal of the mission too much. There will be no mention of obvious space applications where control methods are crucial such as re-entry scenarios, the precise positioning and removal of GEO satellites, active space debris removal and many more. It is preferred to insist on the particular case of small satellites that seem the most relevant for the concept, as mentioned in Section 2.3.

2.4.1. Cubesats

A large amount of effort is nowadays put into Micro Systems Technology (MST) for space missions in order to reduce size, mass and power consumption as these are driving parameters for both launch and development cost [Ubbels et al., 2005]. This is why payload constraints are all the more crucial for small satellites. A concept emerged back in 2000 in a collaboration between California Polytechnic State University San Luis Obispo (CalPoly), and Stanford University's Space Systems Development Lab, for a new type of small satellite called cubesats, first launched in June 2003. Both industries and universities worldwide soon saw the huge potential of cubesats and were not long to follow the trend. Cubesats were originally a very affordable way of reaching space for educational projects only, but their small costs made them extremely attractive for testing new technologies in space. Cubesats are developed nowadays to be used in real and practical commercial missions.

A cubesat weighs no more than 1.33 kilograms per unit[3]. Compared to bigger satellites, cubesats seem to be excellent candidates for an orbit control-free mission with reduced risks. The very first generation of cubesats had no propulsion system, and at the time when the book was printed (2011), [Wertz et al., 2011] mentioned that only one cubesat flew using a cold-gas propulsion system: CanX-2 launched in April 2008 by the Canadian Cubesat Program. It could however be said that another one was first, namely a picosatellite called MEMS Pico Sat Inspector (MEPSI), deployed from the Space Shuttle Discovery in 2006, whose goal was to highlight the potential of small satellites into observing larger ones, also using a cold-gas propulsion system [Wertz et al., 2011].

An up-to-date database of all designed cubesats can be found at *https://www.nanosats.eu/database*. It could in fact be interesting to investigate the number of operational cubesats that do not have a propulsion system in 2021. Such exercise was not performed during the thesis due to time constraint and the fact that the use of a propulsion system is not clearly specified among the thousands of entries which one would have to go through individually. It is however believed that the lack of a propulsion system for cubesats, especially originally, was due to the education-oriented vision with limited budget having a direct impact of the complexity of the design. This vision is not the mainline nowadays, as the new trend is toward cost-efficient and innovative miniatured propulsion systems to mimic bigger spacecraft [Wertz et al., 2011]. Developing a cubesat is also very interesting to test out unconventional technologies, that more expensive missions with bigger spacecraft could not afford.

Delfi-C3 and the No-Propulsion Cubesats

As mentioned earlier, the first generation of cubesats usually did not integrate a propulsion system due to budget constraints mainly. One example that is very familiar to the Aerospace Engineering Faculty of Delft University of Technology (TU Delft) in the Netherlands is Delfi-C3. It was developed by the Aerospace Engineering (AE) and the Mathematics and Computer Sciences (EWI) Faculties of TU Delft, in a collaboration with Dutch Space (nowadays Airbus Defense & Space Leiden) and TNO Science & Industry. The project aimed at exploring the exciting concept of cubesats for educational purposes, and at being an opportunity for the testing of thin-film solar cells (TFCs) in space [Ubbels et al., 2005].

Delfi-C3 was part of this first generation of cubesats, and in that logic did not have a propulsion system for orbit control as the main objectives of the mission could do without. Attitude control was not even needed as a small tumbling could ensure a uniform solar radiation exposition of the cubesat, beneficial for the mission's goal, although the rotation rates of the cubesat needed some constraining [Ubbels et al., 2005]. A visual representation of Delfi-C3 can be seen in Figure 2.2.

[3] https://en.wikipedia.org/wiki/CubeSat

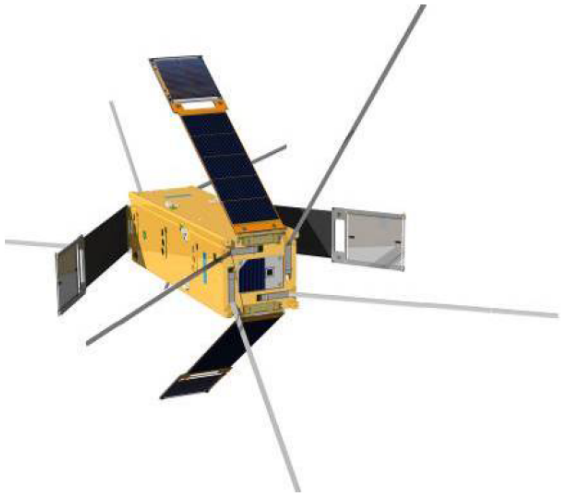

Figure 2.2: The Delfi-C3 cubesat [van Breukelen et al., 2006].

This example highlights that a propulsion system is not always needed depending on the mission requirements, the level of risk that the development team is willing to take, and the financial budget. This thesis is more interested in this cubesat concept with no propulsion system rather than the perceived current trend towards miniaturization of bigger spacecraft. Some nuance must however be put as another trend emerges with even smaller satellites called PocketQubes [4] which were first proposed in 2009 in reaction to the increasing costs of the trendy cubesats. With a total mass lower than 250 grams, a propulsion system is even more considered a luxury and challenging segment to integrate in a PocketQube, which could furthermore not be needed depending on the mission.

Mars Cube One

The Mars Cube One (MarCO) mission is also a recent and very iconic mission involving cubesats. The mission was launched along the Interior Exploration using Seismic Investigations, Geodesy and Heat Transport (InSight) mission in 2018, whose aim is to better understand the internal structure of Mars by positioning the very first seismometer on the surface of the planet.

The MarCO mission was the very first mission involving cubesats at an interplanetary level. The two cubesats called MarCO A and MarCO B were launched together for redundancy purposes, and were used to provide a real-time communication between the Earth and InSight during the entry, descent and landing where InSight was out of sight of the Earth. An overview of the Mars flyby performed by the MarCO cubesats can be seen in Figure 2.3.

[4] https://en.wikipedia.org/wiki/PocketQube

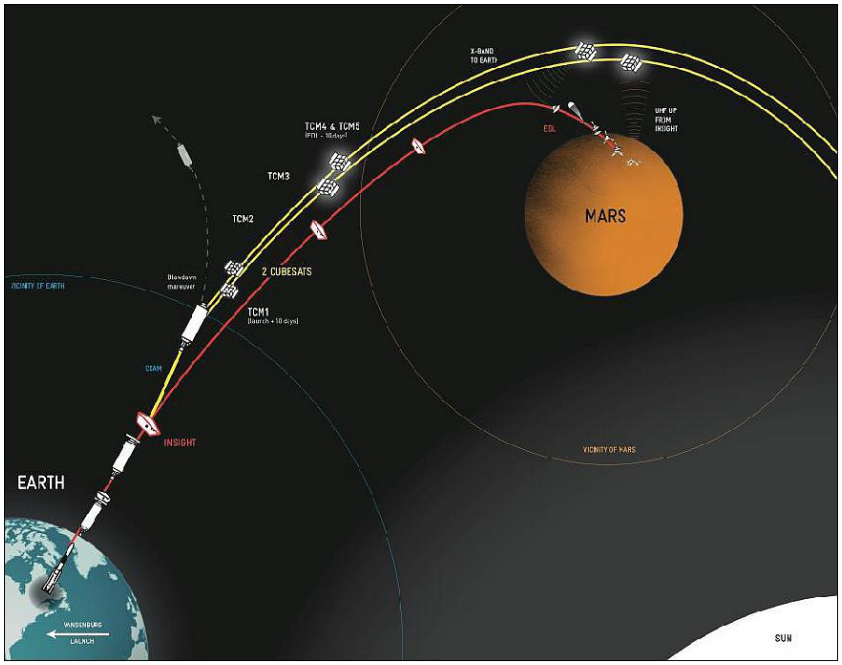

Figure 2.3: MarCO concept of operations (Image Credit: NASA/JPL).

The two MarCO cubesats were not designed to orbit Mars, but only for communication during a short period of time. The contact to the two cubesats was lost afterwards on February 2nd 2020. In theory, a propulsion system could be left aside for this particular mission, but both cubesats did have an orbit maintenance and control system using cold-gas propulsion [Schoolcraft et al., 2016]. This propulsion system had a wet mass of 3.490 kg for a thrust capability of 755 Ns, providing a Trajectory Correction Manoeuvres (TCM) ΔV of 40 m/s [5]. As each cubesat had a launch mass of about 13.5 kg [6], this propulsion system would represent about 25 % of the total mass of each cubesat, which is in accordance with estimations by [Sanders et al., 2007]. Two cubesats were used for redundancy, and they were only used as a relay during a flyby. Could the same mission have been a success as well without propulsion capabilities while being less costly? With what level of risk?

2.4.2. Missions to Asteroids

Asteroids attract the attention of many upcoming missions, such as Psyche to the eponym asteroid planned to launch in August 2022, or also Hera to the Near-Earth Asteroid (NEA) Didymos binary asteroid system in 2023 (see Section 3.1). The latter mission will even serve as a test scenario for new cubesat technologies launched alongside the mothership. This whole mission, combined with the will to focus on cubesats for this thesis, actually led to the idea of considering a mission with control-free motion around asteroids, which was expected to be challenging but one of the most interesting area of research for this concept.

A study that greatly inspired this thesis project is the one by [Damme et al., 2017], who studied the motion of a spacecraft in the vicinity of the two binary systems 1996 FG3 and 1996 GT (Didymos). The study was furthermore interesting in comparing such motion for a medium-sized spacecraft of 400 kg and cubesats of 4.5 kg.

The motion of a spacecraft was investigated in these binary environments using so-called Bounded Input, Bounded Output (BIBO)-stability criteria to distinguish between stable and unstable motion in the orbital plane (see Section 4.2 for the notion of BIBO-stability). The first criterion is whenever a collision happens between the spacecraft and either the primary or the secondary, and the second one is when the spacecraft is considered to escape the system when its distance w.r.t. the primary is larger than 6 km. The third criterion is when the eccentricity of the orbit of the spacecraft exceeds 0.4, as it is considered by the authors that large

[5] https://cubesat-propulsion.com/wp-content/uploads/2015/11/JPL-MarCO-Micro-CubeSat-Propulsion-System-datasheet.pdf

[6] https://www.jpl.nasa.gov/news/press_kits/insight/launch/download/mars_insight_launch_presskit.pdf

eccentricities are more likely to lead to collision or escape in these short time scales.

The authors highlighted the presence of equilibrium points in the system that were very similar to the Lagrange points in the circular restricted three-body problem and showed particularly stable regions as shown in Figure 2.4, where the moonlet of the binary is shown as a green point.

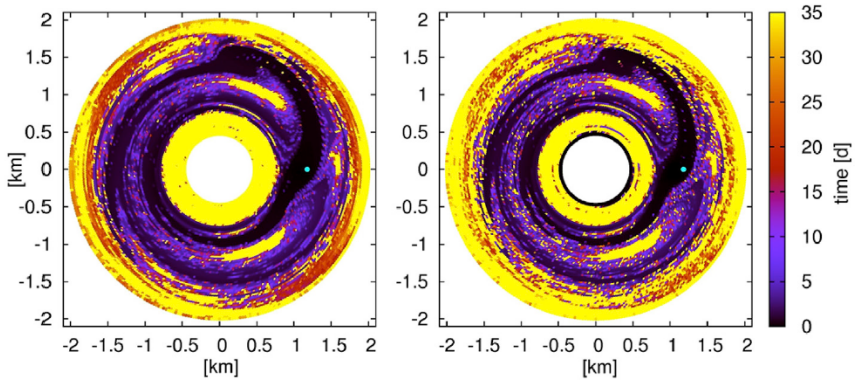

Figure 2.4: Lifetime analysis for cubesat orbits around Didymos. Each orbit is characterized by its initial semi-major axis and its mean longitude. In the left figure, colors indicate the time until $e > 0.4$ is reached; in the right figure, colors indicate the time until the spacecraft either collides with the primary or secondary, or escapes the system (distance to the primary exceeding 6 km) [Damme et al., 2017].

The authors showed that some orbits that are in the orbital plane and close to the primary are stable for at least 35 days, which could be explained by the fact that such orbits are less sensitive to the Solar Radiation Pressure (SRP) and perturbations from the secondary. The model for the primary was however a tri-axial ellipsoid with uniform rotational state, and one remark was that a more irregular shape was more likely to reduce this stability region.

It was also shown in their study that regions corresponding to resonant orbits with the secondary presented some stable properties. Such regions are in fact more stable than if the secondary did not exist, so the perturbations added by the secondary are not always detrimental. Stability regions for resonant orbits are shown in Figure 2.5, with the case of a cubesat on the left and a medium-sized spacecraft on the right. It can be observed that stable regions for the cubesat are actually larger than the ones for the medium-sized spacecraft, due to the fact that the SRP decreases for decreasing area-to-mass ratio, which is significantly smaller for cubesats. This is believed to be one strong argument in favour of a cubesat mission in such perturbed environments.

[Damme et al., 2017] also investigated the stability properties of retrograde orbits versus prograde orbits. Figure 2.6 shows that retrograde orbits seem to be more stable in essence. Retrograde orbits with a semi-major axis smaller than 1 km are seen to be always stable for at least 90 days, independently of the mean longitude of the orbit. This observation was very encouraging for the possibility of an orbit-control free mission in such environments. It appears in Figure 2.6 that increasing the semi-major axis leads to an unstable zone where the cubesat enters in collision with the secondary in less than two days on average. A second vast stable region then appears once again between 1.4 and 1.65 km for retrograde orbits, and the authors remarked that it disappeared when the secondary did not exist. This particular region is in fact created by a balance between the gravitational attraction of the secondary and the SRP. This is actually the argument that led this thesis work to focus more on binary asteroids rather than single ones, as such added stable regions were in essence more beneficial for a mission with control-free motion. Retrograde orbits with a semi-major axis larger than 1.7 km showed to be unstable again as the SRP now becomes the dominant perturbing force over the gravitational attraction of the primary.

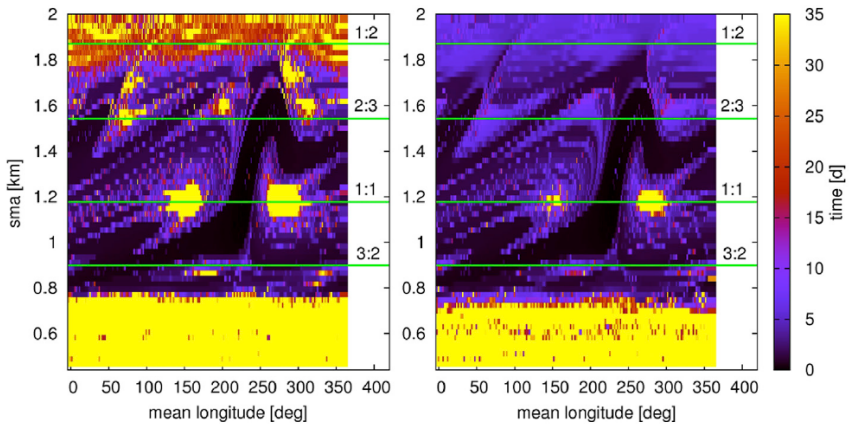

Figure 2.5: Lifetime analysis for orbits around Didymos. Colors indicate the time of stable orbiting with criterion $e < 0.4$. The left figure corresponds to a cubesat, the right one to a medium-sized spacecraft. Green lines correspond to resonant modes [Damme et al., 2017].

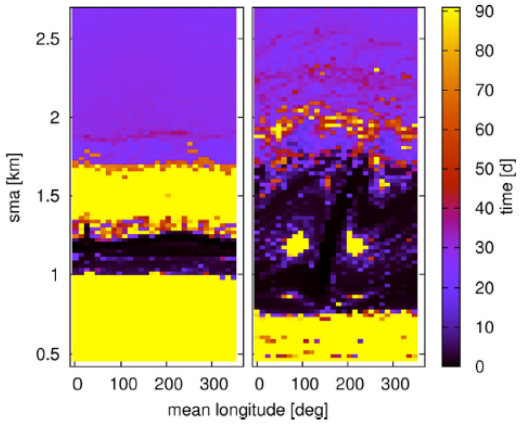

Figure 2.6: Lifetime analysis of cubesats orbiting Didymos. The stability criterion is $e < 0.4$. Orbits in the left figure move retrograde w.r.t. the secondary, while orbits in the right move prograde [Damme et al., 2017].

The authors were not interested in maximum lifetimes to be achievable in a binary asteroid environment, and only investigated the orbital plane of the binary. A sensitivity analysis was also not performed on promising solutions. This thesis work plans to investigate those points with the study of the representative NEA binary asteroid 1999 KW4.

2.5. Conclusions

This chapter first gave a brief introduction on GNC as the usual way of ensuring that a spacecraft follows a nominal path while being subject to perturbations. It was then concluded that small satellites seemed to offer very promising applications for a mission without orbit control, due to the lowered risk of such a mission as well as the inherent cost and mass-efficient vision of their design. While many directions could have been taken from that point, it is furthermore concluded that an orbit control-free mission would be the most interesting and challenging if investigated in a highly perturbed environment. With the increasing number of asteroid missions these days, that particular direction was preferred. The environment around binary asteroids also seem to present more inherent stability zones in comparison to single asteroids as shown in [Damme et al., 2017], which could be beneficial for the whole concept. So it was chosen to focus entirely on binary asteroids. This research is thus all about the feasibility of removing the guidance and control systems for a cubesat mission around a binary asteroid. The navigation system is however preserved as to be able to retrieve scientific data outcome.

3

Orbital Dynamics

This chapter is aimed at discussing the orbital dynamics in the environment of a binary asteroid. Section 3.1 provides some information on this particular family of asteroids, while Section 3.2 focuses on the (66391) 1999 KW4 binary asteroid system that was chosen to explore in this thesis. Section 3.3 highlights the physical environment around any celestial body, with a focus on binary asteroids. Section 3.4 then highlights some relevant ways of expressing the motion of a spacecraft in such environment, while Section 3.5 presents the choice of reference frame and coordinate system that was chosen to further carry out this thesis work.

3.1. Binary Asteroids

Asteroids in general are direct windows to a better understanding of the formation of our entire Solar System, and understanding their dynamics is at the key. New ideas also arise in the direction of asteroid mining, or asteroid deflection in the hypothetical scenario of an Earth impact (see the upcoming Hera mission). Such ideas, among others, are why asteroids are in the collimator of future space missions. Among asteroids, there exists a category that may be even more interesting, if only in their formation.

A binary asteroid system is a system of two asteroids, with a smaller asteroid called the secondary or Beta orbiting a larger one called the primary or Alpha. The discovery of the satellite named Dactyl to the asteroid (243) Ida during a fly-by of the Galileo spacecraft in 1993 enabled to definitely shed light on the binary asteroids population, which was disputed beforehand. An intensified ground-based effort then enabled to discover a satellite around (45) Eugenia a few years later [Zannoni et al., 2017].

Many binary asteroids have been discovered since then from various types of observations, and a classification arose for different populations. Binary asteroids actually represent a significant portion of the Near-Earth Asteroid (NEA) population, namely $15\% \pm 4\%$ [Pravec et al., 2009]. Binaries are less frequent in the main asteroid belt, but they are still estimated to account for a few percent of the total population. It was further estimated that approximately 9% of the overall NEA population consists of so-called contact binaries, which may have formed via the collapse of the mutual orbit of the two asteroids coupled with a low-speed collision.

The original theory regarding the formation of binary asteroids was tidal disruption during planetary flyby, but more recent studies indicate that this mechanism could only account for 1 to 5% of binaries among the NEA population [Fahnestock and Scheeres, 2008]. Alternatively, the Yarkowski-O'Keefe-Radzievskii-Paddack effect (YORP) effect affecting binary asteroids (or BYORP effect for "binary" YORP) has been proved to be a very important mechanism. This effect is caused by scattered sunlight and the re-radiation of energy when heated up by the Sun, creating a torque than can modify the rotation states of the asteroids.

3.2. Binary System 1999 KW4

This thesis work could have gone many directions regarding the choice of a binary system to investigate. The first candidate that came to mind was the promising target of the upcoming Hera mission, the Didymos system. The problem with this system is that the mass ratio between the secondary and the primary is very small, meaning that Beta would be less acting as a counterbalance for the gravitational field of Alpha, but also for the SRP. As the primary goal of this study is to identify stable regions in a binary system for a mission with control-free motion, it seemed that investigating a binary system with a more representative secondary-to-primary mass ratio among the population of binary asteroids was better suited for this thesis work.

A classification of all known binary asteroids and their parameters has been made and regularly updated by Pravec and al., which the interested reader can find at `http://www.asu.cas.cz/~asteroid/binastdata.htm`. Based on this data, Figure 3.1 shows the distribution of primary spin rates as a function of the primary-to-secondary mass ratio, for all known binaries, and for both Didymos and what appears to be a promising candidate : the binary asteroid (66391) 1999 KW4.

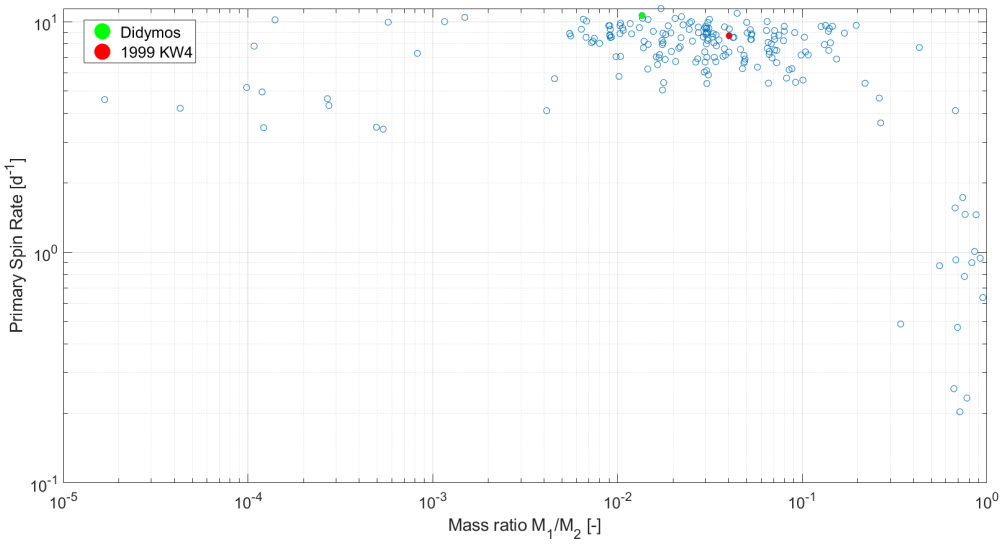

Figure 3.1: Distribution of primary spin rates as a function of the primary-to-secondary mass ratio for binary asteroids. From `http://www.asu.cas.cz/~asteroid/binastdata.htm`.

Classified as a near-earth object and potentially hazardous asteroid of the Aten group, 1999 KW4 has a primary of about 1.3 km in diameter while its secondary is about 360 m at a mean-distance of 2.6 km. The binary appears to be one if not the best characterized binary asteroid, observed using the Arecibo radar in 2001. A detailed model of the binary was constructed by [Ostro and al., 2006] while the dynamical configuration was studied by [Scheeres and al., 2006]. The characteristics of this binary asteroid in fact appear quite typical of the NEA population. The dynamics in this binary system are often used as a test case for models of the Full Two-Body Problem (F2BP) such as in [Compère and Lemaître, 2014]. For these reasons, it has been chosen to further investigate this particular binary asteroid system.

3.3. Physical Environment

The environment around Solar System bodies may vary significantly. A spacecraft orbiting a large body such as a planet would on one hand be expected to experience relatively smooth perturbations, but a spacecraft orbiting a small body is on the other hand expected to experience significant and high-frequency perturbations due to the weak surrounding gravity field and the very irregular shape of the body at stake. As the second case is the focus of this thesis research, it is important to describe such physical environment in a general way. Subsubsection 3.3.1 will briefly explain the choice that was made for a gravitational field model. Subsubsection 3.3.2 will then discuss non-gravitational perturbations and their relevance for a cubesat mission around a binary asteroid.

3.3.1. Gravitational Field

The gravitational field around any celestial body can be approximated through different existing models. The most common one is a spherical-harmonics expansion but other dominant ones may include the polyhedron model developed by [Werner, 1994] or the geometric shape ones for which the equations describing the gravitational potential of a body are derived in [MacMillan, 1958] and [Feng, 2016].

Each of these models has some interesting particularities. The spherical-harmonics expansion is a straightforward and practical model often used for applications in planetary geodesy. Its main drawback, especially for asteroid missions, is that the validity of the expansion relies on the fact that the series describing the potential must be converging, which is not the case when close to the surface of the body. It is common to assume that the expansion is valid outside the circumscribing sphere of the body, i.e. the smallest sphere containing the entire body.

The polyhedron model allows for a closed-form solution of the potential of an arbitrary body approximated as a polyhedron split into triangular faces and edges [Feng, 2016]. Its main advantage is that the potential derived from this model is still valid close to the surface or even directly at its surface, countering the main drawback of the spherical-harmonics expansion. The polyhedron model is thus highly relevant when designing a landing mission. It has even been proven that a better estimation of the gravitational potential of an irregular asteroid can actually be obtained with a polyhedron model instead of the spherical-harmonics expansion, while a method also exists to convert the first one into the other [Werner, 1997]. The main drawbacks of the polyhedron model are however that it requires accurate knowledge about the shape of the body at stake, and that it is computationally demanding.

A geometric shape model is actually quite relevant as it is mainly used for irregular bodies such as asteroids, as an ellipsoid with constant density is a representative shape model for asteroids. Similarly to the polyhedron model, this model is also valid near and on the surface of the body at stake.

For the purpose of this thesis work, the spherical-harmonics expansion model is the one that was used. It was chosen because of its simplicity and because most works found in literature do use this model. Especially for the binary asteroid 1999 KW4, all spherical-harmonic coefficients up to degree and order 4 were provided in [Compère and Lemaître, 2014]. This model is furthermore fully implemented in TUDAT, the software used during this research work (see Chapter 5 for more information about TUDAT). As the goal is also to identify relevant orbit control-free applications in a binary asteroid system, considerations about landing are out of the question, meaning that there is actually no rationale for not choosing a spherical-harmonics expansion.

Spherical Harmonics Expansion

This paragraph aims at presenting the theory behind the spherical-harmonics expansion of the gravitational field of an arbitrary body.

Following the notations of [Wakker, 2015], the gravitational potential of an arbitrary body experienced at a point exterior to this body can be expressed as:

$$U = -\frac{\mu}{r}\left[1 + \sum_{n=2}^{\infty}\sum_{m=0}^{n}\left(\frac{R}{r}\right)^{n} P_{n,m}(\sin\Phi)\{C_{n,m}\cos m\Lambda + S_{n,m}\sin m\Lambda\}\right] \tag{3.1}$$

In Equation 3.1, the parameters r, Φ and Λ are the spherical coordinates of the considered point in the body-centric frame. More exactly, r is the distance between the point and the center of mass of the body, while Φ and Λ are the body latitude and longitude respectively. The gravitational parameter of the central body is expressed by the parameter μ, while R is its mean equatorial radius, and $P_{n,m}$ are Legendre functions of the first kind of degree n and order m.

With the constant model parameters $C_{n,m}$ and $S_{n,m}$, it is possible to define:

$$J_n = J_{n,0} = -C_{n,0} \tag{3.2}$$
$$P_n(\sin\Phi) = P_{n,0}(\sin\Phi) \tag{3.3}$$
$$C_{n,m} = J_{n,m}\cos m\Lambda_{n,m} \tag{3.4}$$
$$S_{n,m} = J_{n,m}\sin m\Lambda_{n,m} \tag{3.5}$$

leading to Equation 3.6 which is an alternative formulation of Equation 3.1.

$$U = -\frac{\mu}{r}\left[1 - \sum_{n=2}^{\infty} J_n(\frac{R}{r})^n P_n(\sin\Phi) + \sum_{n=2}^{\infty}\sum_{m=1}^{n} J_{n,m}(\frac{R}{r})^n P_{n,m}(\sin\Phi)\{\cos m(\Lambda - \Lambda_{n,m})\}\right] \tag{3.6}$$

where $J_{n,m}$ and $\Lambda_{n,m}$ can be computed from:

$$J_{n,m} = \sqrt{C_{n,m}^2 + S_{n,m}^2} \tag{3.7}$$
$$\Lambda_{n,m} = \frac{1}{m}\arctan\frac{C_{n,m}}{S_{n,m}} \tag{3.8}$$

Regarding the Legendre functions of the first kind, the following relations hold:

$$x = \sin\Phi \tag{3.9}$$
$$P_n(x) = \frac{1}{(-2)^n n!}\frac{d^n}{dx^n}(1-x^2)^n \tag{3.10}$$
$$P_{n,m}(x) = (1-x^2)^{m/2}\frac{d^m P_n(x)}{dx^m} \tag{3.11}$$

A spherical-harmonics expansion of the gravity field is practically used by truncating the expansion to a certain degree n and order m that is required for the application at stake. The accelerations in any desired direction can be derived from Equation 3.1 or Equation 3.6 by differentiating them in that specific direction.

[Wakker, 2015] mentions that the most modern gravity field models for the Earth may include coefficients up to degree and order 2150, but most applications in astrodynamics only keep the most contributing/perturbing terms in their models. On a more basic level, the gravitational field of a given Solar System body may also not be known to a very high accuracy from Earth observations. While in-situ observations would offer a better knowledge of the gravitational field, a mission still needs to be designed to provide such data. Regarding this particular thesis research, the spherical-harmonics coefficients of both the primary and the secondary of the 1999 KW4 binary system were found in literature in [Compère and Lemaître, 2014] where the authors derived them up to degree and order 4. The authors estimated that this truncation was sufficient for their own applications, and as this thesis work is all about a proof of concept, this truncation is also deemed good.

3.3.2. Other Perturbations

A cubesat placed in orbit in the 1999 KW4 binary asteroid system will experience several perturbations, some being of course more impactful than others. The dominant perturbations are third-body perturbations as well as solar radiation pressure (SRP). A special note goes to tidal interaction that is known to occur between binary asteroids, but was chosen to be left aside for this preliminary thesis work. A further phase of research with the same subject could take it into account.

Third-body Perturbations

Any spacecraft orbiting a celestial body will also experience the gravitational attraction from other bodies, for instance of the Moon and the Sun in the case of a satellite orbiting the Earth. Let body k be the central body, body i a spacecraft orbiting body k, and body j a perturbing body. The expression of the acceleration of the spacecraft due to the gravitational attraction of j can be written as [Wakker, 2015]:

$$\overrightarrow{f} = -\overrightarrow{\nabla}\left[-\mu_j\left(\frac{1}{r_{ij}} - \frac{x_i x_j + y_i y_j + z_i z_j}{r_j^3}\right)\right] \tag{3.12}$$

where $\mu_j = Gm_j$ and $r_{ij}^2 = (x_j - x_i)^2 + (y_j - y_i)^2 + (z_j - z_i)^2$. In this expression, x, y and z represent Cartesian coordinates, while r is the radial distance, m the mass and G the gravitational constant.

The projection along each direction further leads to:

$$f_x = \mu_j\left(\frac{x_j - x_i}{r_{ij}^3} - \frac{x_j}{r_j^3}\right) \tag{3.13}$$

$$f_y = \mu_j\left(\frac{y_j - y_i}{r_{ij}^3} - \frac{x_j}{r_j^3}\right) \tag{3.14}$$

$$f_z = \mu_j\left(\frac{z_j - z_i}{r_{ij}^3} - \frac{x_j}{r_j^3}\right) \tag{3.15}$$

[Feng, 2016] mentions that third-body perturbations coming from planets are usually negligible for an asteroid system unless the asteroid at stake follows a trajectory that leads to a close encounter, or if extreme accuracy is required for the orbit determination process. This is something that will be validated for the particular case of this thesis work.

Solar Radiation Pressure

SRP is due to the momentum exchange created from solar photons impacting a body. It is also at the origin of a phenomenon where small bodies are heated up and will re-emit energy through thermal radiation, generating in parallel a small force and a torque respectively known as the Yarkowski effect and the YORP effects [Scheeres, 2012]. These effects are however very small and also only involved for long time scales that are very often much longer than the timescale of a typical asteroid mission. This is why they will be left out as first approximation in this thesis work.

[Feng, 2016] highlights that the SRP may be the dominant acceleration over the gravitational attraction from the Sun actually, especially for a large area-to-mass ratio spacecraft. It can however be neglected when dealing with large asteroids of a few kilometers size. As this is not the case for the 1999 KW4 binary asteroid system, SRP must be considered with great attention in this thesis work.

From a theoretical point of view, the total momentum acting on a given spacecraft from incident solar photons can be decomposed into four dominant contributors [Scheeres, 2012]:

1. A momentum resulting from the impact on the surface of the spacecraft that is directed along the line between the Sun and the spacecraft.

2. A momentum resulting from photons that are specularly reflected, i.e. symmetrically of the incident photon flux w.r.t. the normal of the surface. Let ρ the albedo of the body and s the fraction of photons that are specularly reflected among the ones that are reflected, the fraction of specularly reflected photons can be expressed as ρs.

3. A momentum coming from diffusely scattered photons from the surface. The fraction of such photons is the complementary of the above specularly reflected photons and is in that sense equal to $\rho(1-s)$. These photons are not reflected in a single direction, so a factor B is added for the fraction of photons scattered in the normal direction from the surface, equal to 2/3 in an ideal case corresponding to what is called Lambertian surfaces.

4. A momentum resulting from the fraction $1-\rho$ of photons that are not reflected, but instead absorbed by the spacecraft, raising its temperature. While re-radiating those photons, this momentum is created in the direction normal to the surface, with a magnitude once again scaled down by the factor B.

[Scheeres, 2012] provides the complete expression of SRP including those four contributions, but it is usually too complex and can be simplified assuming that the photons are not absorbed by the surface ($\rho = 1$), which is a fair assumption as it is usually the case for the materials used for the spacecraft panels. Another simplification is that photons are specularly reflected ($s = 1$) which is again a fair assumption for most planar surfaces. One last simplification is that the surface is always perpendicular to the Sun-surface line. In this particular case, the acceleration of the spacecraft due to acSRP can be expressed as [Scheeres, 2012]:

$$\vec{a}_{SRP} = -\frac{(1+\rho)P_0 A_{SC}}{M_{SC}} \frac{(\vec{d} - \vec{r})}{|\vec{d} - \vec{r}|^3} \tag{3.16}$$

In this expression, $\vec{d}$ represents the vector from the central body to the Sun, while $\vec{r}$ represents the vector from the central body to the spacecraft, and P_0 is a solar pressure constant, equal to the Solar Constant (1361 W/m^2) if $\vec{d}$ and $\vec{r}$ are expressed in AU. This expression is also known as the cannonball solar radiation pressure model which is the one used in this thesis.

In space applications where the spacecraft is close to the central body, which will be the case in this thesis, it is actually fair to assume that $\vec{r} << \vec{d}$ which leads to the further simplified expression of the acceleration due to the SRP [Scheeres, 2012]:

$$\vec{a}_{SRP} = -\frac{(1+\rho)P_0}{B_{SC} d^3} \vec{d} \tag{3.17}$$

where the mass-to-area ratio $B_{SC} = M_{SC}/A_{SC}$ is introduced, which is tabulated and often ranging between 20 and 40 kg/m^2 [Scheeres, 2012]. This last expression is the most commonly used to model SRP, and assumes that it is only dependent on $\vec{d}$.

3.4. Equations of Motion

This section focuses on the basic set of equations that can describe the motion of a spacecraft orbiting any celestial body. Several forms of these equation do exist and may be of relevance for specific applications.

The Newtonian formulation is the most fundamental form of the equations of motions. This is the way in which dynamics are actually represented in TUDAT, so for the sake of simplicity this is the one that is used in this thesis. Mention can however briefly be made of the Lagrangian and Hamiltonian formulations for which a more detailed description can be found in literature, for instance [Morbidelli, 2002].

According to [Scheeres, 2012], the Lagrangian form of the equations of motion does not provide a particularly good insight on the interpretation of the results, but is still interesting for computation purposes. It is furthermore often used when dealing with small bodies, and can be used either in a rotational body-fixed frame or a quasi-inertial frame fixed to the small body orbiting the Sun. The first frame is useful for applications that are close to the surface of the small body, while the second one is more useful when dealing with orbital motion that is perturbed by SRP or solar gravity [Scheeres, 2012].

The Hamiltonian formulation is an alternative, providing further insight on the results at hand. It is actually strongly correlated to the Lagrangian form, and can be particularly interesting to investigate for the computation of so-called periodic orbits, which could be a very interesting focus for this thesis research. The current work is however designed to be broad on the subject of orbit control-free applications in a binary system, so there is no particular reason to only focus on periodic orbits.

3.4.1. Newtonian Formulation

The Newtonian formulation of the equations of motion can be simply expressed as:

$$\ddot{\vec{r}} = \sum \frac{\partial \mathscr{R}_{\text{gravitational}}}{\partial \vec{r}} + \sum \frac{\partial \mathscr{R}_{\text{spacecraft}}}{\partial \vec{r}} + \sum \frac{\partial \mathscr{R}_{\text{non-gravitational}}}{\partial \vec{r}} \tag{3.18}$$

This expression is based on the usage of potential formulations $\mathscr{R}$, and highlights three contributions:

1. Gravitational accelerations exerted by other bodies on the spacecraft
2. Accelerations coming from the spacecraft itself such as thrust
3. Non-gravitational accelerations including among others SRP

In this thesis work, the second contribution is left equal to zero as the whole point is to get rid of the propulsion system. Also other spacecraft-related accelerations (thermal thrust, ...) are ignored.

Some more assumptions enable to compute a more simplistic expression, following the remarks from [Scheeres, 2012]. It is assumed first that the spacecraft has no effect whatsoever on the motion of the central body with respect to inertial space. If the spacecraft experiences the gravitational attraction of the Sun and other bodies, as well as other non-gravitational accelerations such as SRP, the equations of motion in Equation 3.18 can be rewritten as [Scheeres, 2012]:

$$\ddot{\vec{r}} = \frac{\partial U\left(\vec{C}^T \cdot \vec{r}\right)}{\partial \vec{r}} + \sum_{i=0}^{N} \frac{\partial \mathscr{R}_{p_i}\left(\vec{r}, \vec{d}_i\right)}{\partial \vec{r}} + \frac{\partial \mathscr{R}_{\text{non-gravitational}}\left(\vec{r}, \vec{d}_0\right)}{\partial \vec{r}} \tag{3.19}$$

In this expression, $\vec{r}$ is the position vector of the spacecraft relative to the central body and in an inertial frame, U is the gravitational potential of the central body, $\mathscr{R}_{p_i}$ represents the perturbation from the i^{th} attracting body, and $\mathscr{R}_{\text{non-gravitational}}$ describes the potential coming from non-gravitational perturbations.The position of the central body relative to the Sun is represented by the vector $\vec{d}_0$, while the vectors $\vec{d}_i$ ($i \geq 1$) are the position of the other perturbing bodies w.r.t. the central body. Finally, $\vec{C}^T$ is the transformation matrix from the inertial reference frame to the central body-fixed one in which the potential U is expressed.

3.5. Reference Frames and Coordinate Systems

For the determination of the motion of a spacecraft or any body in general, one needs a reference frame in which its position, velocity and acceleration are expressed, but also a given coordinate system and one for the time. This particular section aims at presenting some relevant options of reference frames and coordinate system for a mission around a binary asteroid, but does not pretend to be exhaustive on the subject. Some basic astrodynamics knowledge is assumed, but the reader can refer to [Wakker, 2015] for some general concepts.

3.5.1. Reference Frames

A reference frame is described by an ordered set of mutually orthogonal unit-length vectors that are possibly time-dependent, and is associated to a center [1].

An inertial frame is one of the most commonly known type of reference frame, derived from Newton's first law: "An inertial reference frame is a reference frame with respect to which a particle remains at rest or in uniform rectilinear motion if no resultant force acts upon that particle.". One can say that an inertial frame is in fact a reference frame in which Newton's second law of motion stands.

The very notion of an inertial frame, although important in theory, is not fully valid in the real physical world. In practice, no truly inertial frame actually exists, so one has to rely on so-called pseudo-inertial frames, which means that one neglects the rotations and accelerations of this pseudo-inertial frame w.r.t. the theoretical true inertial frame [Wakker, 2015].

For the sake of simplicity, it has been chosen in this thesis to express the state of the cubesat in a pseudo-inertial frame centered on the primary Alpha, following the J2000 orientation frame. All angular values provided in literature such as for the mutual orbit elements of the binary are indeed provided in this frame, such as in [Ostro and al., 2006], [Fahnestock and Scheeres, 2008] and [Compère and Lemaître, 2014]. This frame is

[1] https://naif.jpl.nasa.gov/pub/naif/toolkit_docs/Tutorials/pdf/individual_docs/17_frames_and_coordinate_systems.pdf

considered inertial in the remainder of this report.

The rotational model of both Alpha and Beta is then defined in a different frame, following [Compère and Lemaître, 2014]. The X-axis points from the center of Alpha to the initial position of Beta, the Z-axis is orthogonal to the initial orbital plane, and the Y-axis mutually and orthogonally completes this right-handed frame. For a more detailed discussion on the implementation of the rotational model of the binary asteroid for use in future simulations, the reader can refer to Section 6.2.4.

3.5.2. Coordinate Systems

A coordinate system specifies the means of locating points within a given reference frame.

The position and velocity of a spacecraft (or any body) can actually be expressed through different sets of coordinates [Wakker, 2015], the most common ones being:

1. rectangular coordinates: $x, y, z, \dot{x}, \dot{y}, \dot{z}$
2. spherical coordinates: $r, \alpha, \delta, V, \gamma, \Psi$
   r is the radius, α the longitude, δ the latitude, V the velocity, γ the flight-path angle, Ψ the flight-path azimuth.
3. orbital elements: $a, e, i, \Omega, \omega, \tau$
   a is the semi-major axis, e is the eccentricity, i is the inclination, Ω is the right ascension of the ascending node, ω is the argument of pericenter, and τ is the time of pericenter passage.

Figure 3.2 provides a visualization of the spherical coordinates and the orbital elements i, Ω and ω.

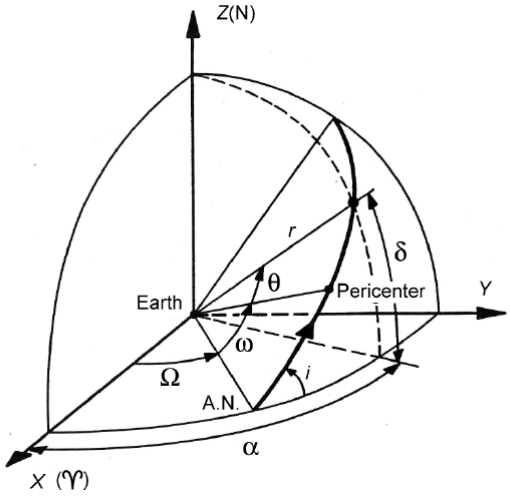

Figure 3.2: Definition of the orbital elements i, Ω, ω and the position of a spacecraft in spherical coordinates around the Earth [Wakker, 2015].

In TUDAT, the initial conditions of the spacecraft are provided in orbital elements w.r.t. the central body Alpha in the inertial frame, and its state can be retrieved and converted to any other representation as desired at any time during the propagation process. The formulation of the coordinates that are propagated during the simulations is however a completely other matter that needs to be treated separately in Chapter 7, as it needs a proper choice based on the required accuracy on the knowledge of the state of the spacecraft, and low cpu time.

3.6. Conclusions

Binary asteroids are an extremely interesting subject to explore. They represent about 15 % of the NEA population and are the focus of the upcoming Hera mission to the Didymos binary. For this thesis work, it has been chosen to work on the binary asteroid commonly known as 1999 KW4 which is typical of the NEA population

having a secondary-to-primary mass ratio that is also average among the binary compendium. This should in theory be beneficial for an orbit-control free cubesat mission as Beta is expected to play as a counterbalance for the gravitational field of Alpha but also the SRP that is very strong in small body environments.

A spacecraft may experience various perturbations in a binary asteroids environment, such as third-body perturbations or SRP, that can actually become the dominant force over gravitational attraction. Three main models are then in use for modelling gravity field around Solar System bodies and the most common one, namely the spherical-harmonics expansion, has been chosen to carry out this thesis work.

Different options also exist to express the equations of motion, and the Newtonian formulation was selected for the sake of simplicity in TUDAT. A quasi-inertial frame centered in Alpha following the J2000 orientation frame has to be constructed, and all simulations will be performed in that particular frame.

4

Stability

Perturbations will always be part of the orbital dynamics of a spacecraft in the Solar System, and such perturbations are even more significant in the vicinity of small bodies as they present very irregular gravity fields. Perturbations may even be so strong that the motion of a spacecraft can drift from a nominal path and become uncontrollable, resulting in various scenarios such as an entry, an impact, or an escape from the entire system. For any kind of mission, but especially for one that aims at being without orbital control, it is desired to stay in orbit as long as possible. To this end, it is crucial to identify "stable" orbits around the binary asteroid, that could be targeted by the mission team depending on the desired scientific outcome. But how to assess this stability? How is it usually understood, and how is it implemented in this thesis work? Section 4.1 serves as a small introduction and briefly discusses the notion of stability via its intrinsic notion of equilibrium. Section 4.2 then refers to the notion of stability that has been implemented in this thesis work, namely via the use of numerical termination conditions, which is a very practical point of view. Section 4.3 will finally discuss other theories that could have been explored further for the assessment of (in)stability within the binary system, and why they were not retained.

4.1. Equilibrium

The notion of stability is intricately linked to the notion of equilibrium, and what a better and simple first approach to the problem than equilibrium points. They are of course at the core of the basic astrodynamics background, so only a few relevant assertions will be stated, but the interested reader can refer to [Wakker, 2015] for instance for some derivations or more detailed information.

In the three-body problem, there exists a total of five equilibrium points that are called Lagrange points. While the first three ones L_1, L_2 and L_3 are located on the X-axis and are always unstable, L_4 and L_5 can be stable depending on the system at hand, with the condition being that the normalized mass of the secondary body is such that $\mu < 0.03852$ [Wakker, 2015] for circular orbits of the two main bodies. It is important to mention that equilibrium points per se only exist in time-invariant systems, which does not stand anymore in real-life applications. It is however possible to reach a sort of quasi-equilibrium around such points in time-variant systems where the spacecraft remains within a bounded region.

In the particular case of the binary asteroid 1999 KW4, the normalized mass of the secondary is approximately equal to 0.0543 so it is actually expected that the motion of a spacecraft around L_4 and L_5 is divergent, as no stable motion can be found for this value; this is even more the case when considering that the two main bodies move in elliptical orbits [Wakker, 2015].

4.2. Termination Conditions-Stability

The notion of stability has a strong mathematical background as will be seen in Section 4.3 where various theories are briefly explored. An eigenvalues analysis is often performed in dynamical systems to that purpose, but many other theories do exist in that field and are still under research. While this is a completely valid approach, it mainly focuses on assessing linear stability around equilibrium points or around periodic solutions. The current thesis work could benefit from a more practical point of view such as in [Hu and Scheeres,

2004] and [Araujo et al., 2015].

This is where orbital elements come into consideration. One usually considers stability in the sense that no secular drift occurs in the actions variable (semi-major axis a, eccentricity e, inclination i), while a drift in the angular variables (longitude of ascending node Ω, argument of periapsis ω, mean anomaly M) is not impactful [Villac and Aiello, 2005].

[Hu and Scheeres, 2004] present in their work such numerical stability condition derived from the evolution of the orbital elements of a given trajectory, in the context of spacecraft orbiting a binary asteroid system. One possible choice for a criterion is that the change in the eccentricity is never larger than a chosen value during a certain duration of propagation T_f:

$$|e(t) - e_0| < \Delta e_{\max}, \quad 0 \leq t \leq T_f \tag{4.1}$$

As stated in [Hu and Scheeres, 2004], $\Delta e_{\max}$ should be chosen between 0.2 and 0.6 but this choice is really application-dependent. For this thesis work, it was chosen to be open to all kind of perturbed orbits so no constraints were added on the eccentricity. Tracking changes in semi-major axis is not necessary in parallel, as a change in semi-major axis cannot be performed appreciably without a change in eccentricity [Hu and Scheeres, 2004].

This idea of relying on constrained orbital elements to assess stability is what Mast [2018] calls Bounded Input Bounded Output - stability or BIBO-stability. It is for instance at the core of the work of [Damme et al., 2017] which inspired this thesis research significantly as explained in Subsection 2.4.2.

One other possible stability criterion to track is to choose a range of available distances w.r.t. a given body, although the choice of boundaries is again quite arbitrary and dependent on the application:

$$r_{\min} < r(t) < r_{\max}, \quad 0 \leq t \leq T_f \tag{4.2}$$

One end of this equation may be more constraining than the others: for instance it could be considered that avoiding an impact is much more critical than an escape situation so the difference between $r(t)$ and $r_{\max}$ could be allowed to be larger.

These two stability criteria were investigated in parallel by Mast [2018] in the case of a second-degree and order gravity field, with the conclusion that they led to very similar results. This is why the author only used the radius criterion over the eccentricity, as it is more intuitive and better suited for a physical understanding of science mission requirements.

All these types of constraints are very well computationally handled in TUDAT, and are referred for the rest of this thesis as termination conditions with a very simulation-oriented view. The underlying principle is simple: as long as the spacecraft does not violate some desired constraints, the motion of the spacecraft is considered stable, in the sense of what we call termination conditions-stability. The termination conditions that were chosen in this particular thesis work are described in detail in Subsection 5.1.4.

4.3. Other Ways of Assessing Stability

Many theories exist in order to assess stability in various systems, and often come from a strong mathematical background. It is still a vast area of research, and this section is not written as an exhaustive one on the subject. Rather, it should be seen as an introduction to some paths that have been investigated for this particular study regarding stability, but were not retained.

One way of introducing the concept of stability is to discuss the concept of Poincaré maps derived from the so-called surfaces of section. This enables afterwards to introduce the concept of periodic orbits in view of those Poincaré maps, which are inherently stable. This section follows the reasoning from [Scheeres, 2012], where the interested reader can find many more details.

4.3.1. Surfaces of Section, Poincaré Maps and Periodic Orbits

One useful way to reduce the dimensionality of a time-invariant system is to rely on a so-called surface of section. It is a geometrically defined surface or condition in phase-space, for which each intersection with a trajectory in a given coordinate frame is reported. One simple visual example is to report every time a trajectory crosses the x-axis in the (x,y) phase-plane, which can be further restricted to only consider intersection points with $\dot{y} > 0$ to only obtain one intersection per orbit.

In a more mathematical point of view, let a surface of section be defined by the scalar equation $S(\boldsymbol{x}) = 0$, with $\boldsymbol{x} \in \mathbf{R}^{2n}$. In order to be properly defined, this surface must not be tangent to the flow but transversal instead, which requires the condition $\frac{\partial S}{\partial \boldsymbol{x}} \cdot \dot{\boldsymbol{x}} > 0$ (where a preferred direction of crossing is defined). This configuration can be visualised in Figure 4.1.

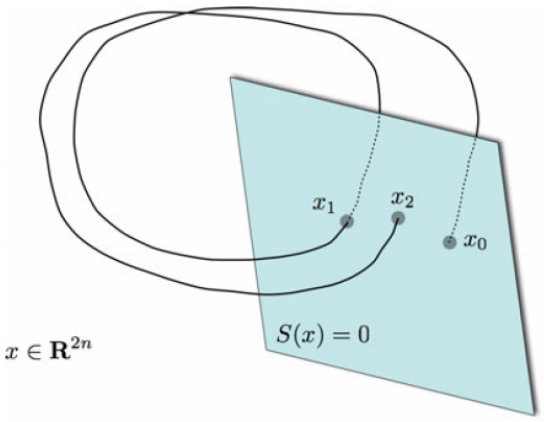

Figure 4.1: Illustration of a surface of section [Scheeres, 2012].

Surfaces of section are usually used in time-invariant systems, because if a trajectory crosses the same point again on the surface, the motion can be defined as periodic by definition. It is however not always the case for time-varying systems as highlighted by [Scheeres, 2012]. Surfaces of section enable in theory to transform a time-continuous solution into a time-independent discrete map.

Such surfaces of section can be used for the computation of so-called Poincaré maps which take into account energy levels, and are essentially what [Scheeres, 2012] calls: "A mapping function that returns a trajectory back to a surface of section and maps every initial point chosen on that section with the same value of the Hamiltonian".

The potentially interesting thing for us about Poincaré maps is that they are useful in the computation of so-called periodic orbits in time-invariant systems which are fixed points on a Poincaré map. They could in essence be very interesting to target for an orbit-control free mission due to their inherent stability, and can be grouped into whole families of periodic orbits. A binary asteroid environment is of course a real physical environment, but it could in theory be possible to target so-called pseudo or quasi-periodic orbits which are essentially perturbed periodic orbits that still maintain a sort of periodicity.

The computation of Poincaré maps was not chosen for the assessment of stability due to their complex implementation and because they would not bring much more insight on our particular research compared to a very practical and space-mission oriented termination conditions-stability. Periodic orbits were also not necessarily focused for this thesis work, although very interesting for the whole concept. This choice comes from the fact that the study is aimed at a broad proof of concept on what is doable or not for an uncontrolled cubesat within a binary-asteroid environment.

The mathematical equations coming from those other theories can be found in [Scheeres, 2012] for the interested reader, and will not be written in this report for the sake of clarity and because these theories were not used for the stability assessment done here.

4.3.2. Chaos Quantification Methods

One particular area of study in the assessment of stability are the so-called chaos quantification methods relying on what are called chaos indicators, theoretically derived from the variational equations.

Many chaos indicators exist, the most famous being maybe the Fast Lyapunov Indicator (FLI) first derived by [Froeschlé et al., 1997] to distinguish between what is called regular versus chaotic motion, and its upgraded version called the Orthogonal Fast Lyapunov Indicator (OFLI) in [Fouchard et al., 2002]. These chaos indicators do not seem very useful for our particular study, especially because they need an absolute reference to measure chaoticity, and thus need reference orbits that could be computed using other chaos indicators for example. Their main advantage is that they are computationally very fast, but they also require numerical integration.

Other well-known chaos indicators include the Mean Lyapunov Exponent (MLE), the Mean Exponential Growth factor of Nearby Orbits (MEGNO), the Dynamical Spectra of Stretching Numbers (SSNs), the Smaller Alignment Index and Generalized Alignment Index (SALI and GALI), the Relative Lyapunov Indicator or other chaos indicators coming from frequency analyses. The interested reader can refer to [Morbidelli, 2002] and [Darriba et al., 2012] for more details on these methods.

[Mast, 2018] investigated the FLI and the OFLI in the context of a second-degree and order gravity field within the Psyche asteroid, which are known to perform well and be representative of the chaos indicators family, and compared the results with regular termination conditions-stability. The results proved to be very similar, showing that chaos indicators are an interesting way of assessing stability. They seem also faster to observe instability for a given orbit. The problem is that they are computationally demanding compared to traditional methods, with a factor 7 in the case of the author, and that they will not bring much more insight for our particular application. An interesting topic could be the implementation of these chaos indicators in TUDAT, but this is left for a different thesis.

4.4. Conclusions

This chapter was all about detailing how the notion of stability was implemented in this particular thesis via the use of termination conditions, which are heavily computation-oriented and thus very interesting in a software like TUDAT. Other ways of assessing stability were mentioned such as via the computation of inherently stable periodic orbits or the use of chaos indicators. Periodic orbits could on the one hand be very interesting to target but this study has been chosen to be broad on the search of stable regions around a binary asteroid. Chaos indicators, on the other hand, are computationally costly while not providing more insight on results compared to when using a simple termination conditions-stability, and were left aside for that reason.

5

Numerical Tools

In order to compute stable orbits in a binary-asteroid environment, one needs to model the orbital dynamics of the cubesat in this environment, which requires a software to numerically evaluate all the equations of motion and integrate them. Some astrodynamics toolbox exist to alleviate the load. This chapter aims at discussing the different numerical tools that are used in this thesis, which are the TU Delft Astrodynamics Toolbox (TUDAT, see Section 5.1) and MATLAB (see Section 5.2).

5.1. TUDAT

TUDAT was used in previous projects and was thus preferred over other existing astrodynamics tools that are publicly available. All TUDAT features that are of relevance for this thesis are highlighted in this section, but the interested reader can find an in-depth documentation for far more content at `http://tudat.tudelft.nl/`.

5.1.1. Perturbing Forces

All perturbing forces highlighted in Chapter 3 are already implemented in TUDAT. This enables to make use of the point-mass gravity or other gravitational potentials exerted by third bodies through different models. The solar radiation pressure is also implemented in TUDAT, though only as a cannonball radiation pressure, which assumes that the generated force is directed along the line from the Sun to the target, which is a fair assumption.

5.1.2. Propagators

A propagator is a way of numerically expressing the equations of motion of a dynamical system, which implies that they are not all well suited for every type of space application. TUDAT has various built-in options for a choice of propagator during the simulations:

- **Cowell and Encke propagators**
  The Cowell propagator fully propagates the Cartesian state of a body and is in that sense very straightforward, while the Encke propagators only propagates the difference between the state of the body and the one of a Keplerian orbit of reference [Dirkx and Mooij, 2019]. The Encke propagator is better suited when this difference is small, so when the spacecraft is in a nearly Keplerian orbit with no large perturbations, which is definitely not the case in this thesis research, so it is expected that this particular propagator will not perform very well.

- **Gauss Planetary equations** are expressed either in Keplerian elements or Modified Equinoctial Elements.
  Propagators based on Gauss Planetary Equations are better suited for perturbed motion. The choice between the Keplerian elements form or the one with the Modified Equinoctial Elements depends on the fact if the motion gets close to singularities at some point, namely when the inclination and/or the eccentricity of the orbit come close to zero. Such singularities are indeed removed when using the Modified Equinoctial Elements.

- **Unified State Model** use either quaternions, Rodriguez parameters or the exponential map.
  The Unified State Model (USM) originally propagates seven elements instead of six: four quaternions and three other parameters related to the velocity hodograph. Two modified versions of the USM are however worth mentioning: one replaces the quaternions by so-called Rodrigues parameters while the other replaces them by the Exponential Map [Vittaldev et al., 2012], doing so reducing the number of propagated elements from seven to six.
  The USM has shown to be better performing than Cartesian propagators when dealing with perturbed motion, using either fixed or variable-step size integrators [Vittaldev et al., 2012]. This statement is less and less accurate with smaller step-sizes, but the difference can be quite significant for larger step-sizes. Cartesian propagators however perform more efficiently in highly eccentric orbits.
  Another strong aspect of the USM comes from its efficiency in terms of computational cost when compared to propagators that use Cartesian coordinates. Using the Exponential Map instead of the Rodrigues parameters has also shown to be better performing in general, although these two modified versions of the USM do show some singularities with retrograde orbits that are not present with the original model using quaternions [Vittaldev et al., 2012].

Based on these arguments, some preliminary assessments can already be made regarding the choice of a propagation method in this thesis work. A more in-depth selection in combination with the integration method to be used is however crucial and is performed in Chapter 7. The first conclusion that can be drawn is that the Encke propagator does not seem to be well-suited for applications with large perturbations like these. It can be highlighted that the USM is very efficient in terms of both accuracy and cpu time. The singularity occurring for retrograde orbits could however go against the modified versions of the USM as most stable periodic orbits around small bodies are retrograde. The Gauss Planetary Equations using Keplerian elements may furthermore not be the best choice due to the zero-eccentricity singularity, as most stable periodic orbits around small orbits are circular. The Cowell propagator is a very solid choice as it has no singularities, but it is generally less efficient than other propagation methods. It is however a strong first choice for the first applications of this thesis work, before considering more efficient methods in Chapter 7.

5.1.3. Integrators

An integrator is, as its name suggests, a way of numerically integrating the equations of motion of a dynamical system. TUDAT has many built-in integrators already available. There is no need to implement an integration technique in this thesis work, as it would be very time-consuming while not being the focus of the research. The concept behind an orbit control-free motion should also not require a hard constraint on numerical accuracy in essence, but of course there is still a need to ensure stability somehow. This is why this thesis work will only consider the integration methods that are already implemented in TUDAT, which is more than sufficient to work with. These integrators are separated into three different groups according to their mathematical construction, presented below.

- **Multi-stage integrators:** those include both fixed step-size integrators such as the Runge-Kutta 4, and variable step-size integrators such as the Runge-Kutta-Fehlberg 4(5), 5(6), 7(8) and the Dormand-Prince integrators.
- **Multi-step integrators:** those include the Adams-Bashforth-Moulton integrator: a variable step-size and order integrator relying on the theory behind both the Adams-Bashforth and the Adams-Moulton integrators.
- **Extrapolation-based integrators:** those notably include the Bulirsch-Stoer integration method.

A brief discussion about these three different groups of integrators is provided below for the interested reader. To this extent, let us assume an n-dimensional first-order differential equation of the form [Montenbruck and Gill, 2012]:

$$\dot{\vec{y}} = \vec{f}(t, \vec{y}) \quad \vec{y}, \dot{\vec{y}}, \vec{f} \in \mathbb{R}^n \tag{5.1}$$

This equation can actually always be obtained from the second-order differential equation that describes the motion of a spacecraft in space [Montenbruck and Gill, 2012]:

$$\dot{\vec{y}} = \vec{f}(t, \vec{y}) = \begin{pmatrix} \dot{\vec{r}} \\ \vec{a}(t, \vec{r}, \dot{\vec{r}}) \end{pmatrix} \tag{5.2}$$

where $\ddot{\vec{r}} = \vec{a}(t, \vec{r}, \dot{\vec{r}})$.

Multi-stage integrators

Multi-stage integrators are actually the ones usually known as the Runge-Kutta category of integrators. These are divided into two subcategories, namely the ones with constant step-sizes and the ones with variable step-sizes. The wish to implement a better integration method made Carl Runge and Wilhelm Kuttta to develop their famous original Runge-Kutta integrator in the 19$^{\text{th}}$ century, known today as the Runge-Kutta 4 (RK4) method.

Numerous constant step-sizes Runge-Kutta integration methods have been developed nowadays, but they overall have the same structural understanding. Consider an s-stage Runge-Kutta integrator. The state of the spacecraft can be approximated at time $t_0 + h$ with a general formula provided in [Montenbruck and Gill, 2012]:

$$\vec{\eta}(t_0 + h) = \vec{y}_0 + h\vec{\Phi} \tag{5.3}$$

with the incremental function:

$$\vec{\Phi} = \sum_{i=1}^{s} b_i \vec{k}_i \tag{5.4}$$

The function evaluations $\vec{k}_i$ in the incremental function must obey several equations that the interested reader can find in [Montenbruck and Gill, 2012].

The second type of multi-stage integration methods relies on variable step-sizes, and are known as the Runge-Kutta-Fehlberg integrators. The idea behind them is that they are able to compute the required step-size to the next iteration taking into account a desired accuracy. To that extent, they rely on the so-called embedded Runge-Kutta methods, which are basically two Runge-Kutta integrators with successive orders evaluated in parallel. The higher-order solution is then taken as a reference, and the state difference with the low-order solution is assumed to be an approximation of the error for the low-order integration method. From the knowledge of the current step-size and this estimate of the error, it is then possible to derive a new time-step with the desired accuracy. The step-size is in practice only modified if the change is significant in terms of computational time saving, typically if there is a factor two to five from one step-size to an other. Of course, it is still of the responsibility of the user to come up with a relevant initial step to start the simulation, with some experience. The role of the nominal and the extra order can also be reversed depending on the method. A more detailed explanation of multi-stage integration methods with variable step-sizes can be found in [Montenbruck and Gill, 2012].

Multi-step integrators

Multi-stage integrators presented above do not take into account the information coming from previous time-steps to generate the next one, they only take into account the information coming from the current time-step. This is where multi-step integration methods come into consideration. They were developed in the 19$^{\text{th}}$ century and the beginning of the 20$^{\text{th}}$ century based on the work of famous astronomers such as J.C. Adams, F.R. Moulton and Ph. H. Cowell who used them for an accurate description of the motion of Solar-System bodies [Montenbruck and Gill, 2012].

Among such multi-step integration methods, a well-known one is called the Adams-Bashforth method which takes into account m different steps using a polynomial approximation interpolating those points. Let be a

polynomial $\vec{p}^{\,i}_{m}$ of order m-1 interpolating those m points, then the state vector at time $t_i + h$ given by the Adams-Bashforth integrator is [Montenbruck and Gill, 2012]:

$$\vec{\eta}_{i+1} = \vec{\eta}_i + h\vec{\Phi}_{ABm} \tag{5.5}$$

where the incremental function is:

$$\vec{\Phi}_{ABm} = \frac{1}{h}\int_{t_i}^{t_i+h} \vec{p}^{\,i}_{m}(t)\,dt \tag{5.6}$$

The expression for the polynomial approximation can be found in [Montenbruck and Gill, 2012] for the interested reader.

The problem with the Adams-Bashforth method is that it relies on m evaluations up to time t_i while the integration is performed between times t_i and t_{i+1} where the approximation is not valid anymore. This is why a new integration method was built, called the Adams-Moulton integration method, which instead uses the polynomial $\vec{p}^{\,i}_{m}$ at time $t_i + h$, such that the incremental function is now defined as [Montenbruck and Gill, 2012]:

$$\vec{\Phi}_{AMm} = \frac{1}{h}\int_{t_i}^{t_i+h} \vec{p}^{\,i+1}_{m}(t)\,dt \tag{5.7}$$

The solution can however not be expressed with a form similar to Equation 5.5 as it now depends on the state vector at time t_{i+1} which is the one that is to be estimated. The Adams-Moulton integration method is in that sense called a predictor-corrector integration method. The precise methodology behind the Adams-Moulton method can be found in [Montenbruck and Gill, 2012] for the interested reader. This method originally takes into account constant step-sizes, but it can actually be adapted with variable step-sizes, with a technique very similar to the one for multi-stage integration methods.

Extrapolation-based integrators

The extrapolation-based category of integration methods are single-step based on the Richardson interpolation technique. They are often called Bulirsch-Stoer or Gragg-Bulirsch-Stoer methods from the work of Gragg (1965) and Bulirsch & Stoer (1966).

These types of integrators take their roots in the so-called mid-point rule. To identify the solution at a time t_0+h, the interval $[t_0, t_0+H]$ is divided in n steps of size $h = H/n$. The state $\vec{\eta}_1$ at time t_0+h can be determined using a simple Euler approximation while other values $\vec{\eta}_1$ are determined using this so-called mid-point rule [Montenbruck and Gill, 2012]:

$$\vec{\eta}_1 = \vec{y_0} + h\vec{f}(t_0, \vec{y}_0) \tag{5.8}$$

$$\vec{\eta}_{i+1} = \vec{\eta}_{i-1} + 2h\vec{f}(t_0 + ih, \vec{\eta}_i) \quad (i = 1, ..., n-1) \tag{5.9}$$

The interested reader can refer to [Montenbruck and Gill, 2012] for the theory and the expressions behind this technique. What is interesting is that the extrapolation-based integrators are in essence good candidates for very high accuracy, but have the big inconvenience that they provide a very sparse output density.

Discussion

It can first be highlighted that the extrapolation-based integration methods do not seem particularly interesting for the sake of this thesis work. Their good accuracy combined with their sparse output density indeed makes them an interesting option for the integration of long time-scale dynamics such as the evolution of Solar-System bodies, where dense output is not crucial. For a cubesat orbit control-free mission around a binary asteroid system, with very impacting perturbations to foresee, dense output is important. It is for this particular reason that this type of integration methods is ruled out for this thesis. The reader is invited to refer to Chapter 7 for a proper choice to be made between the various mentioned techniques.

5.1.4. Initial Termination Conditions

Several techniques have been discussed in Chapter 4 about the computation of stable orbits about any celestial body. The one that was proven to be the most practical for numerical purposes was seen to be based on propagation termination conditions. The default termination setting in TUDAT is to end the propagation when a certain termination time has passed, but others are also implemented such as reaching a certain cpu time, reaching a certain criterion for a dependent variable, switching a boolean with a user-defined function, or even fulfilling multiple criteria (simultaneously or not).

It was chosen to be very general at first in the choice of termination conditions, and for this reason multiple criteria termination conditions were implemented, all based on the distance of the cubesat w.r.t. both Alpha and Beta. In view of the scale of the asteroid system 1999 KW4 (mean distance of 2.6 km), it was chosen that the propagation would stop if the distance between the cubesat and either Alpha or Beta would reach 100 m above their respective surfaces. This particular scenario was considered to be an impact situation, even though a safety margin was taken into account and thus it does not mean the end of the mission per se. Another criterion was implemented to take into account an escape situation. Because it could in essence be possible to find less perturbed orbits around the whole binary system, it was chosen that the termination condition for an escape situation of the cubesat would be whenever it would reach 20 km in distance w.r.t. Alpha: this should cover most types of orbits that can be found in the system. Obviously the above termination conditions only need to be triggered individually to end the propagation.

It is emphasized that at least at this point, no termination conditions on the orbital elements of the cubesat (or BIBO-stability conditions) were implemented, to not restrict the possibilities in the results. Later on (Chapter 7), an extra BIBO-condition was added.

It should also be made clear that no requirements are implemented for the stable orbits to be found regarding a mission perspective (e.g. latitude coverage, ...).

5.2. MATLAB

TUDAT does not provide a visual interface for plotting purposes of the retrieved simulation results. This is why a tool like MATLAB is of primary importance when it comes to interpreting the results with regard to the chosen criteria, in both 2D or 3D plots. A general documentation of the software can be found at `https://nl.mathworks.com/help/matlab`.

6

Environment Model Implementation

This chapter focuses on the implementation of a relevant environment model to approximate the orbital dynamics of a cubesat in the proximity of the binary asteroid system (66391) 1999 KW4, to be used in Chapter 7 and further. Section 6.1 first briefly presents how the cubesat is modelled in future simulations, while Section 6.2 highlights how the two asteroids were implemented. Other bodies in the Solar System have been modelled using a point-mass gravity field and will thus not be detailed further. Section 6.3 finally mentions the acceleration model that is used to describe the dynamics of the system.

This chapter is more descriptive in nature, the whole validation process of this environment model can be found in Chapter 10.

6.1. Cubesat Model

The cubesat is modelled in TUDAT using a point mass of 3.5 kg, which is an average mass for a Three-Unit (3U) cubesat[1]. It has a reference surface of 0.02 m^2, enabling it to be subject to the solar radiation pressure. In their work, [Damme et al., 2017] considered for their simulations a reference cross-section surface of a 4.5 kg cubesat ranging between 0.01 m^2 and 0.0425 m^2, so 0.02 m^2 is a representative value.

6.2. Binary Asteroid Model

This section focuses on the modelling of the binary asteroid 1999 KW4. Subsection 6.2.1 first details the main properties of the binary. Subsection 6.2.3 then presents the spherical-harmonics gravity field model used in this thesis, while Subsection 6.2.4 highlights how the rotational model of the two asteroids is modelled.

6.2.1. Main Properties of 1999 KW4

The main parameters of 1999 KW4 can be found in [Ostro and al., 2006] and are repeated in Table 6.1 for convenience. They can also be found in [Fahnestock and Scheeres, 2008] and [Compère and Lemaître, 2014].

All angular values refer to the equatorial J2000 reference frame. It is highlighted that some difficulties were encountered in the precise determination of Beta spin rate such that it was assumed in [Ostro and al., 2006] that it was equal to its mean orbital period, and the same will be assumed in this thesis work.

[1] `https://en.wikipedia.org/wiki/CubeSat`

Parameter (units)	Alpha	Beta
Mass (10^{12} kg)	2.353	0.135
Mean radius (km)	0.6585	0.2255
Spin rate (°.day^{-1})	3125.4	495.0
a, semi-major axis (m)	-	2548
e, eccentricity (-)	-	0.0004
i, inclination (°)	-	156.1
Ω, longitude of ascending node (°)	-	105.4
ω, argument of peripasis (°)	-	319.7

Table 6.1: Main properties for the model of 1999 KW4 with relative orbital elements of Beta around Alpha. The epoch corresponds to calendar date 26 May 2001 09:55:00.5, and represents the time at which Beta is at pericenter. From [Ostro and al., 2006], [Fahnestock and Scheeres, 2008], [Compère and Lemaître, 2014] and Pravec binary database.

6.2.2. Ephemeris

Regarding the motion of the binary system barycentre, an ephemeris was retrieved from the online Advanced Horizons Asteroid & Comet SPK File Generation Request (`https://ssd.jpl.nasa.gov/x/spk.html`), which makes use of the initial orbital parameters from the Jet Propulsion Laboratory (JPL) Small-Body Database (`https://ssd.jpl.nasa.gov/sbdb.cgi`) to generate Spacecraft and Planet Kernel (SPK) files for asteroids and comets with respect to the Solar System barycentre (SSB).

An SPK file is a binary file that can be interpolated to retrieve the state of an object within a desired timespan. Such files are very useful as they enable to quickly retrieve an ephemeris from a database without the need to constantly integrate the equations of motion for this object. SPK files are part of the SPICE system provided by NASA's Navigation and Ancillary Information Facility (NAIF) team at JPL. Although SPK files can contain ephemerides for any object (spacecraft or Solar-System body), the ones produced by the Horizons system are focusing on asteroids and comets alike.

The SPICE library (`https://naif.jpl.nasa.gov/naif/documentation.html`) has been linked to TUDAT, enabling to retrieve various data designated as SPICE kernels and in that manner reducing the computational load without much loss in accuracy. More details on how TUDAT interacts with the external SPICE toolkit can be found here: `https://tudat.tudelft.nl/tutorials/tudatFeatures/otherLibraries/spice.html`.

The retrieved ephemeris for (66391) 1999 KW4 provided data for the binary system barycentre about the Solar-System Barycenter (SSB) for a chosen duration of one year starting January 1^{st}, 2001 as observations from a close encounter to the Earth in May, 2001 enabled to determine some characteristics of the binary system at that time. It was chosen early on in the thesis that the primary asteroid called Alpha would be assumed at the binary system barycentre for simplicity. The position of Alpha is therefore approximated using the retrieved ephemeris of the binary system barycentre. This has the advantage of simplifying the implementation of the model, without impactful consequences on future results.

From there, the secondary asteroid called Beta was propagated for 200 days around Alpha using the initial conditions in [Ostro and al., 2006] as it was considered very unlikely that a reasonable uncontrolled cubesat mission could last for a longer timespan.

A Runge-Kutta 7(8) integrator with tolerances of 10^{-15} in combination with a Cowell propagator was used to that extent as it should be accurate enough while the Cowell propagator is simple and has no singularities. A high-fidelity acceleration model was used including all point-mass third-body perturbations from the Sun, Jupiter, Mars, Venus, Mercury, and also the Earth and the Moon as the implemented initial conditions come from observations in a close-Earth encounter. A third-body mutual spherical-harmonics acceleration between Alpha and Beta up to degree and order 4 was also used, using spherical-harmonics coefficients of the two bodies as presented in Subsection 6.2.3.

A visual representation of Beta orbiting Alpha for 200 days can be seen in Figure 6.1.

The validation process of the ephemeris model is performed in Chapter 10.

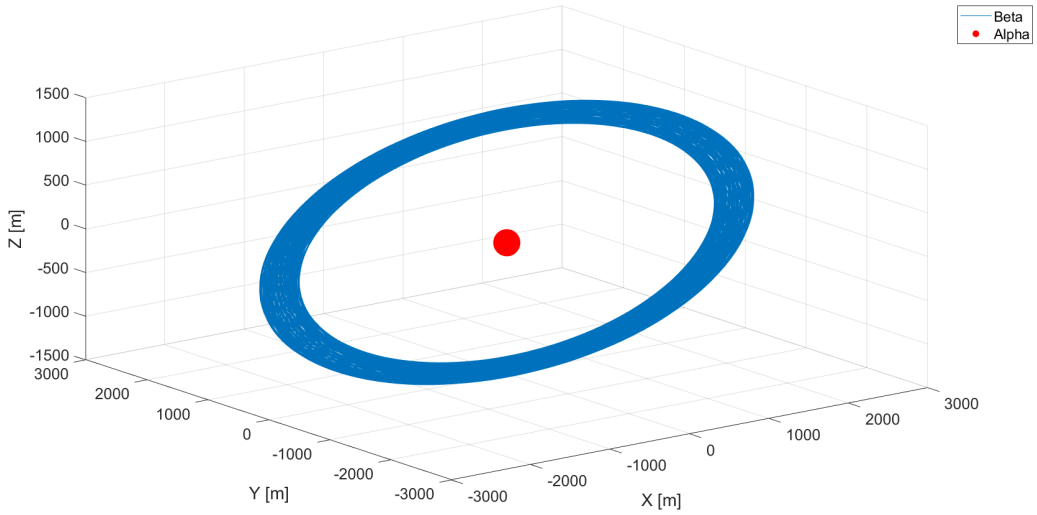

Figure 6.1: Propagation of Beta (blue line) around Alpha (red dot scaled with its nominal radius) for 200 days using initial conditions from [Ostro and al., 2006].

6.2.3. Gravity Field Model

The gravity field model used in this thesis is a spherical-harmonics gravity field model as it is compatible with the implementation of typical dynamical code modelling.

The spherical-harmonics coefficients used in the model are the ones derived by [Compère and Lemaître, 2014] up to degree and order 4 for both the primary and the secondary asteroid of the binary system, called Alpha and Beta respectively. They can be found in Table 6.2.

6.2.4. Rotational Model

The code implemented in this thesis uses a simple rotational model for both Alpha and Beta, already implemented in TUDAT. It assumes a constant rotation axis and a constant rotation rate for the bodies, and is viewed as a fair and sufficient approximation for this thesis work that aims to be a first draft for a proof of concept.

The initial orbital frame in this binary asteroid is defined as having the +X-axis from the system barycenter (assumed to be the center of mass of Alpha) to the initial center of mass of Beta, the +Z-axis perpendicular to the initial orbital plane of Beta, and the +Y-axis completing this frame by mutual orthogonality with the other axes following the right-hand rule. A visual representation of the initial orbital frame can be seen in Figure 6.2.

The Euler angles provided in Table 6.3 are the 3-1-3 Euler angles orienting the asteroids with respect to the initial orbital frame. The two spin axes can be seen in Figure 6.2, and it is worth noticing that the local +Z-axis is the same as Alpha's spin axis.

6.3. Initial Acceleration Model

Regarding the initial acceleration model for the cubesat, a high-fidelity model was used including all point-mass third-body perturbations from the Sun, Jupiter, Mars, Venus, Mercury, the Sun and the Moon. The spherical-harmonics gravity field of both Alpha and Beta were also used up to degree/order 4, with coefficients in Table 6.2. A cannonball radiation pressure is also impacting the cubesat in the system.

This initial acceleration model will be subject to tuning in Subsection 7.8 when the proper relevant applications of this thesis are identified.

Degree (n)	Order (m)	$C_{n,m}$	$S_{n,m}$
Alpha			
2	0	-0.6690×10^{-1}	0
2	1	0.3035×10^{-4}	-0.2391×10^{-4}
2	2	0.4850×10^{-2}	0.2118×10^{-6}
3	0	-0.8729×10^{-2}	0
3	1	-0.4553×10^{-2}	-0.6835×10^{-2}
3	2	0.7255×10^{-3}	-0.2109×10^{-3}
3	3	0.4230×10^{-3}	0.2273×10^{-3}
4	0	0.4680×10^{-1}	0
4	1	-0.3140×10^{-4}	0.2607×10^{-2}
4	2	-0.1441×10^{-3}	0.2361×10^{-3}
4	3	-0.1331×10^{-4}	0.1547×10^{-4}
4	4	0.1422×10^{-4}	-0.1532×10^{-4}
Beta			
2	0	-0.2275	0
2	1	0.8695×10^{-4}	-0.3681×10^{-3}
2	2	0.5391×10^{-1}	-0.1941×10^{-3}
3	0	-0.1079×10^{-2}	0
3	1	-0.3595×10^{-2}	0.3621×10^{-2}
3	2	-0.9628×10^{-3}	-0.3598×10^{-3}
3	3	-0.1864×10^{-2}	0.9309×10^{-4}
4	0	0.9372×10^{-1}	0
4	1	-0.1851×10^{-2}	-0.3506×10^{-3}
4	2	-0.5599×10^{-2}	0.8713×10^{-4}
4	3	-0.2013×10^{-3}	-0.1760×10^{-3}
4	4	0.6153×10^{-4}	-0.5308×10^{-4}

Table 6.2: Unnormalized spherical-harmonics coefficients of the two components of (66391) 1999 KW4 up to degree and order 4, derived by [Compère and Lemaître, 2014].

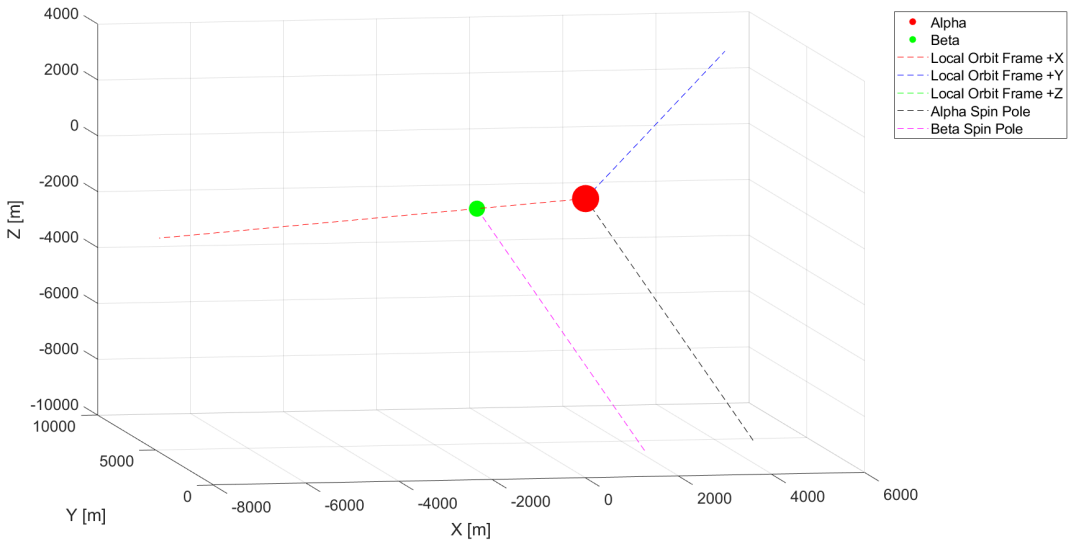

Figure 6.2: Initial orbital frame of (66391) 1999 KW4, angular values from [Fahnestock and Scheeres, 2008].

Alpha			Beta		
$\psi(°)$	$\theta(°)$	$\phi(°)$	$\psi(°)$	$\theta(°)$	$\phi(°)$
117.04	0.0	-173.93	90.0	0.0	90.0

Table 6.3: 3-1-3 Euler angles for the initial rotation axes of the two asteroids of (66391) 1999 KW4, from [Compère and Lemaître, 2014] for the relaxed case, computed from [Fahnestock and Scheeres, 2008].

7

Selection and Tuning of the Propagation and Acceleration Model

One cannot always rely on an existing and available analytical model for most applications in astrodynamics. This is why one usually has to numerically integrate the equations of motion to represent the dynamics of the problem at hand in the most efficient way. There exists however multiple numerical integration and propagation methods briefly exposed in Chapter 5. However, the selection of a given combination of integrator and propagator and the settings is not a straightforward process to ensure the requirements in position while also ensuring a reasonable simulation time.

This chapter focuses on analyzing the impact of different numerical integrators and propagators on the results of a trajectory simulation, and conclude on a sound combination for the application at hand. The final termination conditions used in the simulations are presented in Section 7.1. Section 7.2 then focuses on the selection of applications to perform the tuning of the propagation and acceleration model. Section 7.3 will highlight the benchmark that was assessed and used to compare future results. Sections 7.4 and 7.5 will be about the tuning of the integrator and propagator settings respectively, while Section 7.7 will present in a concise way the main conclusions from this extensive tuning. Section 7.8 will finally present the final acceleration model that was used in this thesis work.

The environment model that is used for the tuning of the propagation model is described in detail in Chapter 6.

7.1. Tuning of Termination Conditions

This section aims at tuning the termination conditions that were chosen initially in Subsection 5.1.4. Indeed, it came out quickly that cubesat flybys around Beta or Alpha had a great impact on the propagation of the cubesat when testing various integrators and/or propagators. It was for instance possible for two different integrators with the same tolerances that one would "crash" into Beta with the 100 m termination condition above its surface very early in the simulation, while the other was just able to remain slightly above this termination condition and pursue the propagation. This would imply hard requirements on position accuracy if good orbits were to be found within the system, which is not something that is desired for an orbit control-free mission. To counter this, it was chosen to modify the termination condition regarding impact on Alpha and Beta to 400 m above their respective surfaces, based on observations that were made. Different values for Alpha and Beta could have been chosen, but for the sake of simplicity the same value of 400 m was used. Plots highlighting this behaviour can be seen in Appendix B.

In an iterative process, it was seen that this sole modification of the distance between the cubesat and Alpha/Beta could still sometimes lead to major differences in propagation time between two integrators/propagators. It was also seen that a flyby introduced the sensitivity to potentially cause the orbit of the cubesat to be highly perturbed afterwards but still pursue the propagation, often with large variations of its semi-major axis. To avoid such scenarios, it was chosen to add a BIBO termination condition on the semi-major axis of the cube-

sat, such that it cannot reach two times its initial value without ending the simulation.

All these changes have the advantage of creating a smoother build-up of differences between integration results, and should also help finding orbits that are less perturbed by the asteroids. Potential stable orbits that are close to the bodies are however more likely to be filtered in the process. It is however seen as a necessity to ensure that the results are not fully dependent on the choice of integration/propagation methods.

To definitely avoid that some simulations get stuck, another termination condition was added regarding the maximum cpu time allowed for an individual simulation, which was set to be 10 s.

To summarize, the final choice of termination conditions used in this thesis are :

- A distance of the cubesat w.r.t. Alpha of less than 400 m (impact scenario).
- A distance of the cubesat w.r.t. Beta of less than 400 m (impact scenario).
- distance of the cubesat w.r.t. Alpha of more than 20 km (escape scenario).
- The semi-major axis of the cubesat around Alpha reaches two times its initial value (BIBO termination condition for smoothing purposes).
- A propagation time of 200 days (simulation end time).
- A cpu time of 10 s (avoids the simulations to get stuck).

7.2. Selection of Case Studies for the Tuning

One particular issue with the tuning of the propagation model is that finding relevant solutions (and therefore initial conditions) that support an orbit control-free motion is at the core of the thesis. It is not a case where the most attractive initial state and the corresponding lifetime are known in advance and where the tuning can be performed in a straightforward way.

There is therefore a need to identify relevant solutions on which to perform the tuning of the propagation model first.

A 3D simulation was thus carried out around the binary system as in a grid search inventory, with each individual simulation corresponding to a given set of initial conditions of the cubesat in the inertial frame. The goal was to identify the best runs in this 3D simulation regarding propagation time, and carry out the tuning of the propagation/integration model on them as they should encompass most future applications.

For computational reasons, it was chosen that the initial eccentricity for the cubesat is zero for all runs, which is also a reasonable choice to not introduce more perturbations from the start in the simulations. This choice of an initially circular orbit also enabled to freeze another initial orbital element, which was chosen to be the initial argument of periapsis kept to zero. The number of variables was therefore reduced from 6 to 4.

The initial semi-major axis of the cubesat was chosen to vary between 1000 m and 5000 m with steps of 200 m, while the initial inclination ranged from 0° to 180° and other angular parameters from 0° to 360° with steps of 20° to reduce the computational load. Another reason is because the goal is not to perform an extensive simulation yet but to identify relevant candidate runs to perform the tuning of the propagation model, i.e. come up with an estimate of a realistic lifetime.

A visual representation of all individual states of the 3D simulation that was carried out can be seen in Figure 7.1.

It can first be highlighted from Figure 7.1 that (although barely noticeable) the best runs in the 3D simulation last for a maximum propagation time of almost 180 days in view of the chosen termination conditions. This duration can be extended to 200 days or even more with less constraining termination conditions, but then the results are not as reliable due to the very perturbed environment.

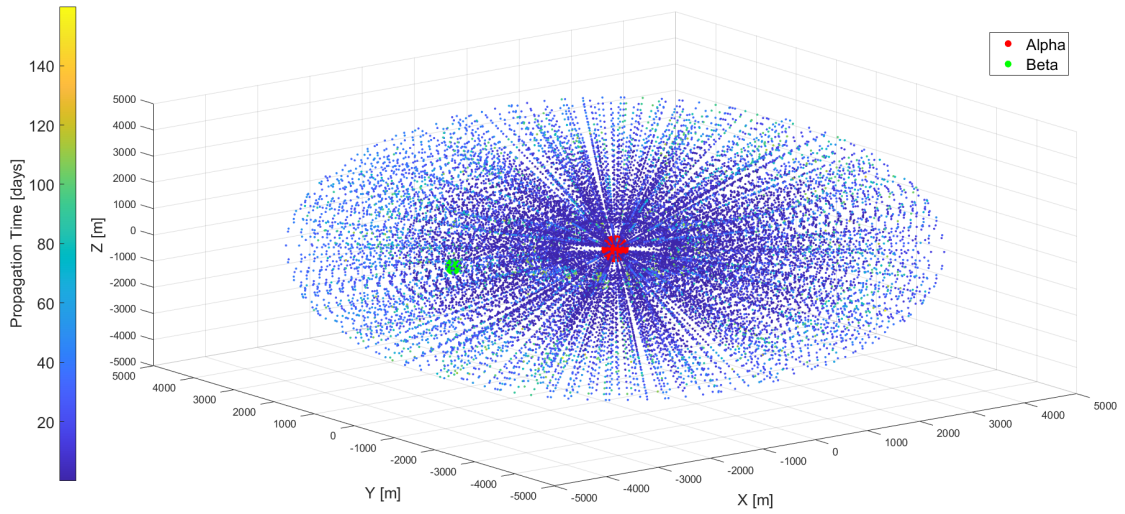

Figure 7.1: 3D simulation. Each set of initial conditions for the cubesat is represented by a small dot in space, and the propagation time using this particular set of initial conditions is represented by the color scale at the left of the figure. The red dot in the center is Alpha scaled with its nominal radius, while the green dot in the left is the initial position of Beta scaled with its nominal radius.

It appeared rapidly in the runs that there was a difference in behavior between the runs starting in the so-called interior ring of the system (with an initial semi-major axis smaller than the semi-major axis of Beta) and the ones starting in the so-called exterior ring (with an initial semi-major axis larger than the semi-major axis of Beta). It was therefore chosen to perform the tuning of the propagation/integration model on two different runs:

- The best run in the **interior** ring from the 3D simulation, in terms of propagation time.
- The best run in the **exterior** ring from the 3D simulation, in terms of propagation time.

This combination should ensure an optimal tuning for most future applications in the binary system, allowing different outcomes for different parts of the geometry of the problem.

The best found run in the **interior** ring has the following characteristics w.r.t. Alpha in the inertial frame:

- Semi-major axis $a = 1400$ m
- Eccentricity $e = 0°$
- Inclination $i = 20°$
- Argument of periapsis $\omega = 0°$
- Longitude of ascending node $\Omega = 260°$
- True anomaly $\theta = 180°$
- Propagation Time = 114 days before reaching the 400 meters termination condition w.r.t. Alpha

The best found run in the **exterior** ring has the following characteristics w.r.t. Alpha in the inertial frame:

- Semi-major axis $a = 4800$ m
- Eccentricity $e = 0°$
- Inclination $i = 80°$
- Argument of periapsis $\omega = 0°$
- Longitude of ascending node $\Omega = 160°$
- True anomaly $\theta = 0°$
- Propagation Time = 179 days before reaching the maximum semi-major axis termination condition

A visual representation of those two runs can be seen in Figure 7.2.

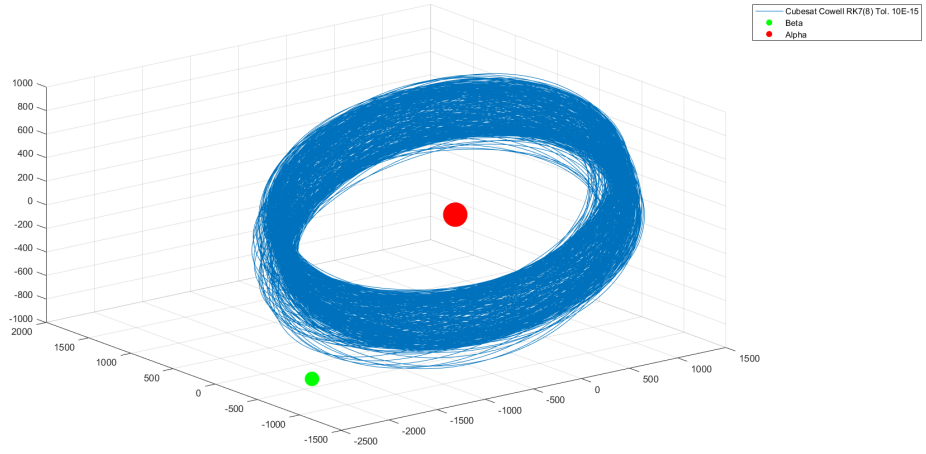

(a) Interior ring.

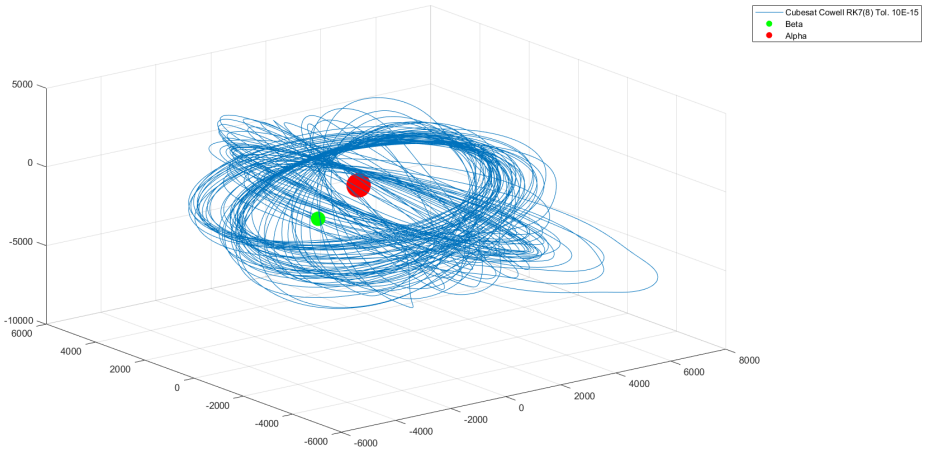

(b) Exterior ring.

Figure 7.2: Initial states and integration results in the interior ring (Figure 7.2a) and the exterior ring (Figure 7.2b) chosen to perform the tuning of the propagation model.

It can be highlighted that the run in the interior ring seems inherently more stable than the one in the exterior ring, and seems relatively close to a pseudo-periodic orbit. It can be expected that the tuning will be more challenging for the simulation in the exterior ring.

7.3. Choice of Benchmark Solution

When assessing the quality of a particular propagation/integration scheme and its settings, the outcome must be compared against a reliable, highly accurate reference solution. This so-called benchmark solution is a propagation model or a particular set of integrator and propagation setting that is assumed relevant for the application at hand, and best representing the dynamics of the system. Also, accuracy requirements need to be defined.

The binary asteroid system 1999 KW4 has a scale in the order of magnitude of 1 km. It has thus been chosen that the requirement for the accuracy of any result is a position error of an order of 100 timer smaller than the scale of the system, so in the order of 10 m. Although arbitrary to some extent, this is a very reasonable value.

The benchmark solution to be chosen therefore needs to be even more accurate. It has been chosen that the requirement for the accuracy of the benchmark results is a position error 10 times smaller than the position requirement for any simulation, so in the order of 1 m. This means that future results will be accurate to 10%, an order of magnitude less than the requirement in position being at the limit of acceptability but still deemed good for the choice of benchmark.

It is emphasized at this point that the propagation duration for which this requirement must still be met is not known yet. The maximum duration for which this requirement is met will drive for how long the results can be trusted and thus the kind of mission that can be designed in the binary system.

Keeping that requirement in mind, the benchmark solution was chosen to be a Runge-Kutta Fehlberg 7(8) with absolute and relative tolerances of 10^{-15} in combination with a Cowell propagator. The minimum and maximum step-size are set to epsilon and infinity respectively in TUDAT.

This choice is motivated by the fact that the Runge-Kutta Fehlberg 7(8) integrators are known to perform reasonably well for a broad range of eccentricities while also not requiring much insight on the problem at hand for the tuning settings [Dirkx and Mooij, 2018]. The choice for absolute and relative tolerances set to 10^{-15} is motivated by the fact that it should provide enough accuracy, and that there is no need to go below such tolerances as the results will not be below the 16 digits accuracy of the *double* type in TUDAT.

To assess whether the quality of a benchmark is good or not, one usually makes a comparison between this benchmark and other numerical solutions, namely Case A (see Subsection 7.3.1) and Case B (see Subsection 7.3.2):

- Case A - The Cowell propagator is changed to USM-EM for the same tolerances which is known to perform reasonably well. The difference between the benchmark solution and Case A is then a measure of the least accurate propagator between Cowell and USM-EM for the application.
- Case B - The tolerances are changed to a higher value, for example 10^{-14}. The difference between the benchmark solution and Case B is a measure of the least accurate integrator for tolerances of 10^{-15} and 10^{-14}.

7.3.1. Case A - Change of Propagator with same Integrator

Results of Case A of the benchmark analysis are presented for both the runs in the interior and the exterior ring in Figure 7.3.

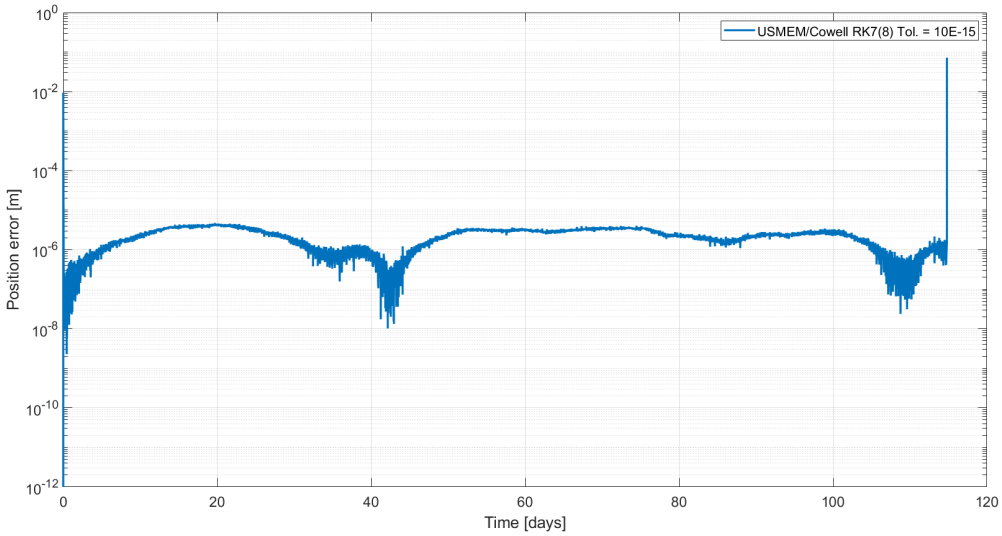

(a) Interior ring.

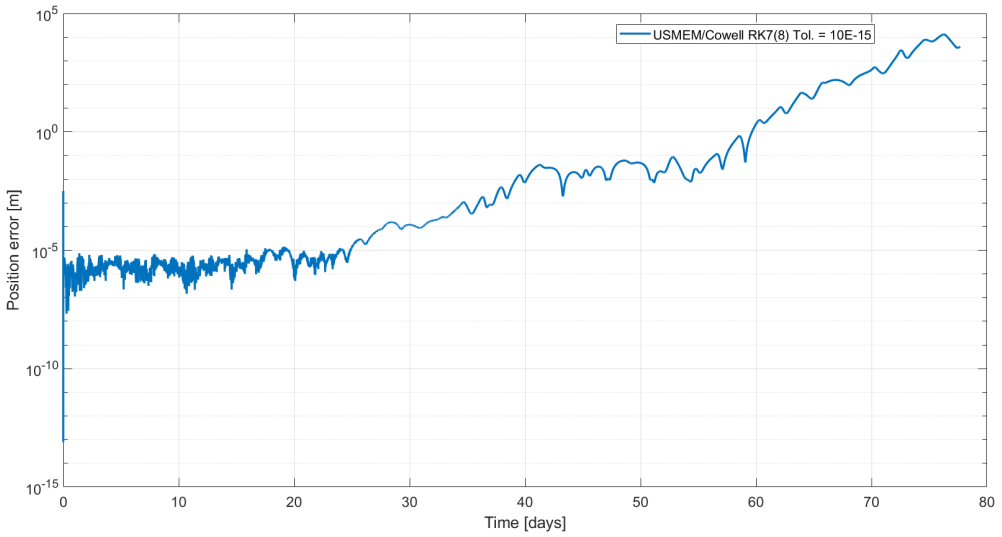

(b) Exterior ring.

Figure 7.3: Case A for both the best runs in the interior (Figure 7.3a) and the exterior ring (Figure 7.3b).

It can be seen in Figure 7.3a that a maximum position error in the order of magnitude of one meter for our benchmark can be easily reached for the whole simulation of 114 days for Case A for the best run in the interior ring (Section 7.2), which suggests that this simulation is particularly stable. It becomes a different matter for the best run in the exterior ring, with an expected lifetime of 179 days (Section 7.2): this duration is reduced to approximately 60 days (Figure 7.3b), which could highlight the fact that the runs starting in the exterior ring are in general more sensitive to perturbations. Clearly, simulation results are also much more sensitive to a choice of propagator.

7.3.2. Case B - Change of Integrator Tolerances with same Propagator

Results of Case B of the benchmark analysis are presented for both the runs in the interior and the exterior ring in Figure 7.4.

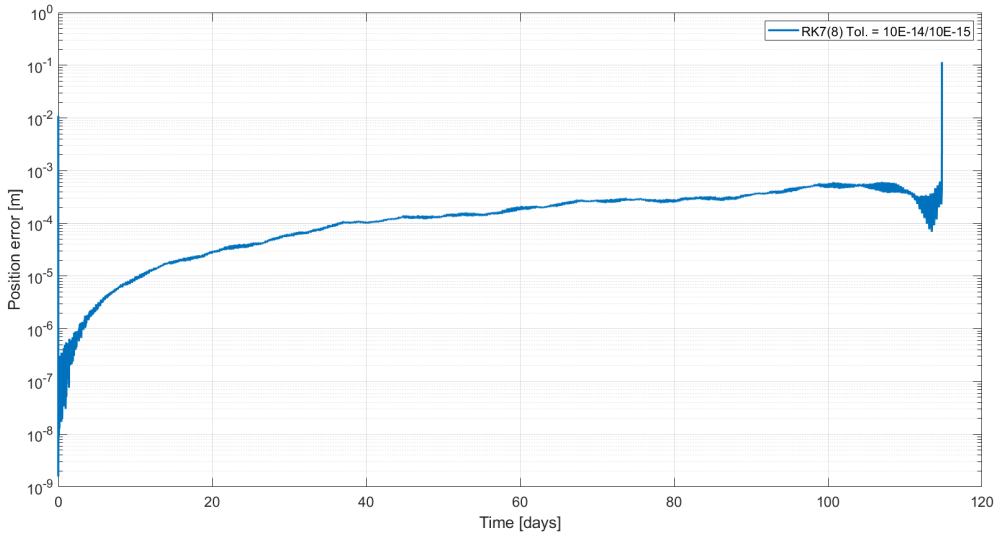

(a) Interior ring.

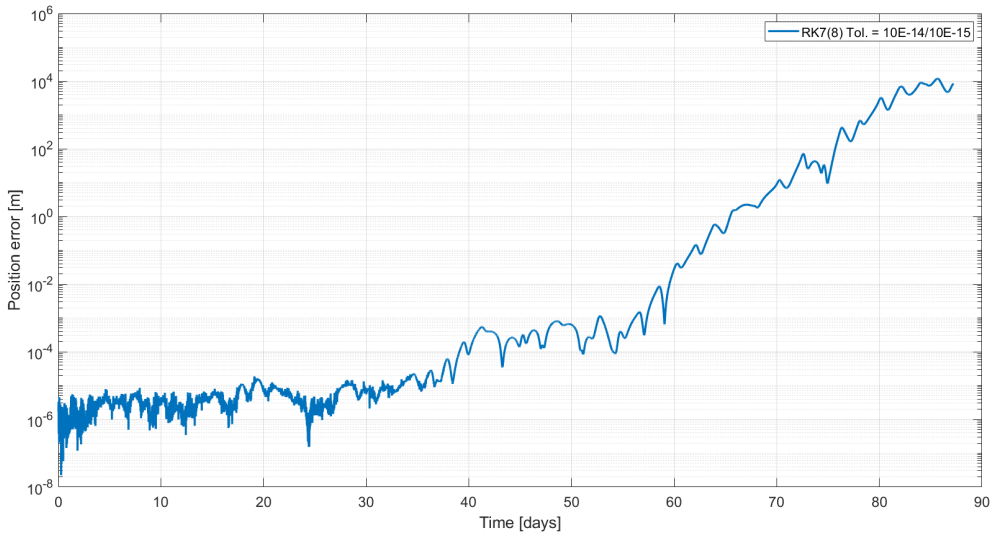

(b) Exterior ring.

Figure 7.4: Case B for both the best runs in the interior and the exterior ring.

It can be seen in Figure 7.4a that a maximum position error in the order of magnitude of one meter for our benchmark can again be reached again for the whole 114 days for Case A for the best run in the interior ring. This duration is again reduced to approximately 65 days for the exterior ring (Figure 7.4b).

7.3.3. Discussion

Taking the consistency between simulations as a direct criterion for the quality of the benchmark solution, it has been shown in Subsections 7.3.1 and 7.3.2 than the chosen benchmark meets the one meter requirement for the whole 114 days for the interior ring, and for approximately 60 days days for the exterior ring. It means that overall, future results in the whole binary system should only be trusted for 60 days but this duration is assumed fairly good in this highly perturbed environment. It is however fair to make a distinction with the stable runs in the interior ring where the results can be trusted for much more than 60 days due to the inherent stability of the pseudo-periodic solution. It is emphasized that it is possible than the cubesat lasts for a longer period of time in the system, but it will be more of a matter of luck after 60 days in the exterior ring as the results are not as reliable. The choice of propagator and integrator based on the interior run will be performed using the 114 days mark as the conclusions can then be extended to 60 days.

In view of those conclusions; the benchmark meets the one meter requirement and is accepted for further analysis.

7.4. Tuning of the Integrator Settings

This section is aimed at evaluating the effect of different integration methods and settings on the accuracy of the solutions. For this purpose, several integrators will be investigated in combination with a fixed Cowell propagator. The various methods already implemented in TUDAT have been presented in Chapter 5.

It can be noted that a small error existed in the implementation of the Adams-Bashforth-Moulton (ABM) integrators back in 2019 in TUDAT, and it is not known if it is has been changed since then. For this reason, the ABM integrators are disregarded for further analysis.

In the same manner, the Bulirsch-Stoer (BS) integrators are disregarded as they provide relatively sparse results while a dense output is preferable when choosing an integrator, especially for our highly perturbed applications in the binary asteroid system.

7.4.1. Interior Ring

Results of the analysis of relevant integration methods for the run in the interior ring are presented in Figure 7.5.

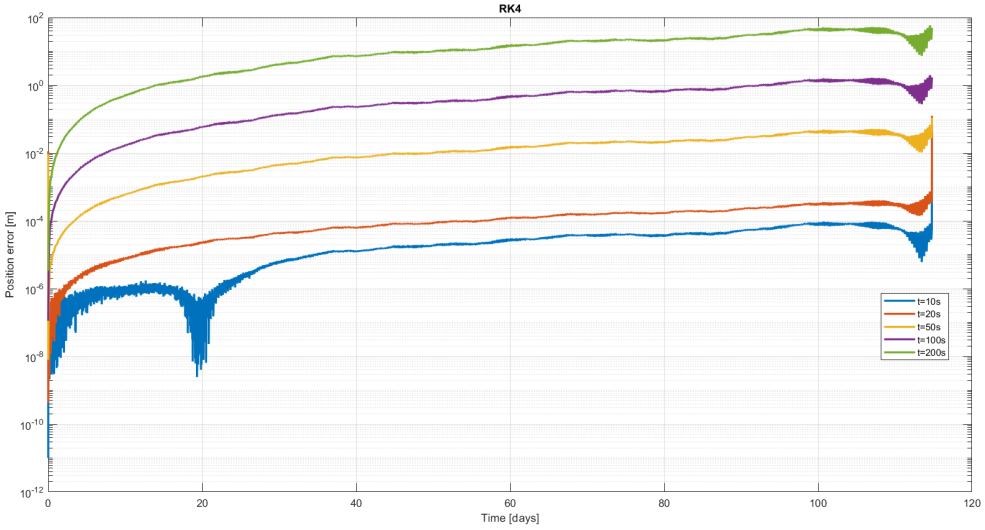

(a) RK4

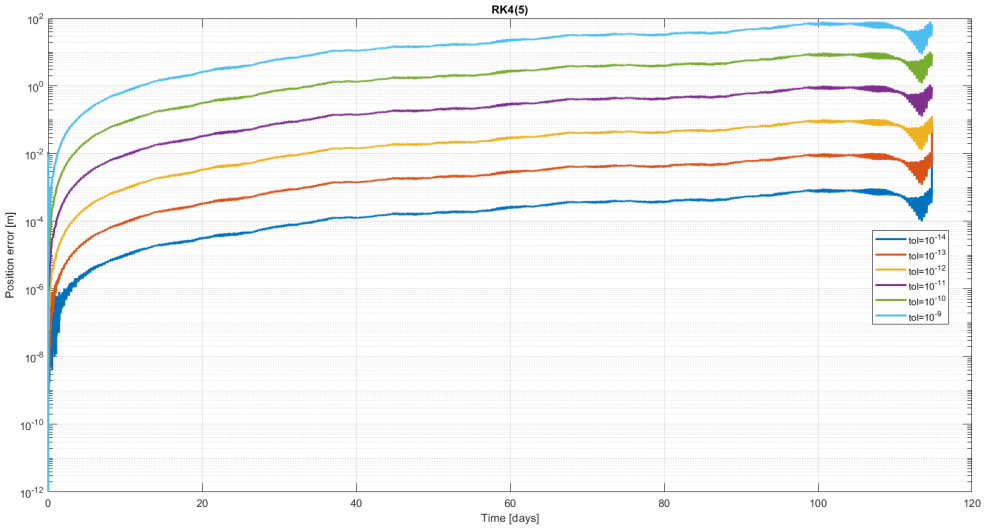

(b) RK4(5)

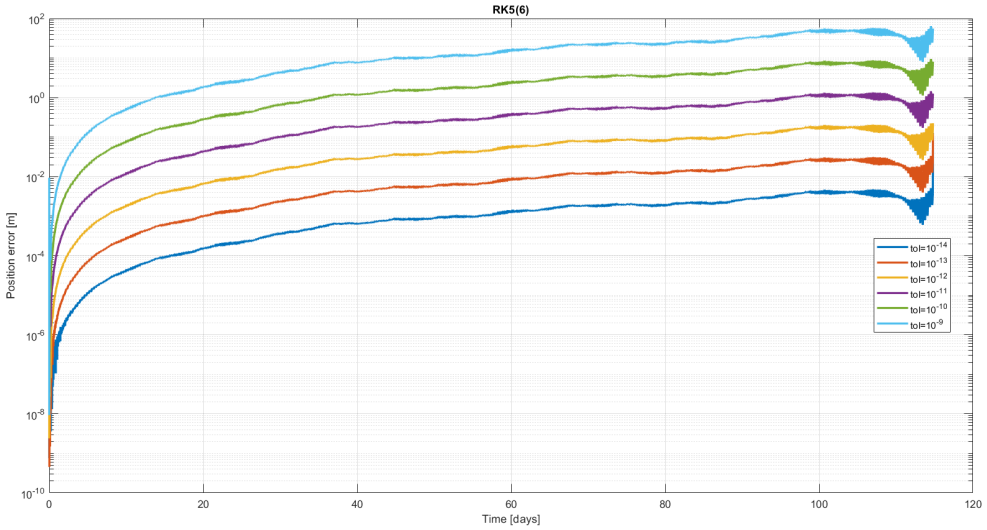

(c) RK5(6)

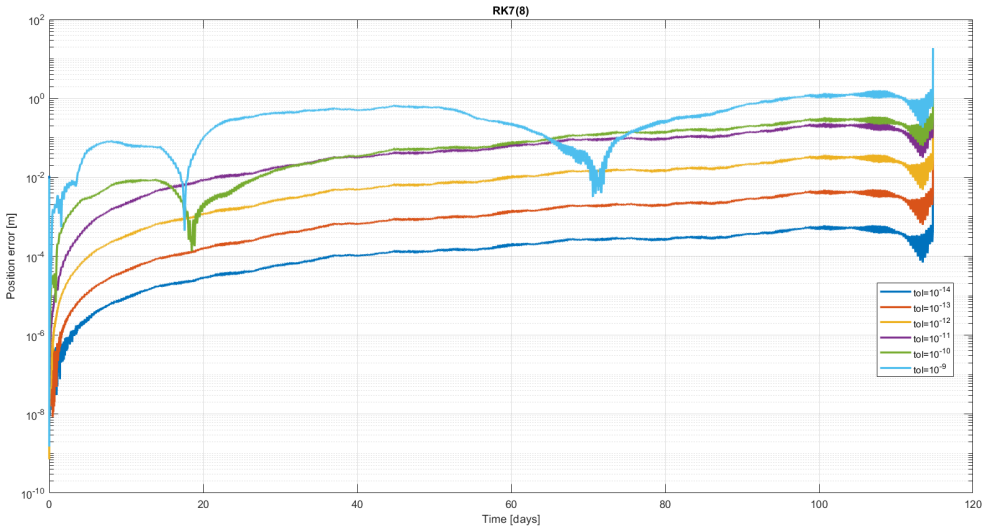

(d) RK7(8)

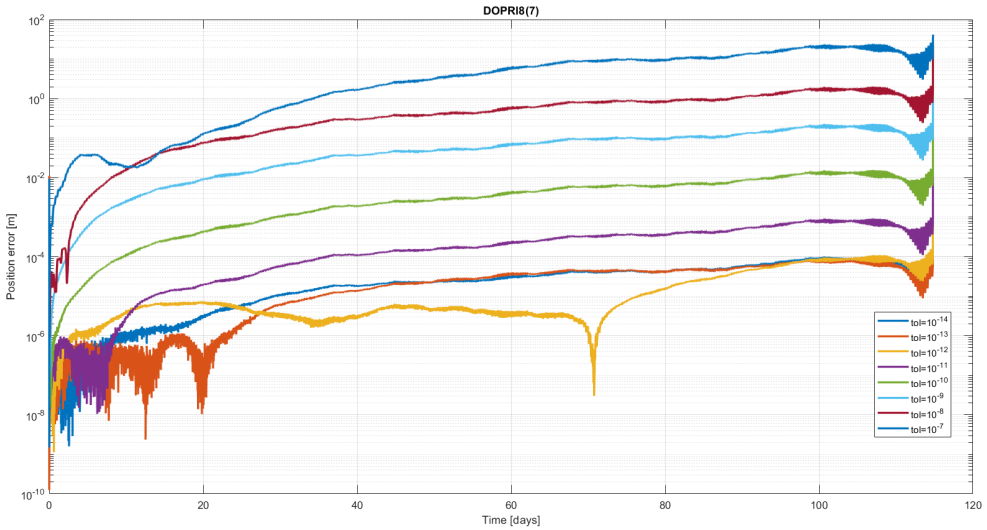

(e) DOPRI8(7)

Figure 7.5: Differences in position between the benchmark solution (Cowell RK7(8) tol. 10^{-15}) and various RK and DOPRI integrators using a Cowell propagator, for the run in the interior ring.

From the results in Figure 7.5, a preliminary choice can be made for the assumed best integrators for this particular run in the interior ring, regarding the requirement for a maximum position error of 10 m after 114 days w.r.t. to the benchmark solution:

- RK4 with a time step of 10, 20, 50 and 100 s
- RK4(5) with tolerances 10^{-14}, 10^{-13}, 10^{-12}, 10^{-11} and 10^{-10}
- RK5(6) with tolerances 10^{-14}, 10^{-13}, 10^{-12}, 10^{-11} and 10^{-10}
- RK7(8) with tolerances 10^{-14}, 10^{-13}, 10^{-12}, 10^{-11} and 10^{-10}
- DOPRI8(7) with tolerances 10^{-14}, 10^{-13}, 10^{-12}, 10^{-11}, 10^{-10}, 10^{-9} and 10^{-8}

Clearly, most of the settings studied here satisfy the requirement.

7.4.2. Exterior Ring

Results of the analysis of relevant integration methods for the run in the exterior ring are presented in Figure 7.6.

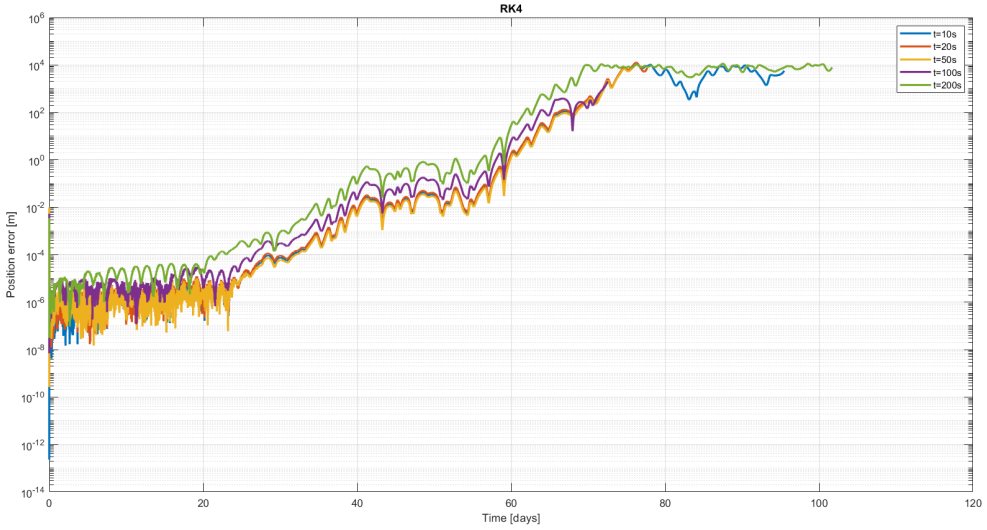

(a) RK4

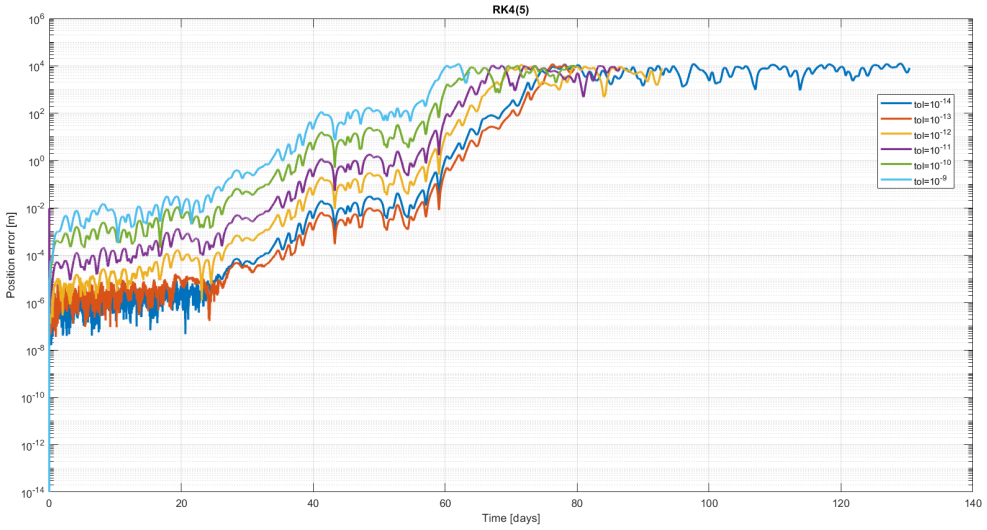

(b) RK4(5)

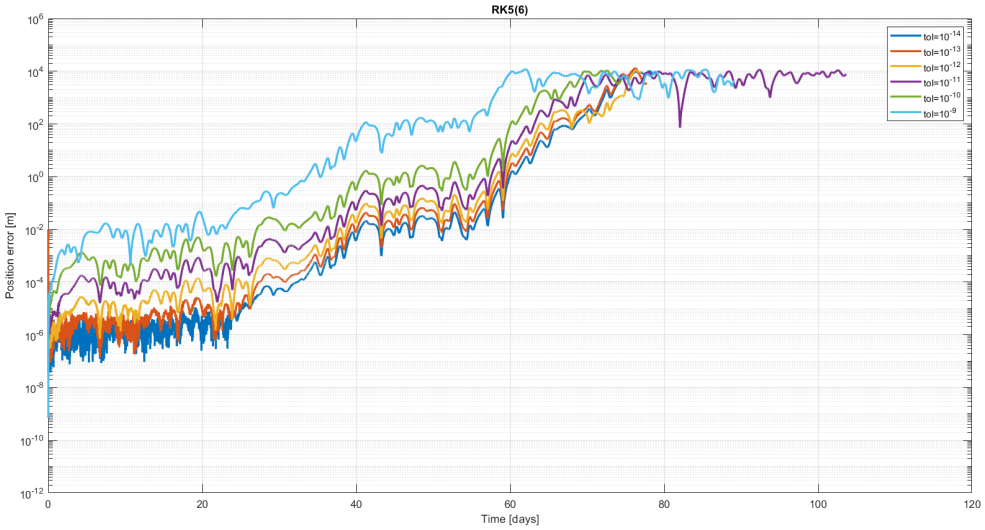

(c) RK5(6)

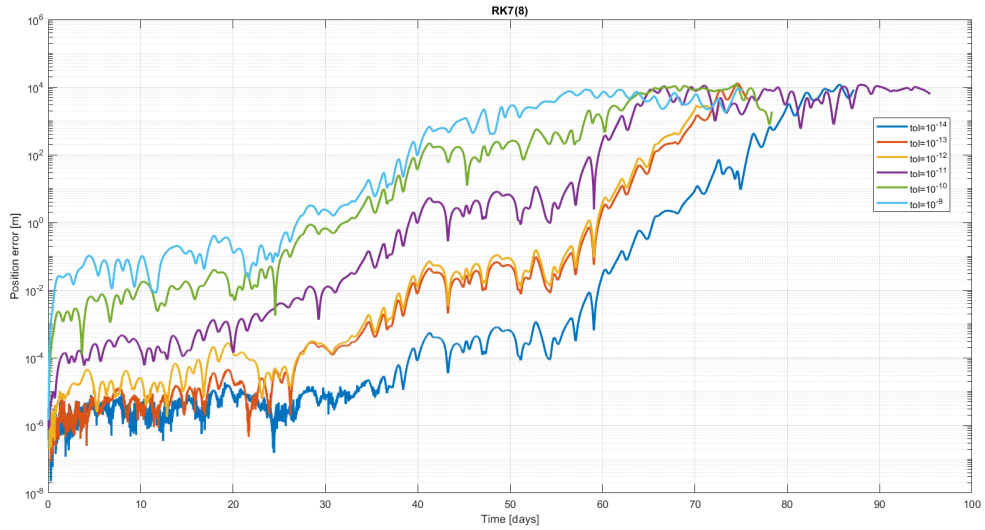

(d) RK7(8)

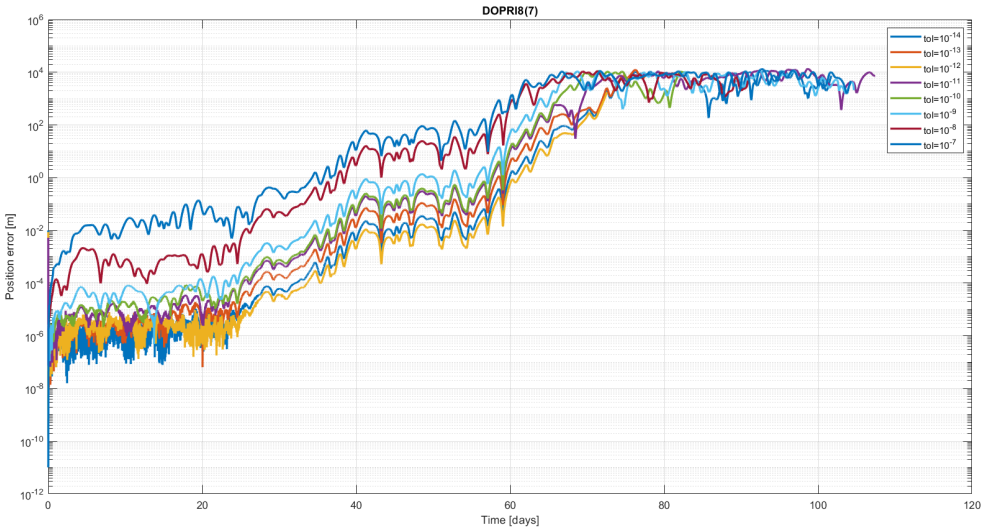

(e) DOPRI8(7)

Figure 7.6: Differences in position between the benchmark solution (Cowell RK7(8) tol. 10^{-15}) and various RK and DOPRI integrators using a Cowell propagator, for the run in the exterior ring.

From the results in Figure 7.6, a preliminary choice can be made for the assumed best integrators for this particular run in the exterior ring, regarding the requirement for a maximum position error of 10 m after 60 days w.r.t. to the benchmark solution:

- RK4 with a time step of 10, 20, 50 and 100 s
- RK4(5) with tolerances 10^{-14} and 10^{-13}
- RK5(6) with tolerances 10^{-14} and 10^{-13}
- RK7(8) with tolerances 10^{-14}, 10^{-13} and 10^{-12}
- DOPRI8(7) with tolerances 10^{-14}, 10^{-13}, 10^{-12}, 10^{-11} and 10^{-10}

7.4.3. Discussion

By combining the results in Subsections 7.4.1 and 7.4.2 for the runs in the interior ring and in the exterior ring respectively, a preliminary choice can be made for integrators that should best capture the dynamics of the entire system, regardless of the choice of initial conditions:

- RK4 with a time step of 10, 20, 50 and 100 s
- RK4(5) with tolerances 10^{-14} and 10^{-13}
- RK5(6) with tolerances 10^{-14} and 10^{-13}
- RK7(8) with tolerances 10^{-14}, 10^{-13} and 10^{-12}
- DOPRI8(7) with tolerances 10^{-14}, 10^{-13}, 10^{-12}, 10^{-11} and 10^{-10}

This is a very wide range of options, still, which will be further addressed later in this chapter.

7.5. Tuning of the Propagator

While Section 7.4 was aimed at evaluating the effect of different integration methods on the accuracy of the solutions, this section is aimed at evaluating the effects of different propagation methods. For this purpose, several propagators will be investigated in combination with a fixed step-size integrator. The various methods already implemented in TUDAT were briefly presented in Chapter 5. A relatively simple integrator that meets the requirements is assumed to be a fairly good option, this is why the choice tends towards the RK4 integrators.

It can be seen in Figure 7.5b and Figure 7.6b and from the conclusions in Subsection 7.4.3 that an RK4(5) with tolerances 10^{-14}, 10^{-13} or 10^{-12} performs fairly well for both the runs in the interior and the exterior ring and meets the requirement in position. The RK4(5) with tolerances 10^{-12} is preferred for both the runs in the interior ring and the exterior ring as it should be faster and no significant rounding errors are observed so it should be more reliable.

When investigating the time steps used by these integrators in combination with a Cowell propagator, it has been found that a mean time step of 58 s was used in the interior ring run and 272 s in the exterior ring run. The various propagation methods are thus investigated in combination with an RK4(5) integrator with those fixed step-sizes.

It is pointed out that propagation models that are based on equinoctial and Keplerian elements did not perform well and lead to errors during the runs, so they were ruled out as potential propagation methods. The fact that the Keplerian elements did not perform well is however expected as the motion of the cubesat starts in a zero-eccentricity orbit, as mentioned in Subsection 5.1.2. The propagation models that were investigated are therefore Cowell, the Encke formulation, and the Unified State Model using either quaternions (usm7), modified Rodriguez parameters (usm6) and equinoctial elements (usmem).

7.5.1. Interior Ring

Results of the analysis of relevant propagation methods for the run in the interior ring are presented in Figure 7.8.

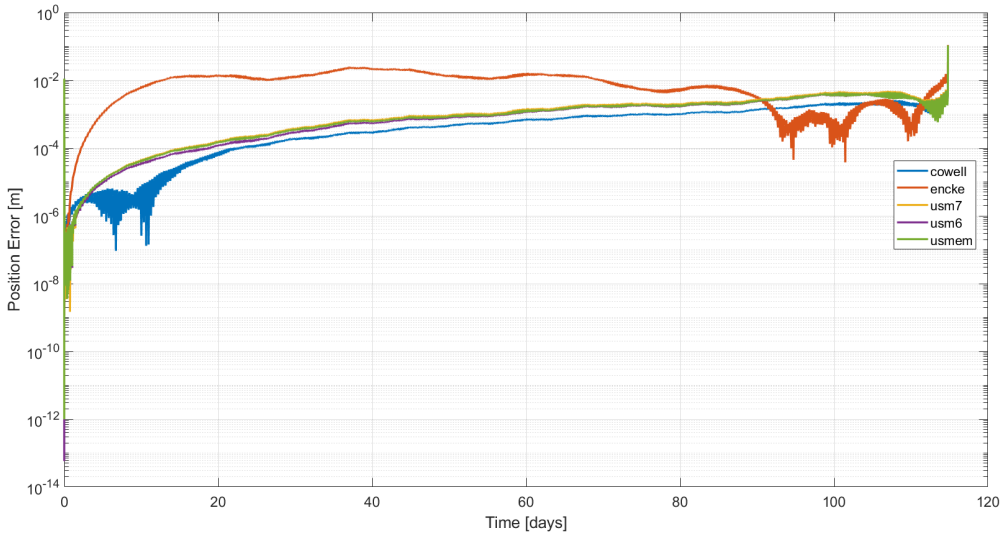

Figure 7.7: Differences in position between the benchmark solution (Cowell RK7(8) tol. 10^{-15}) and a fixed-step integrator for different propagators using the run in the interior ring.

From Figure 7.7, it can be seen that the 10 m requirement after 114 days for the maximum position error w.r.t. the benchmark solution is easily reached for all propagation methods:

- Cowell (cowell)
- Encke formulation (encke)
- Unified State Model - Quaternions (usm7)
- Unified State Model - Modified Rodrigues parameters (usm6)
- Unified State Model - Equinoctial Elements (usmem)

7.5.2. Exterior Ring

Results of the analysis of relevant propagation methods for the run in the exterior ring are presented in Figure 7.8.

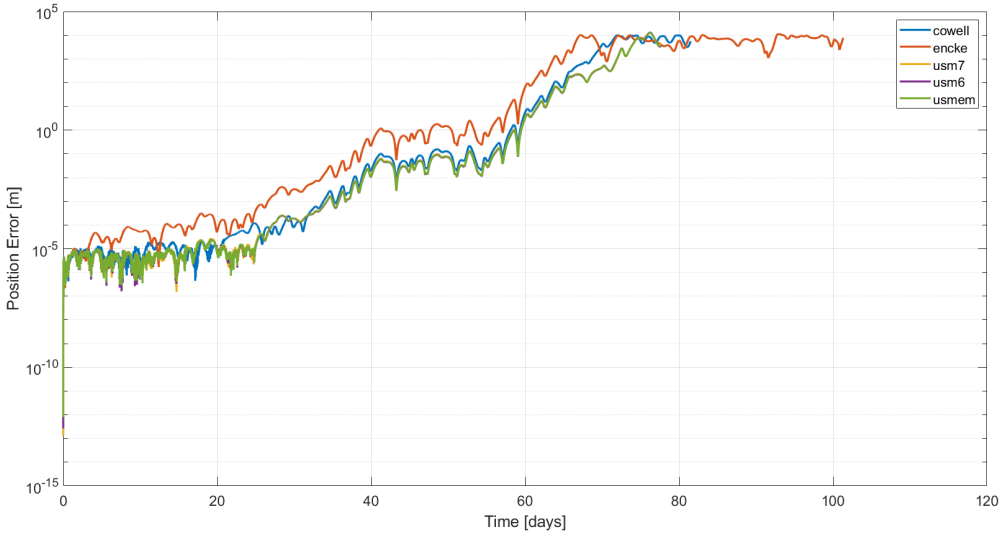

Figure 7.8: Differences in position between the benchmark solution (Cowell RK7(8) tol. 10^{-15}) and a fixed-step integrator for different propagators using the run in the exterior ring.

From Figure 7.8, it can be seen that the 10 m requirement after approximately 60 days for the maximum position error w.r.t. the benchmark solution is reached again for all propagation methods.

7.5.3. Discussion

All investigated propagators seem to perform fairly well in view of the results presented in Subsections 7.5.1 and 7.5.2. All propagation methods will therefore be kept for further analysis in Subsection 7.6.

The fact that the Encke propagator is performing worse than the others was actually something expected as highlighted in Subsection 5.1.2, because it is better suited for orbits that are nearly Keplerian with no large perturbations.

7.6. Combined Propagator and Integration Analysis

While Sections 7.4 and 7.5 were aimed at evaluating the separate effect of different integration and propagation methods on the accuracy of the solutions respectively, this section is aimed at evaluating the effects of combining the relevant integrators and propagators that were identified. For this purpose, each combination of integrator and propagator is investigated concerning its maximum position error and the required cpu time. For ease of analysis, this maximum position error is taken at 114 days for the interior run and 60 days for the exterior one, due to the validity of the benchmark for these runs discussed in Subsection 7.3.3.

7.6.1. Interior Ring

Results of the combined analysis of integration and propagation methods for the run in the interior ring are presented below in Figure 7.9.

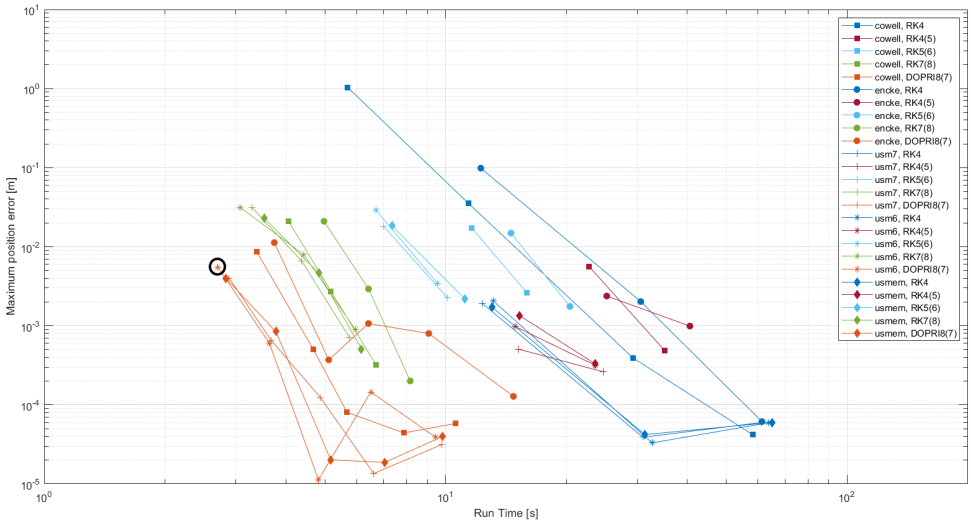

Figure 7.9: Maximum position error between the different relevant options of integrators and propagators w.r.t the benchmark as function of cpu time, for the best run in the interior ring.

Joined points correspond to different sets of tolerances for the same combination of integrator and propagator.

First of all, it can be seen in Figure 7.9 that the overall behaviour is what could be expected: for each integrator/propagator combination, the maximum position error decreases with lower tolerances while cpu time increases. Some strange behaviours however occur where smaller tolerances for a given combination lead to a larger position error. This could be due to the fact that this particular combination is in the domain of rounding errors w.r.t. the benchmark. It can be noted that this interior run is rather computationally demanding, with the faster combinations being in the order of a few seconds.

Regarding the requirement in position error of 10 m after 114 days and cpu time, it can be concluded that RK7(8) and DOPRI8(7) seem to perform fairly well. RK4, RK4(5) and RK5(6) are indeed more computationally demanding.

Between all combinations for the interior ring run, the ones below seem to be a fair choice for future applications:

- DOPRI8(7) with tolerances 10^{-10} with usm7
- DOPRI8(7) with tolerances 10^{-10} with usm6
- DOPRI8(7) with tolerances 10^{-10} with usmem

7.6.2. Exterior Ring

Results of the combined analysis of integration and propagation methods for the run in the exterior ring are presented below in Figure 7.10.

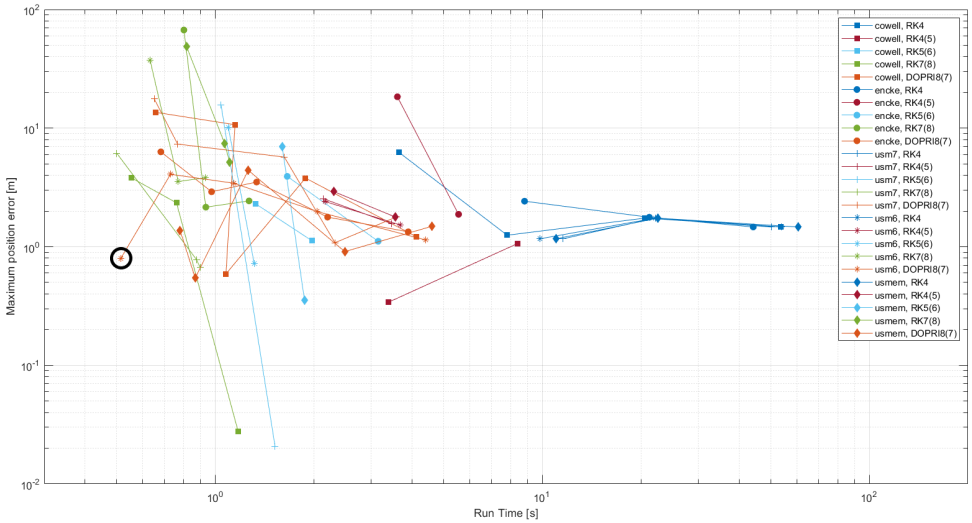

Figure 7.10: Maximum position error between the different relevant options of integrators and propagators w.r.t the benchmark in function of cpu time, for the best run in the exterior ring.

It can first be noted in Figure 7.10 that the overall behaviour is more flat than in Figure 7.9. In addition, it is strange for some combinations, as sometimes smaller tolerances for a given combination lead to a larger position error. It should again be due to the fact that this particular combination is in the domain of rounding errors w.r.t. the benchmark solution.

The overall behaviour highlights how perturbed this run can be compared to the interior ring. Again, the RK7(8) and DOPRI8(7) integrators seem to be the most well-performing integrators independently of the coupled propagator.

Between all combinations for the exterior ring run, the ones that seem to be the best trade-off are:

- DOPRI8(7) with tolerances 10^{-10} with usm6
- RK7(8) with tolerances 10^{-12} with usm7
- RK7(8) with tolerances 10^{-12} with cowell

7.7. Conclusions for Propagation Settings

In view of the conclusions drawn in Subsections 7.6.1 and 7.6.2, the DOPRI8(7) integrator with tolerances of 10^{-10} combined with the usm6 propagator seems to be the best choice in terms of low cpu time and reaching the 10 m requirement in maximum position error w.r.t. the benchmark after 114 days in the case of the interior ring, and 60 days in the case of the exterior ring. This particular combination is the one that is encircled in black in both Figure 7.9 and Figure 7.10.

7.8. Acceleration Model

While a high-fidelity acceleration or dynamics model was previously used as described in Section 6.3, not all of the accelerations in this model are necessarily useful for our particular applications. Now that the propagation/integration settings have been tuned, a proper choice can be made w.r.t. the relevant forces acting on the cubesat.

To this extent, a nominal acceleration model is chosen and all accelerations from the high-fidelity acceleration model are then individually added to assess their impact on the integration results.

The nominal acceleration model that was chosen is consisting of:

- The point mass gravity of the Sun
- The spherical-harmonics gravity field of Alpha up to degree/order 4
- The spherical-harmonics gravity field of Beta up to degree/order 4
- The solar radiation pressure

It is indeed known that the solar radiation pressure has a drastic impact on the dynamics, while the spherical harmonics gravity fields of both Alpha and Beta up to degree/order 4 is a fair choice in this highly perturbed environment. The elements in the dynamics environment that need to be investigated are third-body perturbations in particular.

7.8.1. Interior Ring

The effect of each third-body perturbation on the integrated orbit in the interior run can be seen in Figure 7.11.

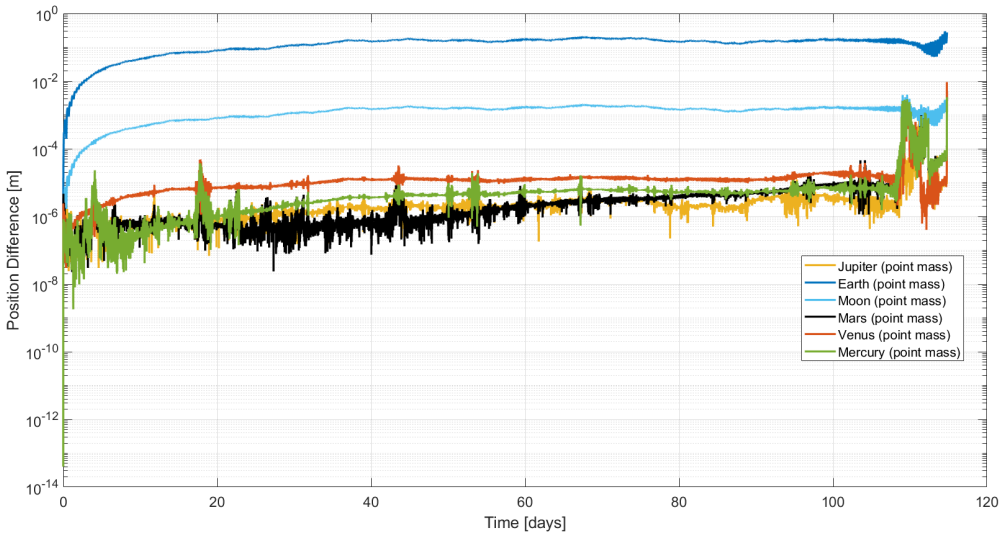

Figure 7.11: Impact of third-body perturbations on the integrated orbit in the interior run.

It can be observed in Figure 7.11 that even if the binary asteroid 1999 KW4 is at a close encounter to the Earth at the start of the simulation (as mentioned in Subsection 6.2.2), even the Earth has a negligible impact on the dynamics of the cubesat in view of our requirement in accuracy. It can however be highlighted that the Earth and the Moon are the first two most important contributions, at 0.1 and 0.001 m respectively.

7.8.2. Exterior Ring

The effect of each third-body perturbation on the trajectory in the exterior run can then be seen in Figure 7.12.

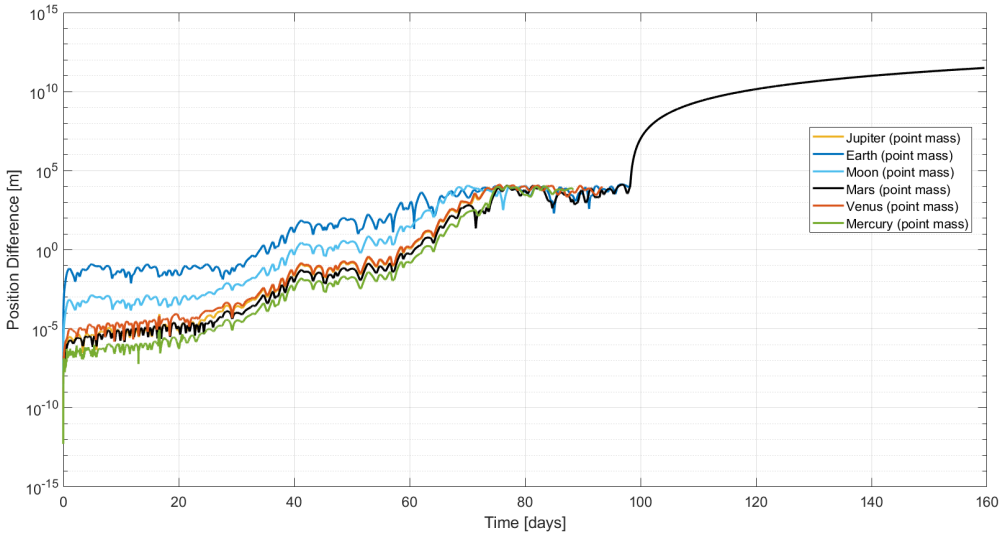

Figure 7.12: Impact of third-body perturbations on the trajectory in the exterior run.

It can be observed in Figure 7.12 that this run is inherently very perturbed, and third-body perturbations tend to pile up over time leading to large position differences. The ones to consider however w.r.t. the requirement in position of 10 m after 60 days in the exterior ring are the Earth and the Moon only, while the remainder can be neglected.

7.8.3. Conclusions on the Acceleration Model

In view of the discussions in Subsections 7.8.1 and 7.8.2, the acceleration model that would best capture the dynamics in the whole binary system (and the one that is further used in this thesis) consists of :

- The point mass gravity of the Sun
- The point mass gravity of the Earth
- The point mass gravity of the Moon
- The spherical harmonics gravity field of Alpha up to degree/order 4
- The spherical harmonics gravity field of Beta up to degree/order 4
- The solar radiation pressure

8

Nominal Results

This chapter presents the main results found in this thesis work, hoping to provide sound argumentation for some applications that seem promising in view of an orbit control-free mission. The methodology that is employed to do so is detailed in Section 8.1, while Sections 8.2 and 8.3 present some promising results found in the interior ring and the exterior ring of the binary asteroid 1999 KW4 respectively.

8.1. Methodology

Now that the propagator/integrator settings and the dynamics model have been tuned in Chapter 7, a new 3D simulation as in Section 7.2 is carried out using the propagation settings chosen in Section 7.7, namely a DOPRI8(7) integrator with tolerances of 10^{-10} combined with the usm6 propagator, and the acceleration model defined in Subsection 7.8.3.

This new 3D simulation enabled once more to identify different promising sets of initial conditions for the cubesat in the inertial frame in terms of propagation time. However, it is possible that such sets correspond to an isolated point in 3D space with high sensitivities to the exact conditions (initial state, uncertainties in dynamics model, ...). Worst case, this point would require hard accuracy requirements to reach, and could very well "disappear" due to various uncertainties, which is detrimental for an orbit control-free mission. Isolated points are overall not attractive because of sensitivity for injection, but also sampling (grid search) itself. For those reasons, it was chosen to identify whether the best initial conditions found in the 3D simulations were located within larger regions with long propagation times of the cubesat. If it were to be the case, this would in theory be highly beneficial regarding position uncertainties during the injection of the cubesat.

In TUDAT, each set of initial conditions is linked to a plane in which the cubesat starts the propagation. For the best initial conditions identified in the 3D simulation, it was investigated whether other points in their corresponding initial plane also led to promising results in terms of propagation time. This enabled to shift an extensive 3D search to a more visual 2D search, while still taking into account the results found in 3D space. For these 2D searches, the initial semi-major axis of the cubesat was chosen to vary between 800 m and 5000 m with steps of 50 m, while the true anomaly ranged from 0° to 360° with steps of 1°.

This work was carried out for the best identified runs in this new 3D simulation, with a clear distinction between the ones starting in the interior ring of the binary system and the ones starting in its exterior ring.

8.2. Interior Ring

In total, 30600 different initial conditions were evaluated. For ease of interpretation, the results are plotted for a 2D subset. The plane in which lies the best found run in the interior ring w.r.t. propagation time is presented in Figure 8.1. Each colored point corresponds to a set of initial condition of the cubesat in the inertial frame w.r.t. Alpha with the corresponding propagation time as a color scale.

This plane corresponds to a set of initial conditions such that in the inertial frame:

- Inclination $i = 20°$
- Longitude of ascending node $\Omega = 260°$

For ease of simulation, a grid search was performed on the entire domain, but the interpretation focuses on the interior and exterior domains independently.

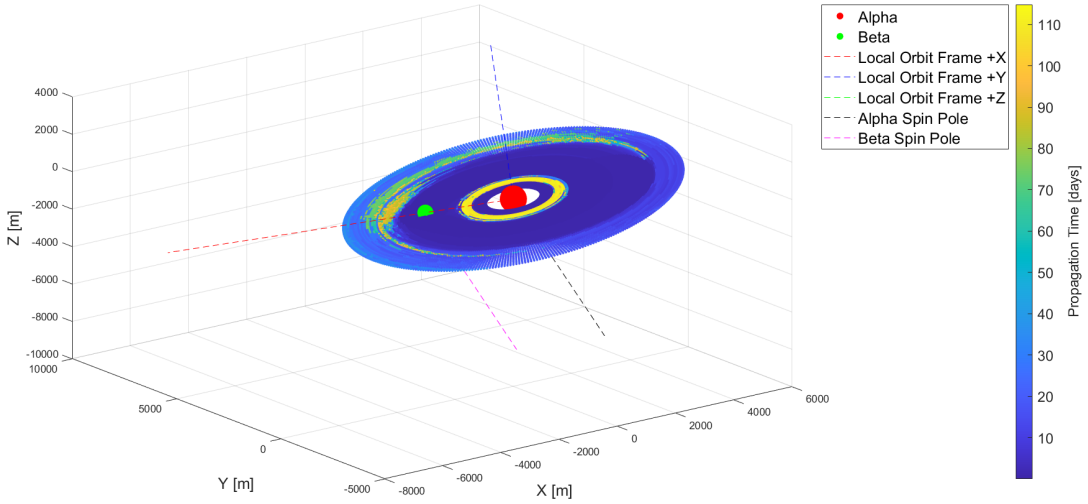

Figure 8.1: 3D view of the plane with the best run found in the interior ring.

First of all, it can be seen that this plane is very close to the initial orbital plane of the binary asteroid, which reinforces the idea that the orbital plane has inherent stable properties. Two yellow stable regions appear clearly on this plot, one around Alpha in the interior ring, and the other at the border of the exterior ring. The point that led to the investigation of this plane lies in the band around Alpha, so the exterior band is more of a surprising discovery at this point.

Figure 8.1 confirms the existence of lifetimes larger than 100 days in the interior ring, but surprisingly, also larger than 60 days in the exterior ring.

Figure 8.2 is a 2D representation of Figure 8.1, restricted to initial positions of the cubesat with a semi-major axis smaller than the initial one of Beta as it is what was investigated in the first place.

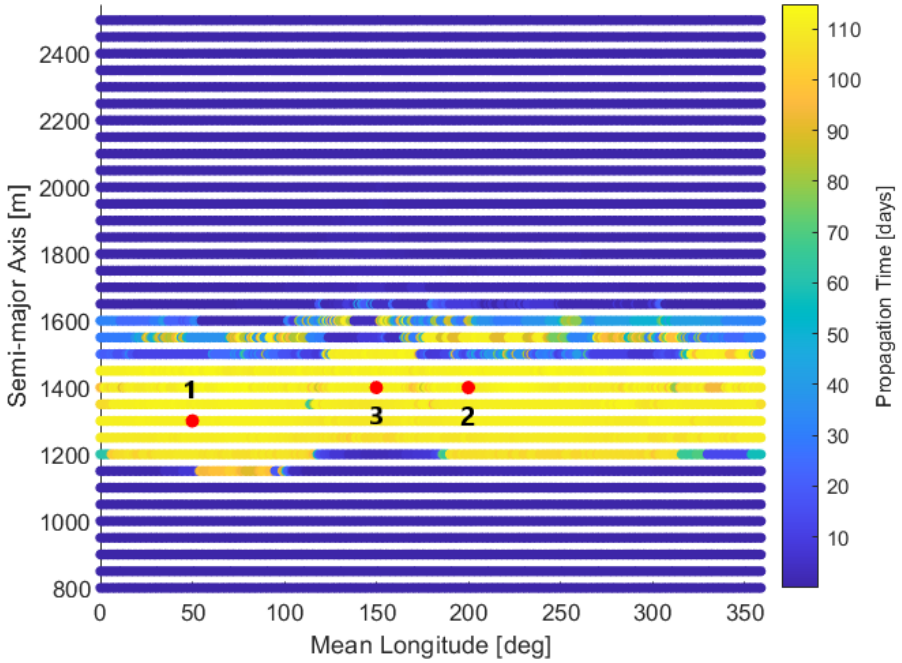

Figure 8.2: Plane with the best found run in the interior ring. The red dots are the points that are further investigated for the sensitivity analysis in Chapter 9.

It can be seen that the idea behind the methodology in Section 8.1 paid off, as it is clear that the most attractive conditions found are associated with a large stable yellow band w.r.t. propagation time around Alpha.

To provide sound argumentation in favour of an orbit control-free mission in this particular region, it is then important to investigate whether any promising (yellow) point could be selected for such a mission. A choice has been made to investigate three points shown in red in Figure 8.2 and perform the sensitivity analysis on them. Three points were chosen because they might encompass different behaviours regarding the sensitivity analysis that will be performed in Chapter 9.

The initial conditions of these interior ring points can be found in Table 8.1 along the resulting propagation time and the termination condition used to end the simulation.

	Point 1	**Point 2**	**Point 3**
Semi-major axis (m)	1300	1400	1400
Eccentricity (-)	0	0	0
Inclination (°)	20	20	20
Argument of periapsis (°)	0	0	0
Longitude of ascending node (°)	260	260	260
True anomaly (°)	150	300	250
Propagation time (days)	111.1	109.1	110.7
Termination condition used	400 meters w.r.t. Alpha	400 meters w.r.t. Alpha	400 meters w.r.t. Alpha

Table 8.1: Points that are investigated in the interior ring, with their corresponding initial conditions in the inertial frame.

Central gravity from Alpha is the dominant term in the dynamics model here, so perturbations are less impactful, leading to those reasonable lifetimes.

8.2.1. Point 1

This point corresponds to the red one on the left of Figure 8.2.

A visual representation of the propagation of the cubesat using this particular set of initial conditions can be seen in Figure 8.3.

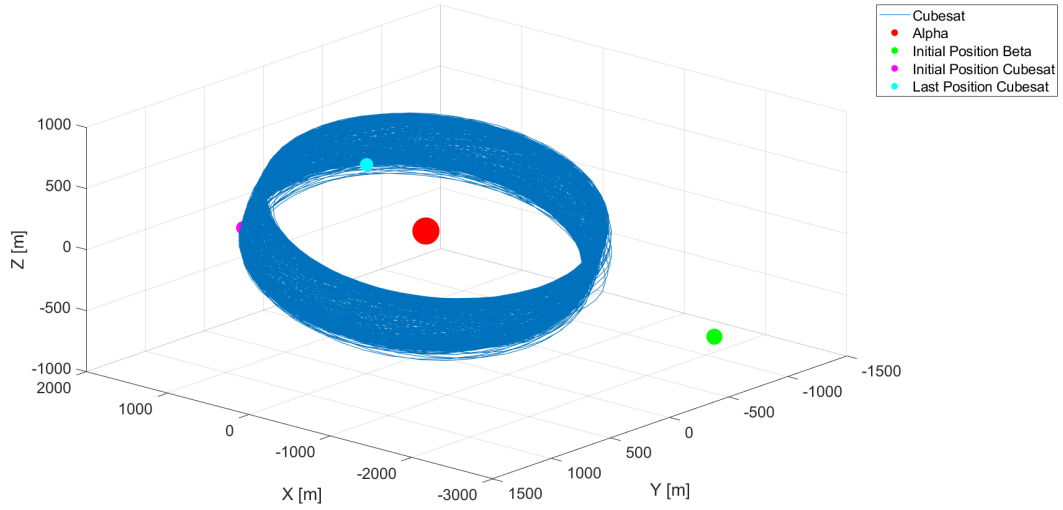

Figure 8.3: 3D representation of the propagation of the cubesat using the initial conditions corresponding to point 1 in Figure 8.2

As can be seen in Figure 8.3, it seems that this orbit has some kind of pseudo-periodic behaviour which explains its stable properties. It is a fair assumption to say that the whole yellow region in Figure 8.2 seems to be associated with periodic physical properties, and it is in that sense expected that points 2 and 3 behave similarly.

It is also emphasized that the termination condition that ends the simulation is the 400 m limit above the surface of Alpha, which is also comparable to the initial semi-major axis of the cubesat (Table 8.1) for these runs. Therefore, the end of the mission is not implied after the duration of approximatively 111 days. It may very much be that the cubesat continues for a much longer time, at the cost of a deteriorated orbit, with higher uncertainties and thus risk. It can however be seen as an end-of-life scenario phase of the mission which could still bring a large amount of insight. In fact after investigation, if the termination conditions on impacting both Alpha and Beta are lowered back to 100 m above their respective surfaces, the cubesat is indeed able to reach the termination limit of 200 days orbiting Alpha. Integration errors are however more likely to pile up in this second phase and cause differences between different integrators/propagators, it is something that could be investigated further.

8.2.2. Point 2

This point corresponds to the red one on the right of Figure 8.2.

A visual representation of the propagation of the cubesat using this particular set of initial conditions can be seen in Figure 8.4.

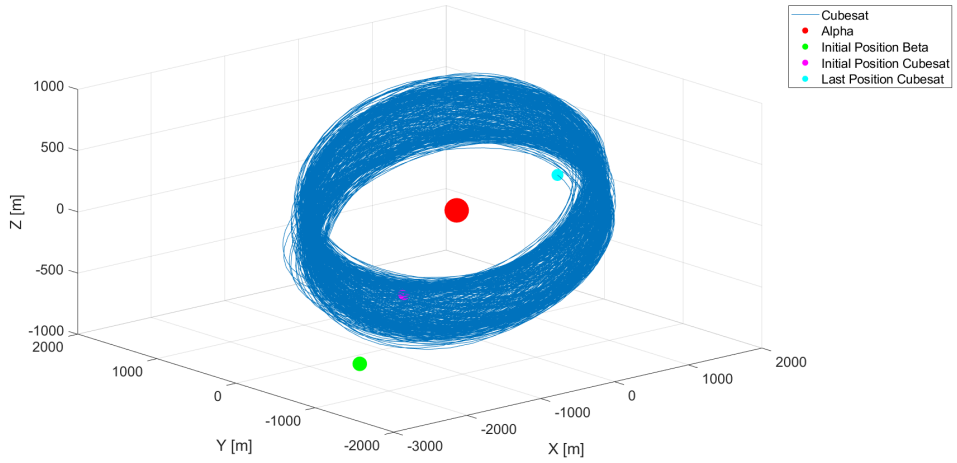

Figure 8.4: 3D representation of the propagation of the cubesat using the initial conditions corresponding to point 2 in Figure 8.2

The pseudo-periodic behaviour of this orbit was expected in view of the one presented by point 1. The same conclusions as in Subsection 8.2.1 apply for this run. It can be noticed that this run starts close to the initial position of Beta which could be detrimental for the sensitivity analysis, but this remains to be seen in Chapter 9.

8.2.3. Point 3

This point corresponds to the red one in the middle of Figure 8.2.

A visual representation of the propagation of the cubesat using this particular set of initial conditions can be seen in Figure 8.5.

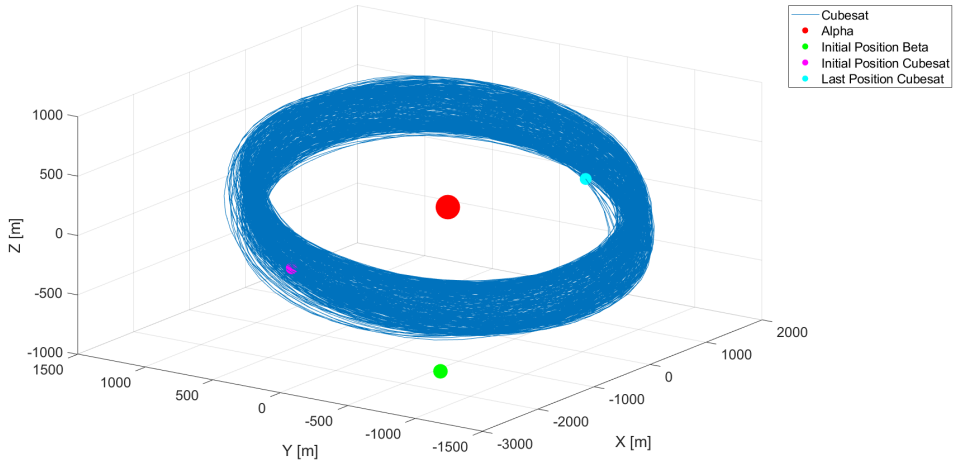

Figure 8.5: 3D representation of the propagation of the cubesat using the initial conditions corresponding to point 3 in Figure 8.2

The pseudo-periodic behaviour of this orbit was once again expected in view of the one presented by point

1. The same conclusions as in Subsection 8.2.1 apply for this run once more. It is also a run that starts close to Beta, like point 2.

8.3. Exterior Ring

The results for the exterior ring are presented and discussed here. Actually, and surprisingly, in view of earlier results, the best runs found in the 3D simulation w.r.t. propagation time are in fact in the exterior ring. Following what is done in Section 8.2, three different planes are here investigated because they correspond to the best found sets of initial conditions for the cubesat in the inertial frame. This choice comes from the fact that unlike the interior ring, it is not clear that there is one stable region that prevails in the exterior ring.

The initial conditions of these exterior ring points in the orientation frame can be found in Table 8.2, along with the resulting propagation time and the termination condition used to end the simulation.

	Point 1	**Point 2**	**Point 3**
Semi-major axis (m)	4500	3600	4150
Eccentricity (-)	0	0	0
Inclination (°)	80	20	80
Argument of periapsis (°)	0	0	0
Longitude of ascending node (°)	140	260	120
True anomaly (°)	258	229	115
Propagation time (days)	196.7	97.8	111.9
Termination condition used	Max. semi-major axis	400 meters w.r.t. Beta	Max. semi-major axis

Table 8.2: Points that are investigated in the exterior ring, with their corresponding initial conditions in the inertial frame.

8.3.1. Point 1

The plane in which lies the best found run in the exterior ring w.r.t. propagation time is presented in Figure 8.8.

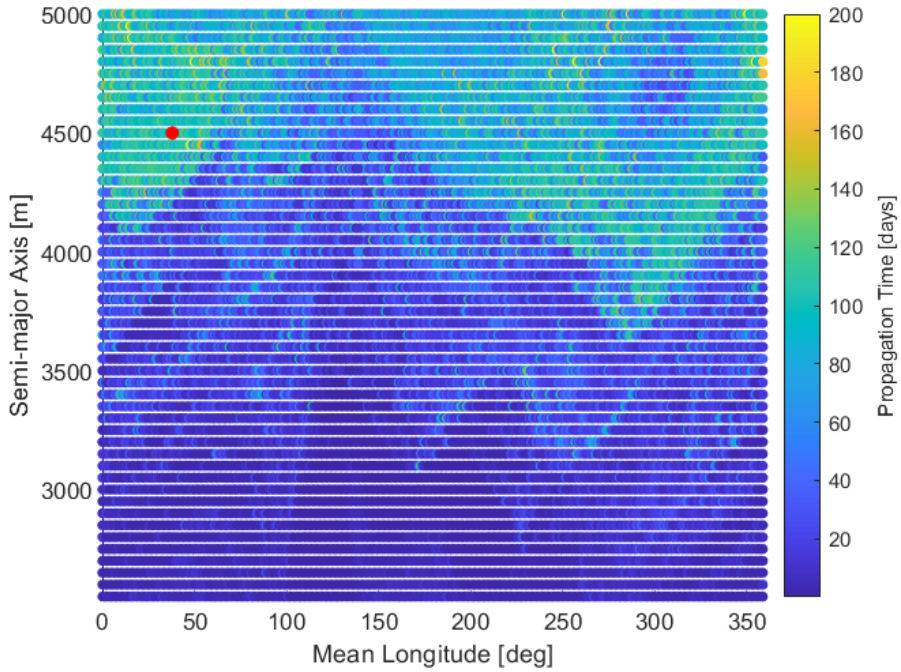

Figure 8.6: Plane in which lies the best found run in the exterior ring. The red dot is the point that is further investigated for the sensitivity analysis in Chapter 9.

It can be seen that a stable region is not so clear to identify, and that it is most likely that the best initial

conditions found in this plane correspond to an isolated point. It is however worth mentioning that because our choice of integrator/propagator settings is only valid for 60 days in the exterior ring (see Section 7.3), regions in the upper part of Figure 8.6 do appear stable w.r.t. to that sole criterion as shown in Figure 8.7, which is why an investigation is still deemed relevant. The point in this plane that is chosen to perform the sensitivity analysis in Chapter 9 is shown in red in both Figure 8.6 and Figure 8.7, as it is located in a more promising area.

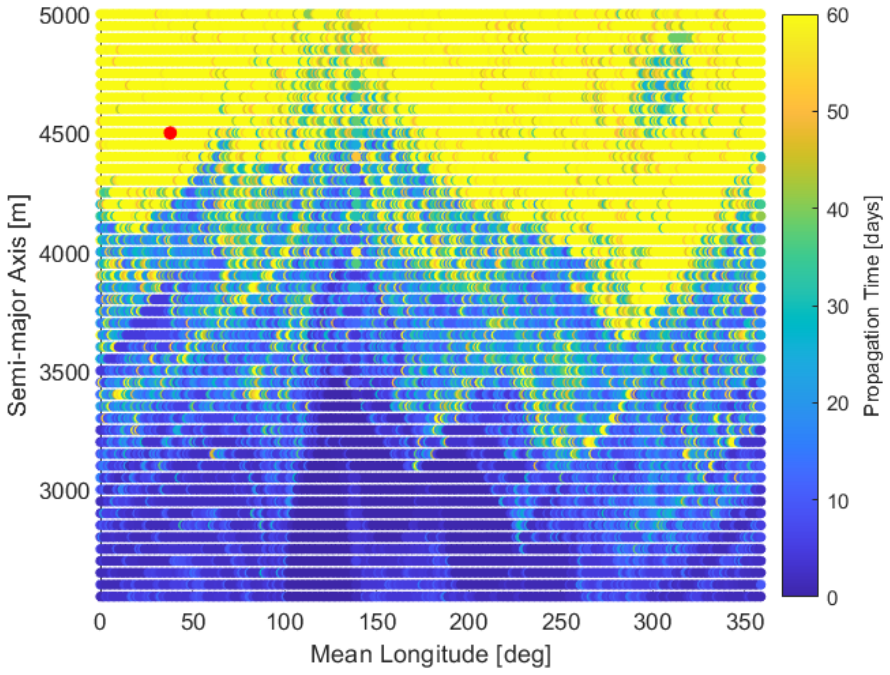

Figure 8.7: Figure 8.6 scaled for a maximum propagation time of 60 days.

A visual representation of the propagation of the cubesat using this particular set of initial conditions can be seen in Figure 8.8.

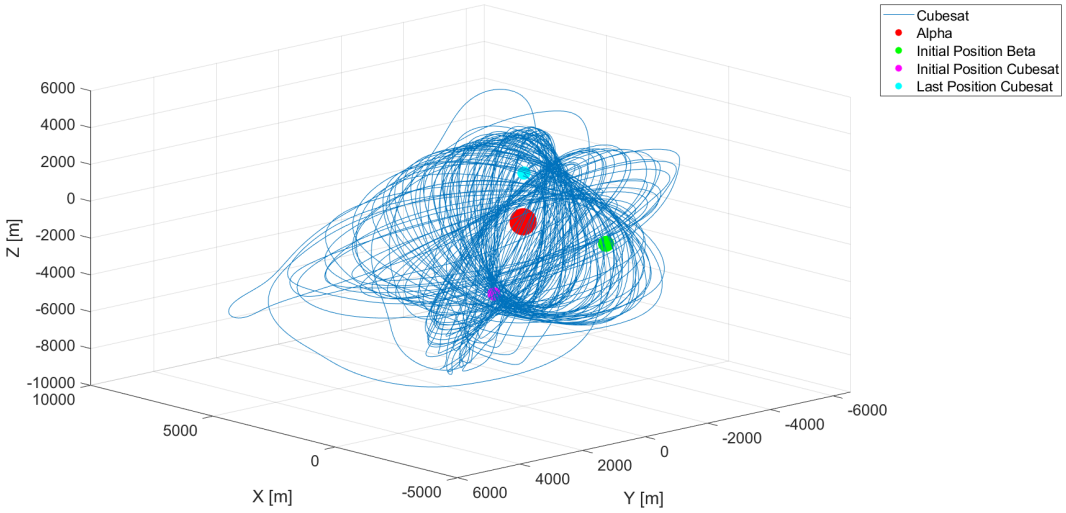

Figure 8.8: 3D representation of the propagation of the cubesat using the initial conditions corresponding to point 1 in Figure 8.6.

It can be seen in Figure 8.8 that the orbit has a precession motion at first around the whole system before reaching out the BIBO termination condition regarding the semi-major axis. This type of orbit seems much more perturbed in essence, so it will be seen during the sensitivity analysis in Chapter 9 whether an orbit-control free mission is still relevant in this context.

8.3.2. Point 2

The second plane that is investigated for the exterior ring, containing point 2 in Table 8.2 with a lifetime of 97 days, is actually the same as the interior plane in Section 8.2: see Figure 8.9. It was indeed chosen to investigate whether the stable region observed in the upper part of Figure 8.9 could lead to interesting results. The point that will be further investigated for the sensitivity analysis in Chapter 9 is the red dot in this graph (cf. Table 8.2).

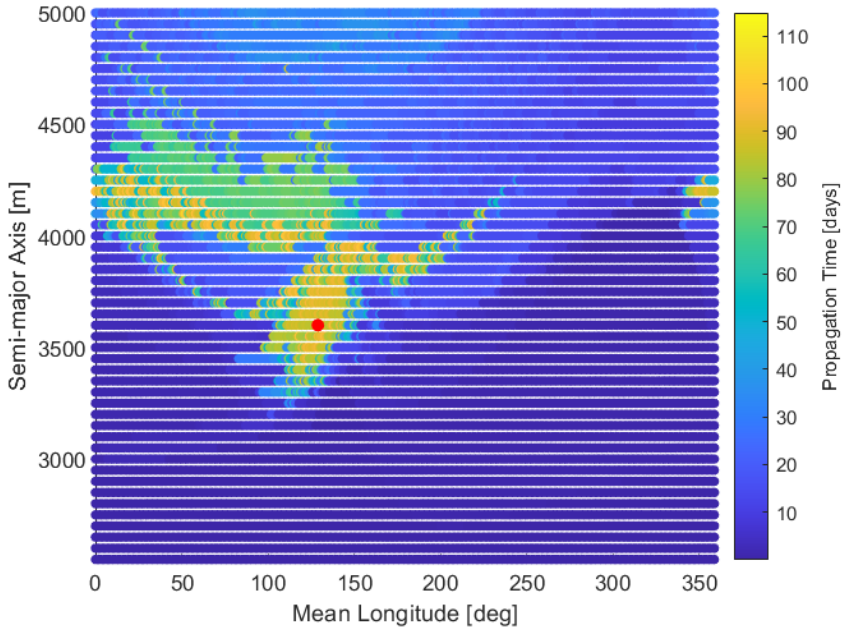

Figure 8.9: Same plane as the interior plane in Section 8.2, for larger values of the semi-major axis. The red dot is the point that is further investigated for the sensitivity analysis in Chapter 9.

A visual representation of the propagation of the cubesat using this particular set of initial conditions can be seen in Figure 8.10.

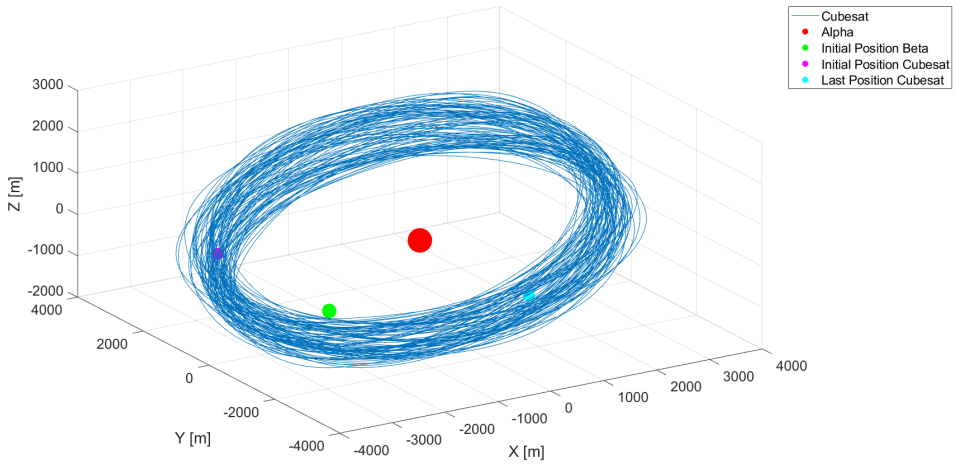

Figure 8.10: 3D representation of the propagation of the cubesat using the initial conditions corresponding to point 2 in Figure 8.9

It seems that this run also leads to a pseudo-periodic behaviour like the ones already seen in the interior ring in Section 8.2, but this time in the exterior ring. The orbit however seems much more perturbed, and only the sensitivity analysis in Chapter 9 will highlight if such orbit is relevant for an orbit control-free mission. It is definitely differently behaving compared to point 1 (Figure 8.9).

8.3.3. Point 3

The plane in which lies one of the best found run in the exterior ring w.r.t. propagation time is presented in Figure 8.13.

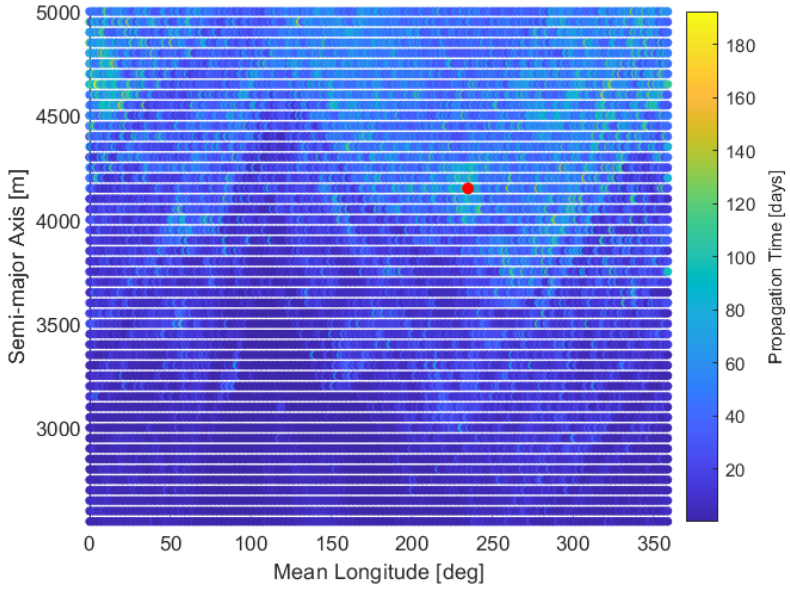

Figure 8.11: Plane with one of the best found run in the exterior ring. The red dot is the point that is further investigated for the sensitivity analysis in Chapter 9.

Again, there does not seem to be a clear stable region in this plane unlike in the interior ring. It is however worth mentioning once more that because our choice of integrator/propagator is only valid for 60 days in the

exterior ring (see Section 7.3), some areas do appear stable w.r.t. to that sole criterion as shown in Figure 8.12, which is why an investigation is still deemed relevant. The point in this plane that is chosen to perform the sensitivity analysis in Chapter 9 is shown in red in both Figure 8.11 and Figure 8.12, as it is located in a more promising area with an average of 100 days propagation time.

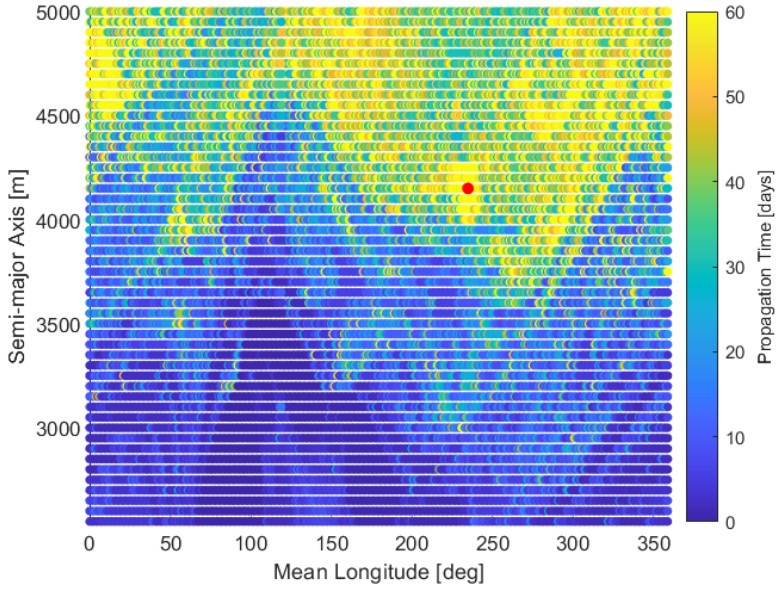

Figure 8.12: Figure 8.11 scaled for a maximum propagation time of 60 days.

Finally, a visual representation of the cubesat orbiting with these particular initial conditions can be seen in Figure 8.13.

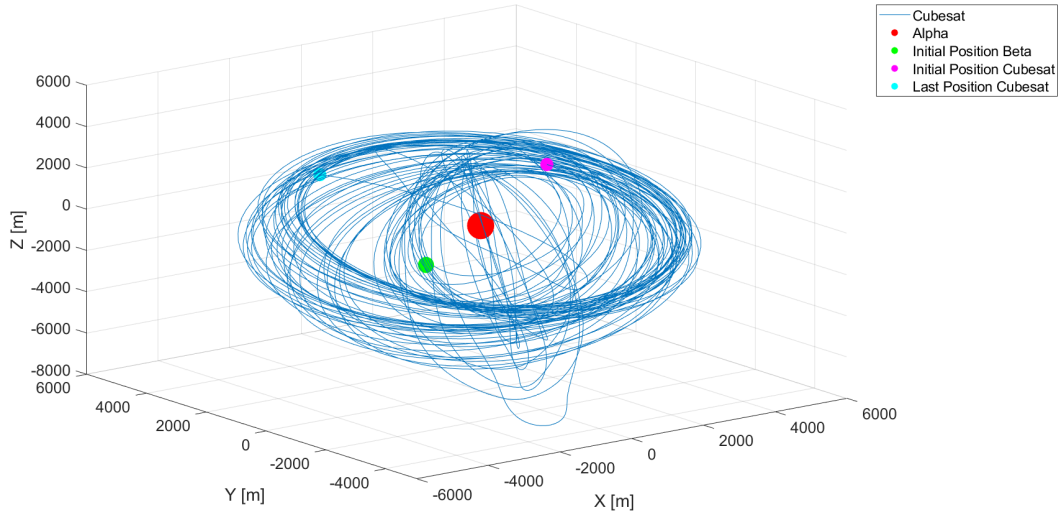

Figure 8.13: 3D representation of the propagation of the cubesat using the initial conditions corresponding to the red dot in Figure 8.11

This particular orbit seems to start in some kind of precession motion like Point 1, before also reaching the BIBO termination condition w.r.t. the semi-major axis of the cubesat. This kind of orbit thus seems to be the most promising in terms of propagation time, but only the sensitivity analysis performed in Chapter 9 will highlight how impactful can the introduction of uncertainties in the model be on this highly perturbed run.

8.4. Conclusions from the Nominal Results

3D runs have revealed lifetimes as high as 110 days and 200 days in the interior and exterior ring respectively.

The best orbits found in the interior ring lie in planes that are very close to the initial orbital plane of Beta, which would imply that it could be the best choice for a long-lasting orbit control-free mission in the interior area. Overall all the best runs found in the interior ring also highlight an interesting pseudo-periodic behaviour, which would also imply that targeting such specific orbits is in fact the best strategy to adopt when it comes to a mission in the interior ring of a binary asteroid system.

Surprisingly, the best orbits found in the whole system w.r.t. propagation time lie in the exterior ring, with some that almost reach a propagation time of 200 days. This information should however be taken cautiously as it was shown in Chapter 7 that the results should only be trusted for a duration of 60 days in the exterior ring due to large perturbations. It is interesting to discover some pseudo-periodic orbits in the exterior ring as well as shown in Subsection 8.3.2. Exterior orbits are overall expected to be much more sensitive to uncertainties in conditions and dynamics parameters, compared to interior ones that present this pseudo-periodic behaviour. The sensitivity analysis performed in the following Chapter 9 will shed light on this matter.

9

Sensitivity Analysis

The sensitivity analysis performed in this chapter aims at investigating whether the chosen optimal points in Chapter 8 (for both the interior and the exterior ring) could still be valid options for an orbit control-free mission in view of various uncertainties in the model. Section 9.1 first describes what uncertainties are considered as relevant, and are introduced in the model and how. Sections 9.2 and 9.3 will then highlight how the nominal results withstand those uncertainties respectively. Section 9.4 will finally present the main conclusions coming from this sensitivity analysis.

9.1. Methodology

One could perform a standard sensitivity analysis using the sensitivity matrix w.r.t. different parameters of our choice, but such an analysis is derived from a linearization of the dynamical equations. In view of the highly perturbed environment at stake, it is assumed that this linearization would only be valid for a small period of time, so it has been chosen to perform the sensitivity analysis via a so-called Monte Carlo simulation instead. The idea here is to generate random values for various parameters of interest within a certain range and assess how the trajectories are impacted. It can be mentioned here that some methods do exist to further reduce the number of runs, for instance the Taguchi methods employed in industry, but were not retained as the Monte-Carlo approach is very straightforward in TUDAT.

It has been chosen to limit ourselves to the investigation of uncertainties in the following elements in the dynamics model when it comes to their impact on the best nominal trajectories in Chapter 8:

- Solar radiation pressure coefficient
- Gravitational parameter of Alpha
- Gravitational parameter of Beta
- Spherical harmonic coefficients of Alpha
- Spherical harmonic coefficients of Beta
- Initial position of the cubesat at injection
- Initial velocity of the cubesat at injection
- All of the above combined

Although one could argue that uncertainties in the ephemerides of Alpha and Beta are worth taking into account as well, the position of the asteroids is one of the best known parameter even from ground-based observations. This statement especially holds for the primary. [Manghi and al., 2017] made a preliminary analysis for a cubesat mission around the binary asteroid Didymos, and only considered the ephemerides' error in the secondary with an order of magnitude of 5 m for the modelling of the Orbit Determination and

Control System (ODCS) error sources of the mothership. This order of magnitude was even assumed conservatively higher in the paper that was expected after the Detailed Characterisation Phase (DCP) (1.1 m) and after the Payload Deployment Phase (PDP) (0.55 m). For our particular work that aims at presenting a proof of concept, it was chosen not to introduce uncertainties in the asteroids' ephemerides in view of such considerations.

All the runs were performed using a seed (which is used to generate quasi-random numbers), equal to 42, and 10 000 runs were performed for each simulation. In view of the large number of runs per simulation, it is assumed a fair choice not to consider additional seeds. The following subsections aims at explaining how the various uncertainties presented above were introduced in the model.

9.1.1. SRP Uncertainties

This subsection aims at defining a good range for varying the solar radiation pressure factor experienced by the cubesat during the mission. A choice has been made to vary the SRP factor from 0.6 to 1.4 using a uniform distribution as in Manghi and al. [2017], which should in that way be a fair representation of all kind of illumination conditions for the cubesat in the binary environment. The value for the nominal simulations was 1.2.

9.1.2. Gravitational Parameter Uncertainties

Uncertainties in the gravitational parameter of both Alpha and Beta were introduced following the uncertainties in the mass of the asteroids presented originally in [Ostro and al., 2006] and [Fahnestock and Scheeres, 2008]. They are repeated in Table 9.1 for convenience using TUDAT built-in value for the universal gravitational constant.

Parameter (units)	**Alpha**	**Beta**
Mass (10^{12} kg)	2.353 ± 0.100	0.135 ± 0.024
Gravitational parameter ($km^3.s^{-2}$)	157.006 ± 6.673	9.008 ± 1.601

Table 9.1: Mass uncertainties for the primary and the secondary of the binary asteroid 1999 KW4 [Ostro and al., 2006], and the resulting gravitational parameter uncertainties.

These uncertainties are introduced in the model using a normal distribution with a $1-\sigma$ uncertainty.

9.1.3. Spherical Harmonics Uncertainties

This subsection aims at defining a good range for varying the spherical harmonic coefficients of both Alpha and Beta, as their knowledge is also subject to uncertainties. It has been chosen to vary each relevant spherical harmonic coefficient of both Alpha and Beta presented in Table 6.2 by a $1-\sigma$ uncertainty of 10% from their nominal value using a normal distribution, which should be a fair assumption.

9.1.4. State Uncertainties

This subsection aims at assessing the initial state uncertainties of the cubesat, may it be from the Orbit Determination and Control System (ODCS) errors of the mothership or from the injection.

Manghi and al. [2017] made a preliminary orbital analysis for a cubesat mission to the Didymos binary asteroid, which is the target of the upcoming Hera mission. They evaluated that the maximum position and velocity errors of the ODCS allowed for safe operations at an L4 parking orbit around the binary are 10 m and 5 mm/s respectively. The rationality of this kind of accuracy was also tackled in the paper and proved to be feasible using an optical navigation method. Manghi and al. [2017] also designed their concept mission around the fact that the release mechanism of their cubseat allowed for deployment speeds down to 5 cm/s (checked and compatible with all our nominal results) with an accuracy of ± 1 cm/s along the deployment axis. With such orders of magnitude in mind, a budget for the state errors in our model is derived in Table 9.2.

	Position (m)	Velocity (mm/s)
ODCS errors	10	5
Injection errors	/	10
RMS	10	11.2

Table 9.2: State errors budget for a cubesat mission around a binary asteroid, derived from Manghi and al. [2017].

For simplification and because only the order of magnitude is important, it was chosen to consider a normal distribution with a $1-\sigma$ uncertainty of 10 m for each component of the initial position of the cubesat, and 0.01 m/s for each component of its initial velocity.

9.2. Interior Ring

The following sensitivity analysis focuses on the nominal interior points in Section 8.2.

9.2.1. Point 1

The first point corresponds to the one in Subsection 8.2.1.

SRP Uncertainties

The uniform distribution of the SRP factor for this particular run is checked and presented in Figure 9.1.

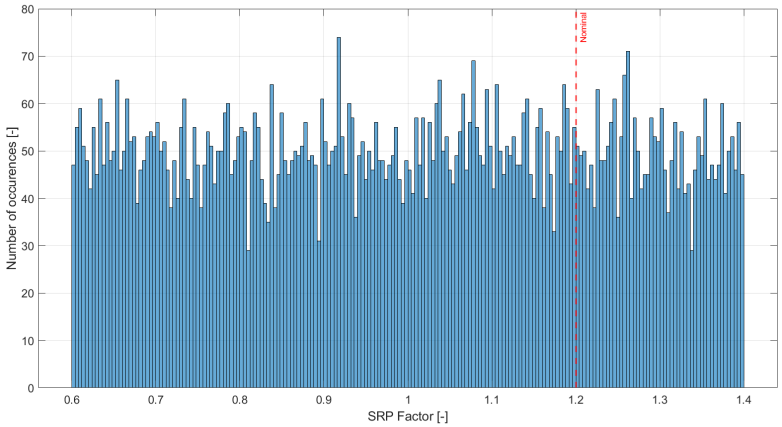

Figure 9.1: Distribution of the SRP factor in the range [0.6 1.4] for 10 000 runs, for point 1 in the interior ring.

The distribution of occurrences w.r.t. propagation time is then displayed in Figure 9.2. It can first be highlighted that the distribution is unusual as the distribution is not uniform anymore and some propagation times seem to be more dominant than others.

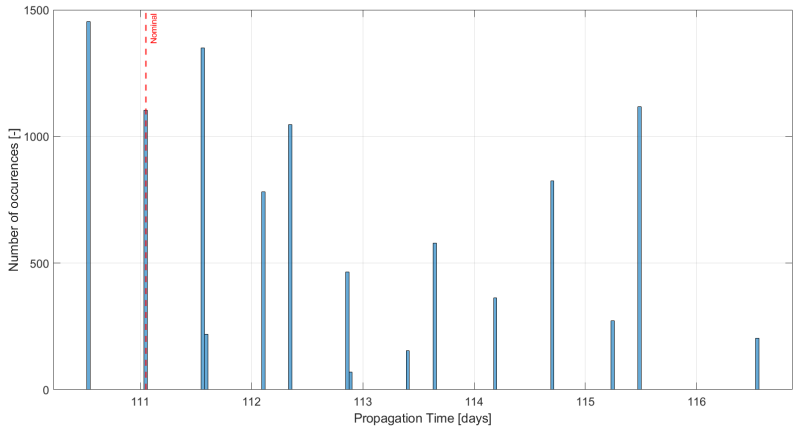

Figure 9.2: Distribution of occurrences with regard to propagation time for 10 000 runs, for point 1 in the interior ring.

This observation can once again be made in Figure 9.3 where the propagation time is shown as a function of the solar radiation pressure factor. The general behaviour is expected: a smaller SRP factor means a smaller perturbation of the cubesat coming from the SRP and thus a longer propagation time in theory, while a larger SRP factor leads to a more perturbed orbit and a smaller propagation time.

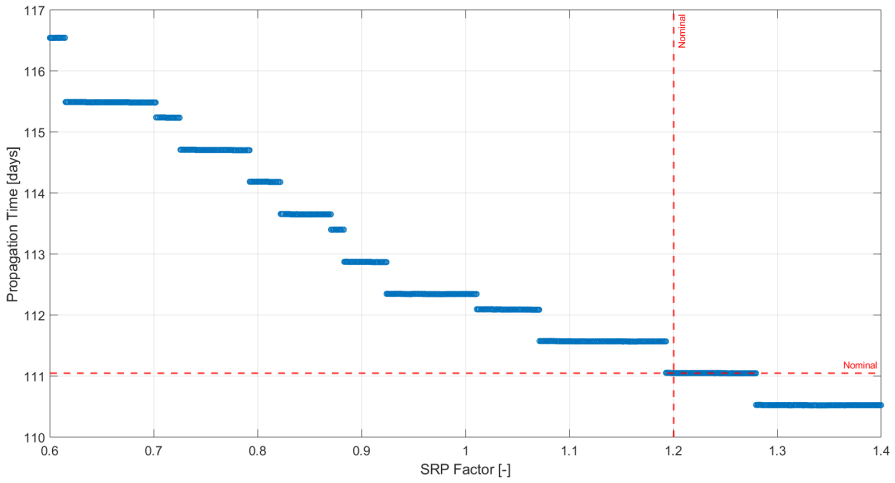

Figure 9.3: Propagation time as a function of SRP factor for 10000 runs, for point 1 in the interior ring.

It can also be highlighted that no runs are found below 110 days which seems promising for an orbit control-free mission.

Nonetheless, the gaps that appear in both Figure 9.2 and Figure 9.3 are surprising. It is believed that such gaps arise from the fact that decreasing the SRP factor at some point leads to a new threshold where the orbit is able to pursue one or more orbital revolutions before reaching the termination condition, which is always the maximum allowed distance w.r.t. Alpha, and always at pericenter.

Considering Kepler's third law and that the cubesat initially lies in a circular orbit, its orbital period can be approximated as:

$$T = 2\pi\sqrt{\frac{a^3}{\mu}} \approx 6.5288 \text{ h} = 0.2720 \text{ days} \tag{9.1}$$

Each propagation time gap in Figure 9.3 was investigated and compared in length to this approximation of the cubesat orbital period in Table 9.3.

Gap	Mean Gap Length L (hours)	L/T (-)
1	25.27	3.87
2	6.06	0.93
3	12.70	1.94
4	12.55	1.92
5	12.74	1.95
6	6.15	0.94
7	12.57	1.93
8	12.66	1.94
9	6.08	0.93
10	12.51	1.92
11	12.50	1.92
12	12.57	1.93

Table 9.3: Comparison between the length of the gaps in Figure 9.3 and a multiple of the average initial orbital period of the cubesat, for point 1 in the interior ring.

It seems indeed that each gap corresponds to a certain integer of orbital revolutions around Alpha which is the hypothesis that was put forward. The comparison is however not perfect due to the rough estimate of the orbital period.

Gravitational Parameter Uncertainties

The sensitivity analysis corresponding to the gravitational parameter of Alpha can be seen in Figure 9.4, while the one for the gravitational parameter of Beta can be seen in Figure 9.5. Figures 9.4a and 9.5a confirm a normal distribution.

The gaps observed in Figure 9.4b and Figure 9.5b seem to be once again related to the orbital period of the cubesat. It seems that changes in the gravitational parameter of Alpha are more impactful than changes for Beta, which is expected due to the close distance of the orbit w.r.t. Alpha. The general behaviour in Figure 9.5c is however not fully understood, but seems to be linked to orbital revolutions once again. Overall, all the runs last for more than 100 days which again seems promising.

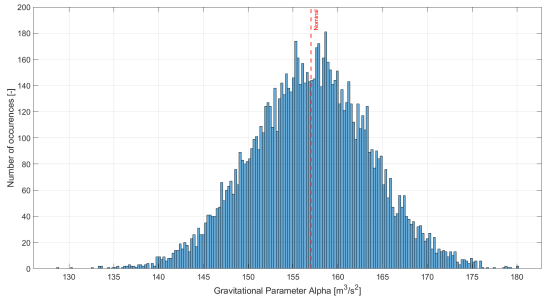

(a) Normal distribution of the gravitational parameter of Alpha.

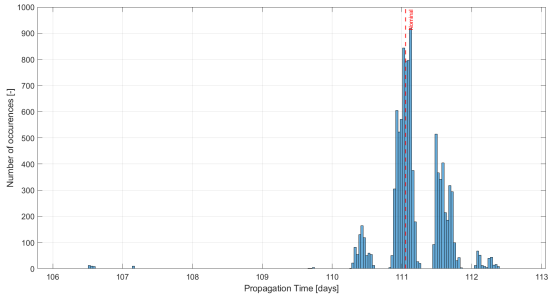

(b) Distribution of occurrences w.r.t. propagation time.

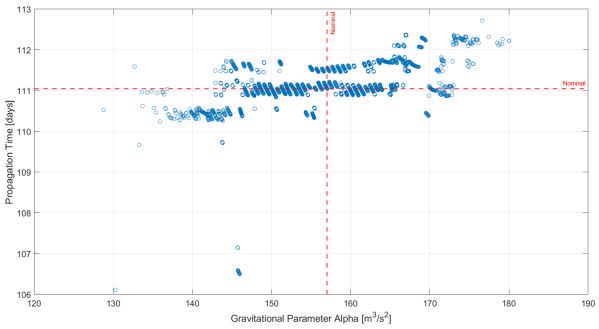

(c) Propagation time as a function of the gravitational parameter of Alpha.

Figure 9.4: Sensitivity analysis for the gravitational parameter of Alpha, for point 1 in the interior ring.

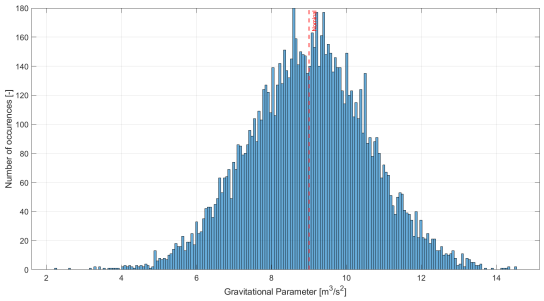

(a) Normal distribution of the gravitational parameter of Beta.

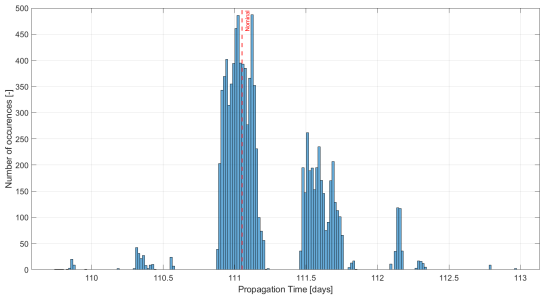

(b) Distribution of occurrences for the propagation time.

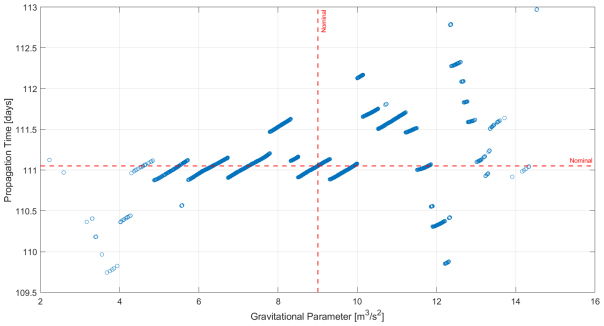

(c) Propagation time as a function of the gravitational parameter of Beta.

Figure 9.5: Sensitivity analysis for the gravitational parameter of Beta, for point 1 in the interior ring.

Spherical Harmonics Uncertainties

The introduction of uncertainties in the spherical harmonics coefficients of Alpha and Beta led to the results in Figure 9.6 and Figure 9.7 respectively.

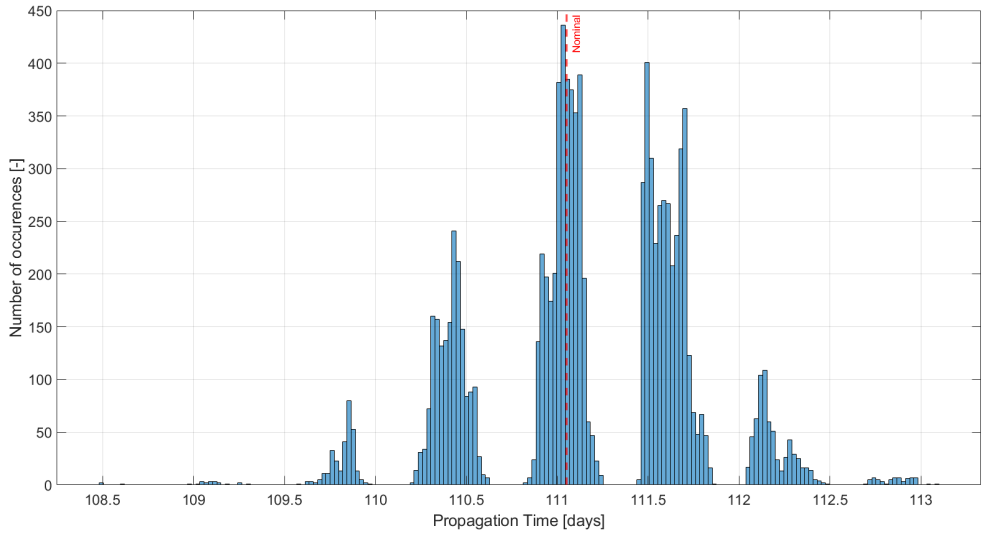

Figure 9.6: Sensitivity analysis for the spherical harmonic coefficients of Alpha, for point 1 in the interior ring.

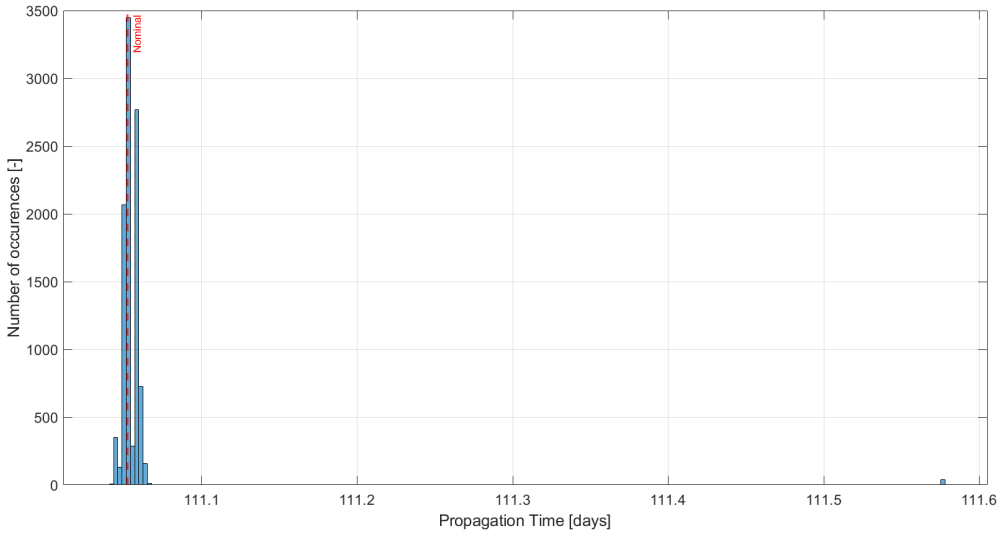

Figure 9.7: Sensitivity analysis for the spherical harmonic coefficients of Beta, for point 1 in the interior ring.

It appears that varying the spherical harmonics of Beta has almost no impact on the runs as the nominal pseudo-periodic orbit around Alpha is more perturbed by the primary. Still, no runs are found below 100 days in both cases.

State Uncertainties

The impact of uncertainties in the initial state of the cubesat is assessed in Figure 9.8 and Figure 9.9 for the position and velocity respectively.

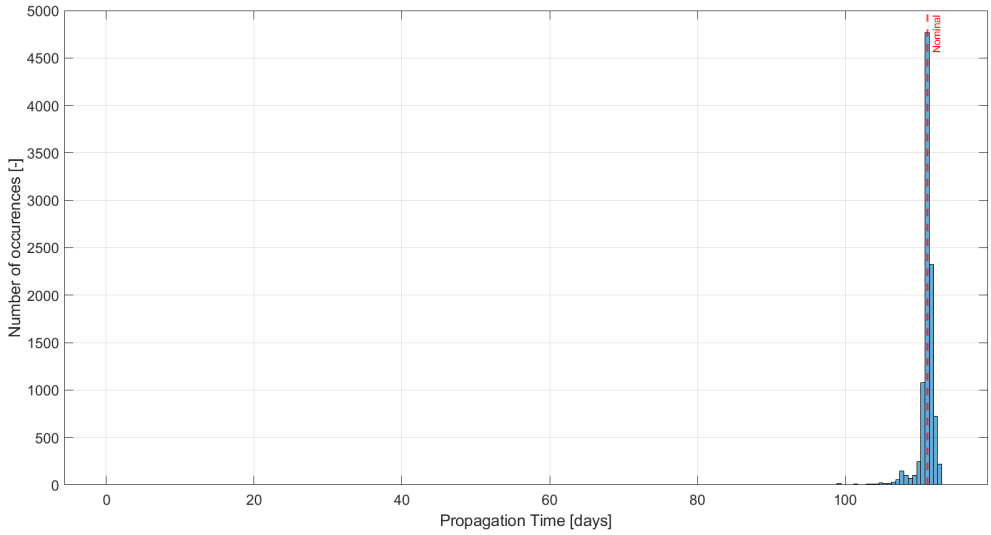

Figure 9.8: Sensitivity analysis for the initial position of the cubesat, for point 1 in the interior ring.

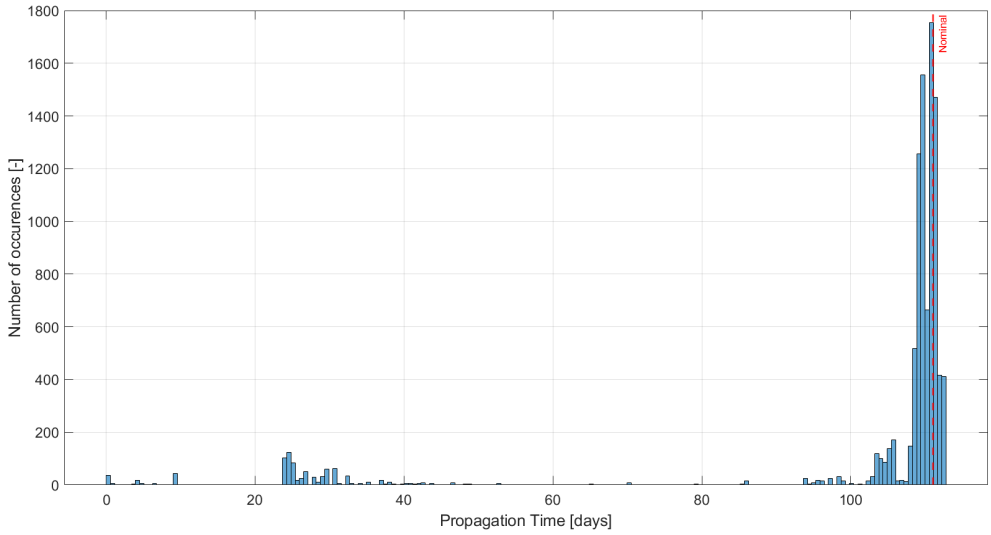

Figure 9.9: Sensitivity analysis for the initial velocity of the cubesat, for point 1 in the interior ring.

While it can be seen in 9.8 that the introduction of position uncertainties does not have a great impact on the result of the lifetime compared with the nominal run, it seems from Figure 9.9 that some particularly bad combinations of velocities lead to propagation times below 40 days. The percentage of runs lasting longer than 100 days is however 89%, which is deemed fairly good.

It is also reminded that the termination condition for all those runs is the one regarding the distance w.r.t. Alpha which is set to 400 m above the surface of the asteroid. The initial conditions for the nominal run are furthermore relatively close to this termination condition, namely a bit less than 250 m above it. The small bulge of unfavorable runs lasting for less than 40 days in Figure 9.9 thus does not imply the end of the

mission at all, just that the risk level acceptance is here maybe too low. It is still an encouragement to have better accuracy for velocity determination.

Combination of all Uncertainties

All the above uncertainties are also combined in one simulation, with results presented in Figure 9.10.

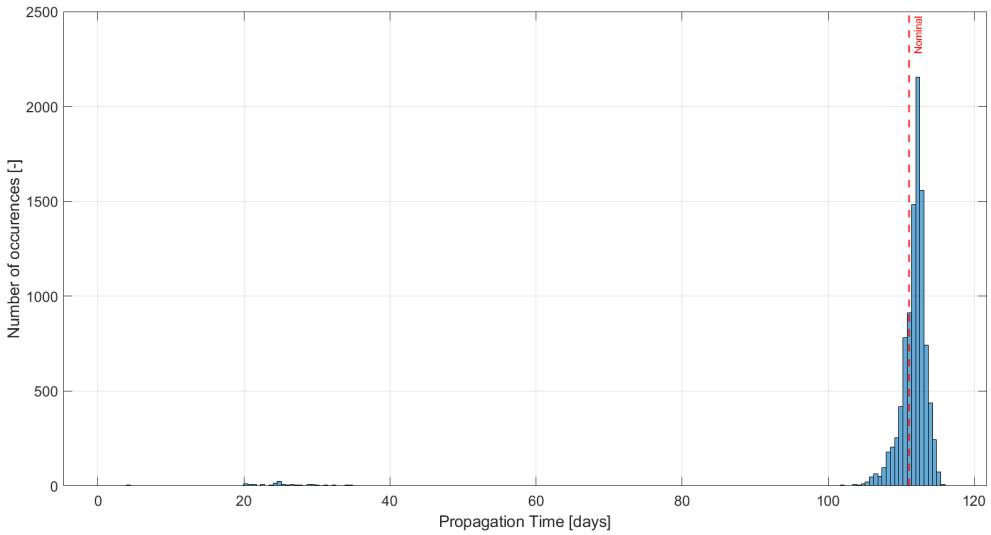

Figure 9.10: Combination of all uncertainties in a 10 000 runs simulation, for point 1 in the interior ring.

Almost all the runs are lasting for more than 100 days, except the visible small bulge between 20 and 40 days that comes from very bad combinations of velocities. This clearly is the dominant error source. Overall, this nominal orbit is deemed performing very well under the introduction of all these uncertainties, which implies that a cubesat mission targeting a pseudo-periodic orbit around the primary in a binary environment can in theory safely last for at least 100 days without orbit control.

9.2.2. Point 2

The second point corresponds to the one in Subsection 8.2.2.

SRP Uncertainties

The distribution of occurrences w.r.t. propagation time is displayed in Figure 9.2. It can first be highlighted that the distribution is unusual as the distribution is not uniform anymore and some propagation times seem to be more dominant than others.

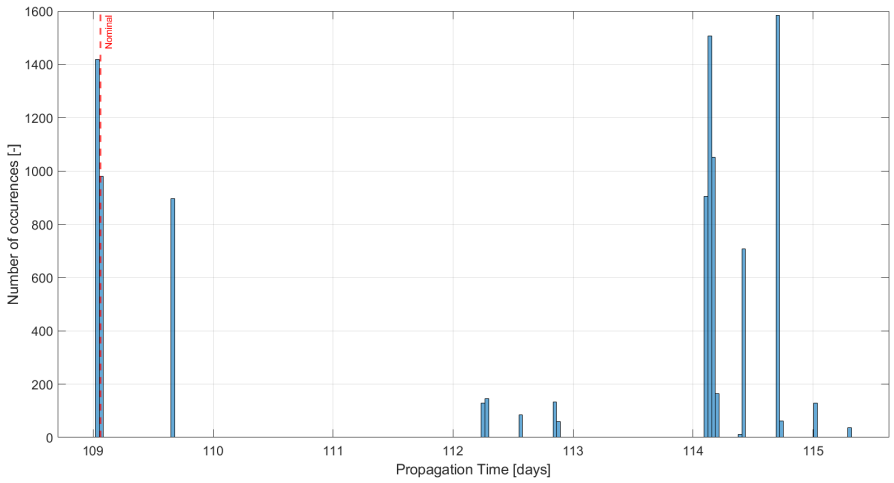

Figure 9.11: Distribution of occurrences with regard to propagation time for 10 000 runs, for point 2 in the interior ring.

This observation can once again be made in Figure 9.3 where the propagation time is shown as a function of the solar radiation pressure, but this also has to do with orbital periods as this is similar to the observation for point 1. A strange behaviour however occurs for large SRP factors where the orbit is able to pursue longer than expected. Although not fully understood, it is believed to be due to a strange combination with perturbations from Beta.

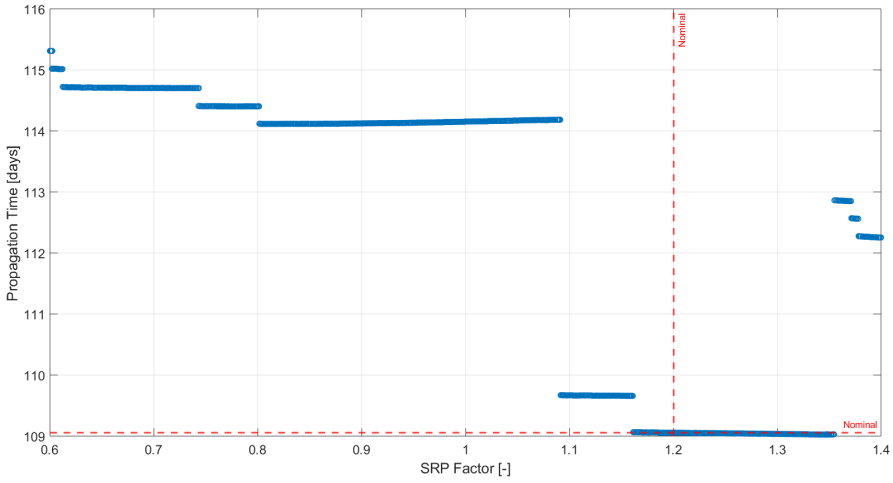

Figure 9.12: Propagation time as a function of SRP factor for 10000 runs, for point 2 in the interior ring.

Nonetheless, it can be highlighted that no runs are found below 109 days which seems once again promising for an orbit control-free mission.

Gravitational Parameter Uncertainties

The sensitivity analysis corresponding to the gravitational parameter of Alpha and Beta can be seen in Figure 9.13 and Figure 9.14 respectively.

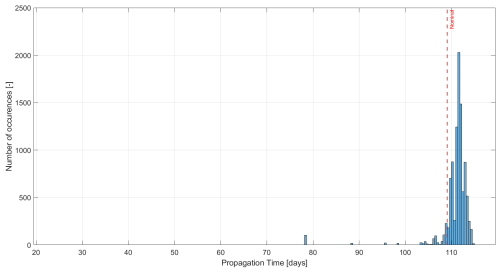

(a) Distribution of occurrences w.r.t. propagation time.

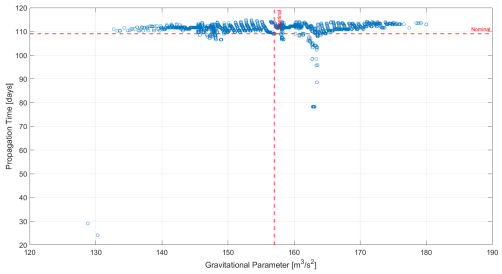

(b) Propagation time as a function of the gravitational parameter of Alpha.

Figure 9.13: Sensitivity Analysis for the gravitational parameter of Alpha, for point 2 in the interior ring.

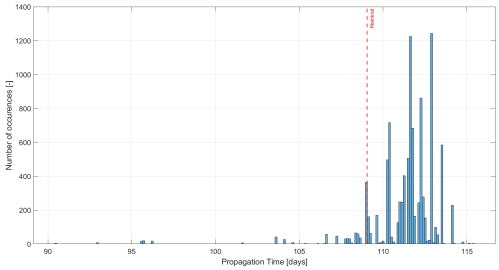

(a) Distribution of occurrences w.r.t. propagation time.

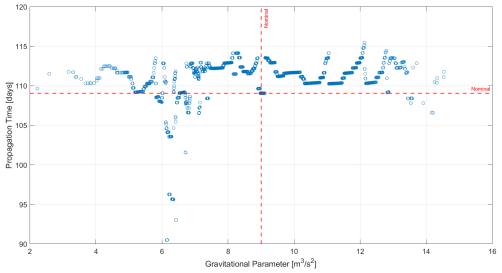

(b) Propagation time as a function of the gravitational parameter of Beta.

Figure 9.14: Sensitivity Analysis for the gravitational parameter of Beta, for point 2 in the interior ring.

It is first interesting to point out that most runs are lasting longer than the nominal one. Then some small peaks appear as low as 80 days for Alpha, which was not seen for Point 1. This would suggest that point 2 maybe lies in a more sensitive region. This could indeed be due to the fact that point 2 starts closer to the initial position of Beta than point 1.

Spherical Harmonics Uncertainties

The introduction of uncertainties in the spherical harmonics coefficients of Alpha and Beta led to the results in Figure 9.15.

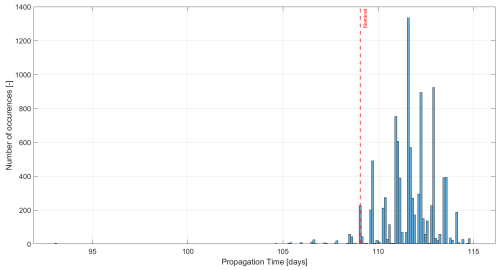

(a) Sensitivity analysis for the spherical harmonic coefficients of Alpha.

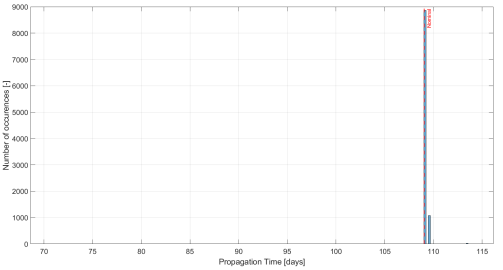

(b) Sensitivity analysis for the spherical harmonic coefficients of Beta.

Figure 9.15: Sensitivity analysis for the spherical harmonic coefficients of Alpha and Beta, for point 2 in the interior ring.

The impact of the uncertainties in the spherical harmonics of Beta is again negligible.

State Uncertainties

The impact of uncertainties in the initial state of the cubesat is assessed in Figure 9.16.

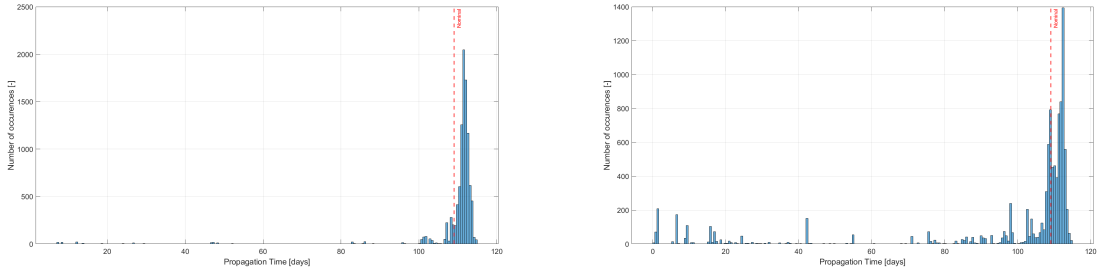

(a) Sensitivity analysis for the initial position of the cubesat.

(b) Sensitivity analysis for the initial velocity of the cubesat.

Figure 9.16: Sensitivity analysis for the initial state of the cubesat, for point 2 in the interior ring.

Real issues again arise with the introduction of velocity uncertainties, with some bad combinations leading to an impact scenario into Alpha in the first few days after the start of the simulation. There seems to be a trend where the velocity uncertainties are the critical aspect regarding the mission design.

Combination of All Uncertainties

All the above uncertainties are combined in one simulation, with results presented in Figure 9.17.

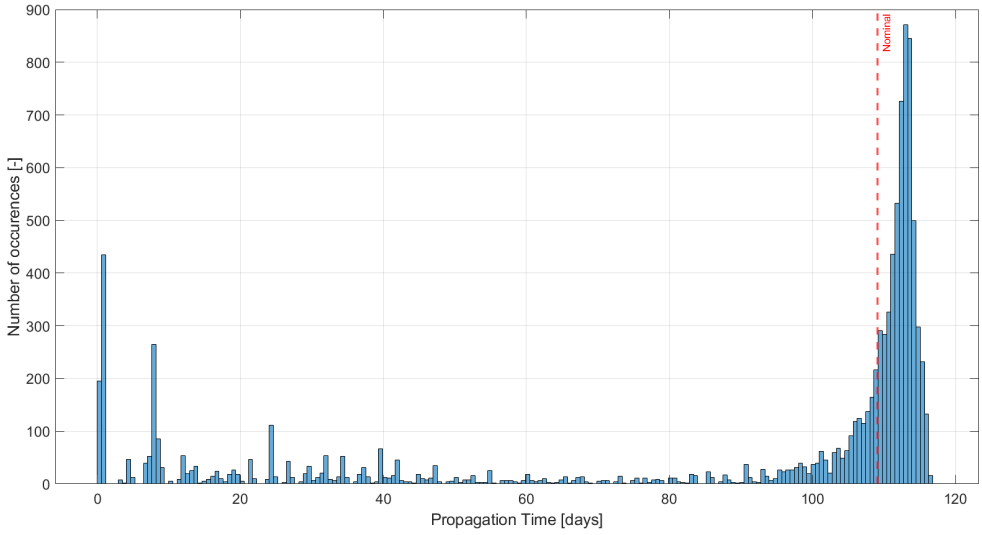

Figure 9.17: Combination of all uncertainties in a 10 000 runs simulation, for point 2 in the interior ring.

Point 2 is not performing as well as point 1 when it comes to the sensitivity analysis, with the introduction of a large number of runs lasting less than 40 days. Again, the quality of the initial velocity estimate is crucial. While they do not mean the end of the mission, it all comes down to the level of risk acceptance for such a mission. The 400 m termination condition is maybe too harsh for a pseudo-periodic orbit around Alpha, and the left bulge would most certainly disappear if it would be lowered. That would however come at this expense of a larger build-up of integration errors, but it should be tolerable in the specific case of an inherently stable pseudo-periodic orbit.

9.2.3. Point 3

The third and last point in the interior ring corresponds to the one in Subsection 8.2.3.

SRP Uncertainties

The performed sensitivity analysis for point 3 can be found in Figure 9.18. The behaviour is very similar to point 1 and 2, although even smoother regarding orbital period gaps in Figure 9.18b.

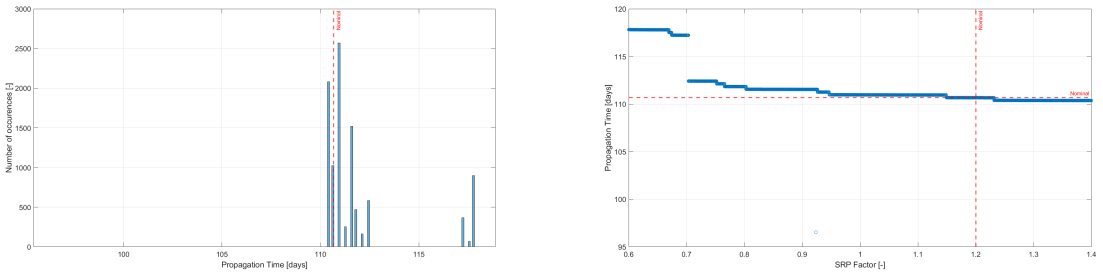

(a) Distribution of occurrences with regard to propagation time.

(b) Propagation time as a function of SRP factor.

Figure 9.18: Sensitivity analysis for the solar radiation factor, for point 3 in the interior ring.

Gravitational Parameter Uncertainties

The sensitivity analysis for the gravitational parameter of Alpha and Beta can be seen in Figure 9.19 and Figure 9.20 respectively.

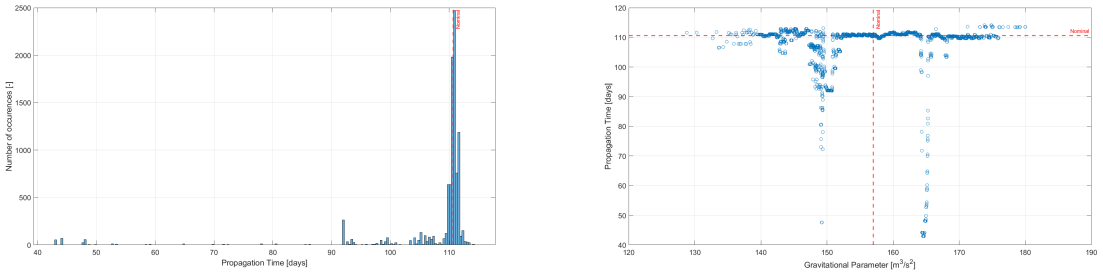

(a) Distribution of occurrences for the propagation time.

(b) Propagation time as a function of the gravitational parameter of Alpha.

Figure 9.19: Sensitivity analysis for the gravitational parameter of Alpha, for point 3 in the interior ring.

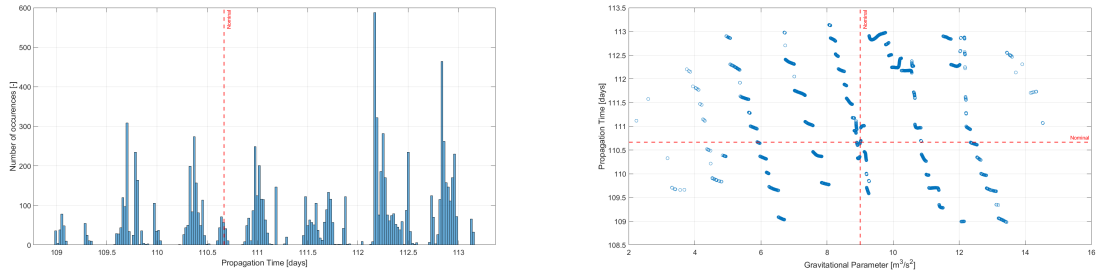

(a) Distribution of occurrences for the propagation time.

(b) Propagation time as a function of the gravitational parameter of Beta.

Figure 9.20: Sensitivity analysis for the gravitational parameter of Beta, for point 3 in the interior ring.

It is interesting to notice in Figure 9.19b that there seems to be two values of the gravitational parameter of Alpha that lead to reduced propagation times in view of our termination conditions. The end condition always

being an impact on Alpha, it could be that these specific values trigger the ending condition as a combined effect with the SRP or Beta.

Although results seem quite sparse in Figure 9.20, all runs lie in a region around 110 days so Beta has a much lesser impact on the dynamics as expected. Gaps due to orbital revolutions of the cubesat can also be seen in Figure 9.20, although the general behaviour in itself is not fully understood.

Spherical Harmonics Uncertainties

The introduction of uncertainties in the spherical harmonics of Alpha and Beta can be seen in Figure 9.21.

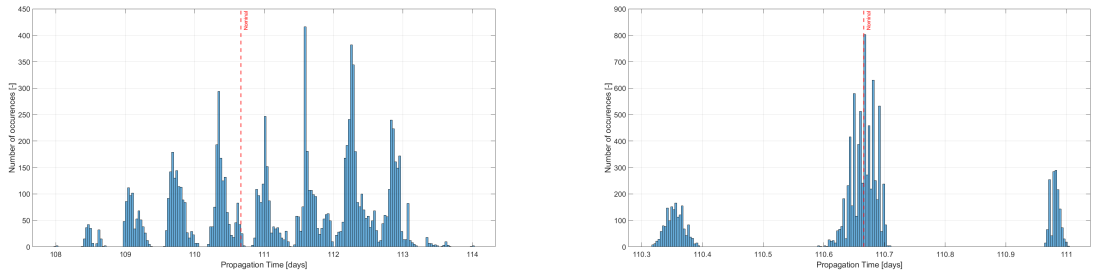

(a) Sensitivity analysis for the spherical harmonic coefficients of Alpha.

(b) Sensitivity analysis for the spherical harmonic coefficients of Beta.

Figure 9.21: Sensitivity analysis for the spherical harmonic coefficients of Alpha and Beta, for point 3 in the interior ring.

The results seem promising here, and the orbital period of the cubesat is clearly visible in each graph. The explanation for the gaps is as before.

State Uncertainties

The impact of uncertainties in the initial state of the cubesat is assessed in Figure 9.22.

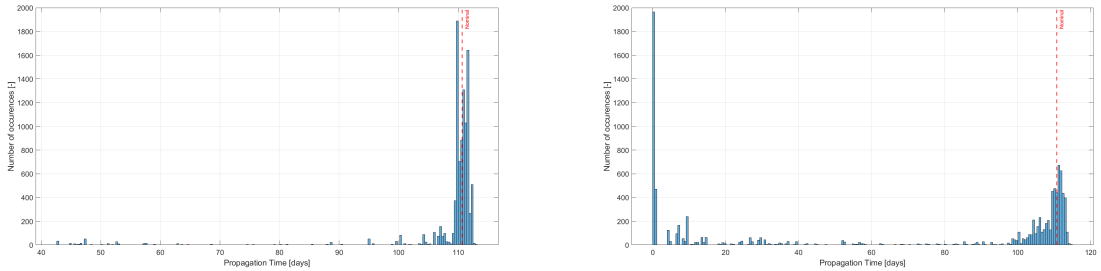

(a) Sensitivity analysis for the initial position of the cubesat.

(b) Sensitivity analysis for the initial velocity of the cubesat.

Figure 9.22: Sensitivity analysis for the initial state of the cubesat, for point 3 in the interior ring.

Some bad combinations can already be seen in Figure 9.22a but it is the velocity results in Figure 9.22b that are striking and show that the simulation can end quickly in view of our termination conditions. The runs lasting between 0 and 30 days end with an almost equal number of impacts on Alpha and Beta, which suggests that point 3 is initially much too close to both these termination conditions and may not be a good mission choice as the orbit is very likely to be sensitive to perturbations afterwards.

Combination of All Uncertainties

All the above uncertainties are combined in one simulation, resulting in Figure 9.23.

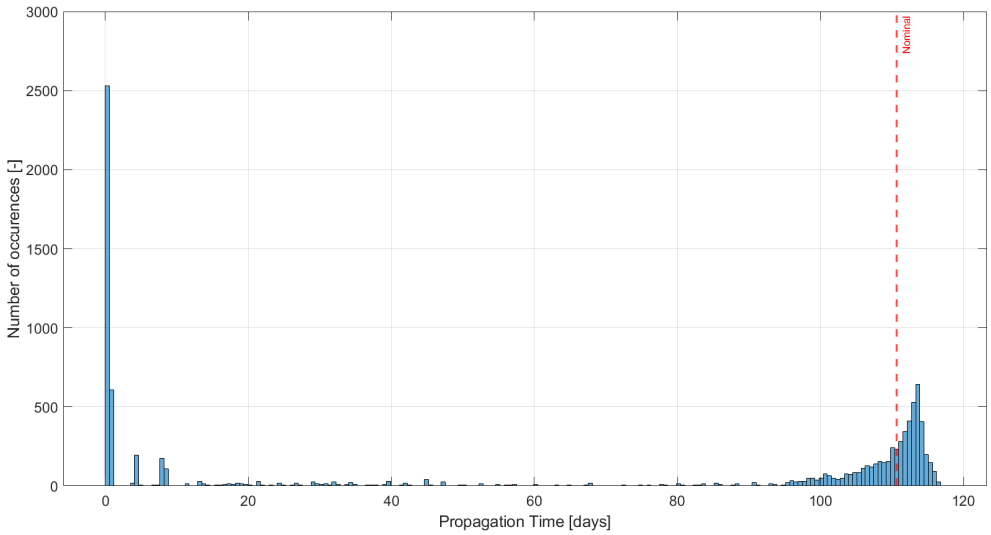

Figure 9.23: Combination of all uncertainties for point 3 in the interior ring.

This point seems too close to both termination conditions regarding Alpha and Beta, actually in an almost equal amount again below 30 days. This is due to the fact that the cubesat is injected almost in between Alpha and the initial position of Beta at the start of the simulation, which seems to be a poor geometry. Choosing such a point does not mean critical failure of the mission, but means that this orbit is more sensitive in the long term.

It would be interesting to investigate whether lowering the uncertainties in the velocity components has an impact on those final results. To that extent, Figure 9.24 was made by halving the uncertainties in the initial velocity of the cubesat to 5 mm/s.

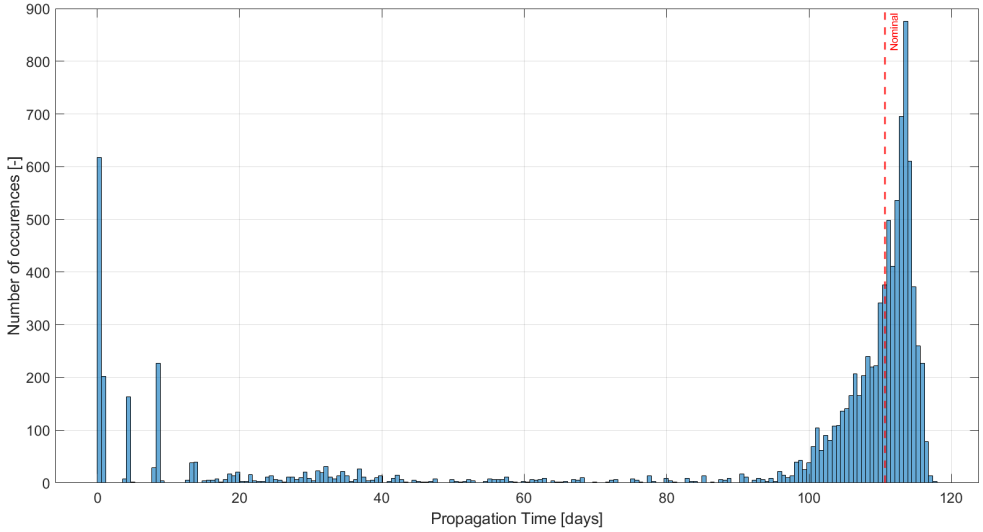

Figure 9.24: Combination of all uncertainties for point 3 in the interior ring, for halved uncertainties in the initial velocity components of the cubesat.

It can be seen that there is a transfer of the low propagation time runs towards the nominal value, which proves that such a mission can greatly benefit from trying to reduce the initial velocity uncertainties, either via a better injection mechanism or smaller ODCS errors from the mothership before injection.

9.3. Exterior Ring

The next step in this sensitivity analysis focuses on the nominal exterior points in Section 8.3.

9.3.1. Point 1

The first point corresponds to the one in Section 8.3.1.

SRP Uncertainties

The sensitivity analysis for point 1 in the exterior ring can be found in Figure 9.25.

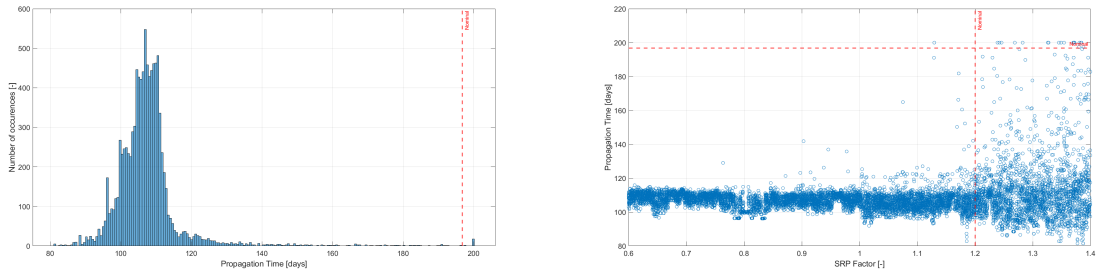

(a) Distribution of occurrences with regard to propagation time.

(b) Propagation time as a function of SRP factor for 10000 runs.

Figure 9.25: Sensitivity analysis for the solar radiation factor, for point 1 in the exterior ring.

The orbital revolution steps are now gone in Figure 9.25b as the motion is not pseudo-periodic anymore. The striking thing about these graphs is that the nominal orbit seems to be a very luck shot, confirming that it corresponds to a very unrealistic isolated point: the far majority of the points has a lifetime of about 50% of the nominal value. One interesting conclusion is also that an increased SRP factor leads to sparser and sometimes longer propagation times in the exterior ring. Point 1 is a very lucky point which otherwise seems to lay in a region of about 100 propagation days w.r.t. our termination conditions. Still, all runs otherwise last for more than 60 days, which is really what was accepted as realistic for missions in the exterior ring. It can be mentioned that the typical termination condition is here on the maximum semi-major axis allowed for the cubesat.

Gravitational Parameter Uncertainties

Confirming the sense of an isolated nominal point, the sensitivity analysis w.r.t. the gravitational parameter of both Alpha and Beta can be seen in Figure 9.26 and Figure 9.27 respectively.

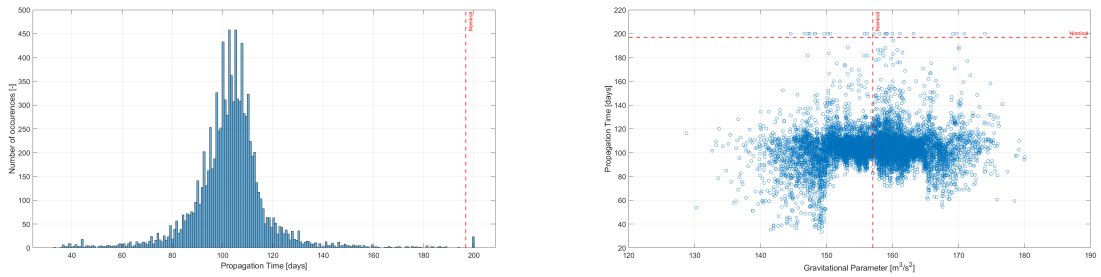

(a) Distribution of occurrences with regard to propagation time.

(b) Propagation time as a function of the gravitational parameter of Alpha.

Figure 9.26: Sensitivity analysis for the spherical harmonic coefficients of Alpha, for point 1 in the exterior ring.

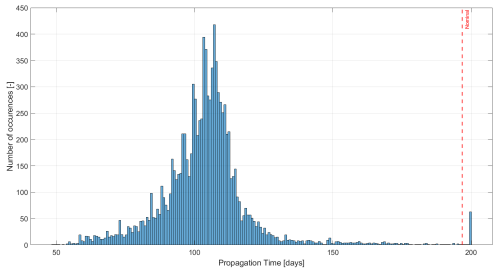

(a) Distribution of occurrences with regard to propagation time.

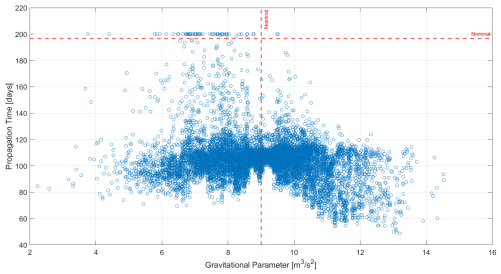

(b) Propagation time as a function of the gravitational parameter of Beta.

Figure 9.27: Sensitivity analysis for the spherical harmonic coefficients of Beta, for point 1 in the exterior ring.

Spherical Harmonics Uncertainties

The introduction of uncertainties in the spherical harmonics of Alpha and Beta can be seen in Figure 9.28.

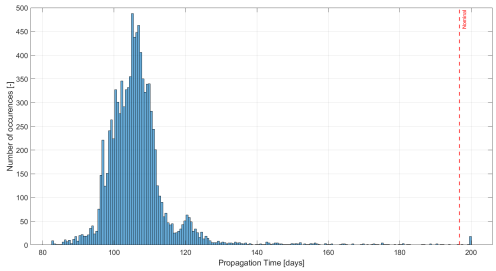

(a) Sensitivity analysis for the spherical harmonic coefficients of Alpha.

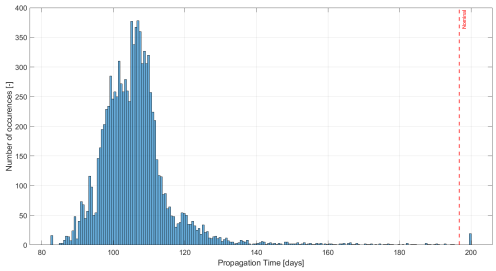

(b) Sensitivity analysis for the spherical harmonic coefficients of Beta.

Figure 9.28: Sensitivity analysis for the spherical harmonic coefficients of Alpha and Beta, for point 1 in the exterior ring.

Uncertainties in the spherical harmonics of Alpha and Beta are more equally impactful on the results compared to the close pseudo-periodic interior orbits, which is understandable: distances are much more comparable.

State Uncertainties

The sensitivity analysis with regard to the initial position and velocity of the cubesat can be seen in Figure 9.29.

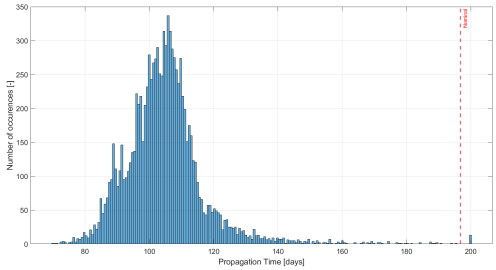

(a) Sensitivity analysis for the initial position of the cubesat.

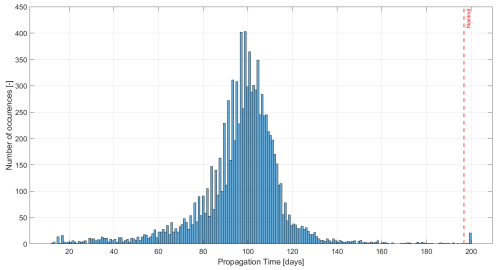

(b) Sensitivity analysis for the initial velocity of the cubesat.

Figure 9.29: Sensitivity analysis for the initial state of the cubesat, for point 1 in the exterior ring.

Some bad combinations appear as low as 20 days in Figure 9.29b which is not very promising.

Combination of All Uncertainties

The combination of all uncertainties for this point can be seen in Figure 9.30.

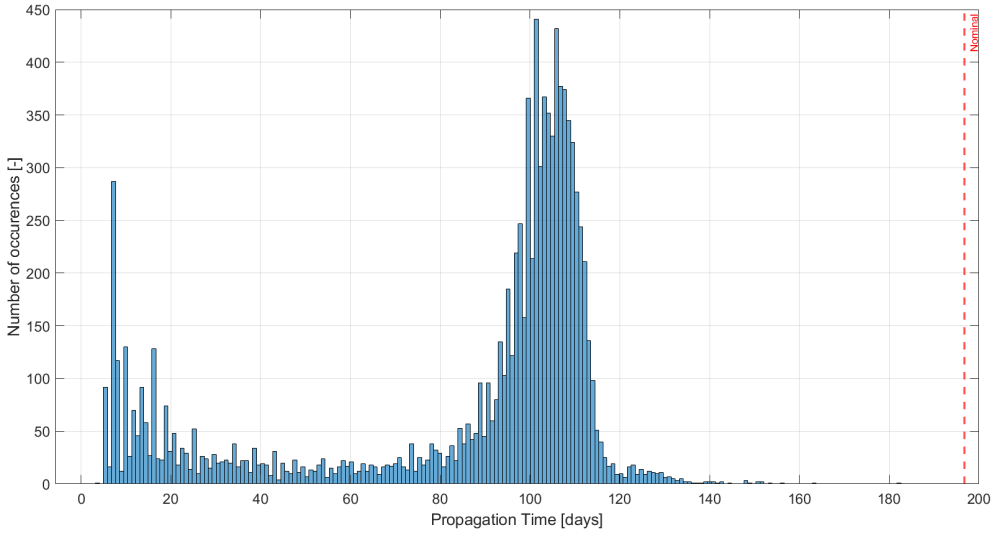

Figure 9.30: Combination of all uncertainties for point 1 in the exterior ring.

Although the percentage of runs lasting longer than 60 days is 78.6 %, the large bulge appearing for (very) low propagation times is deemed to high a risk regarding our own safety margins.

It could once more be interesting to investigate the impact on lowering the velocity uncertainties, which was performed in Figure 9.31.

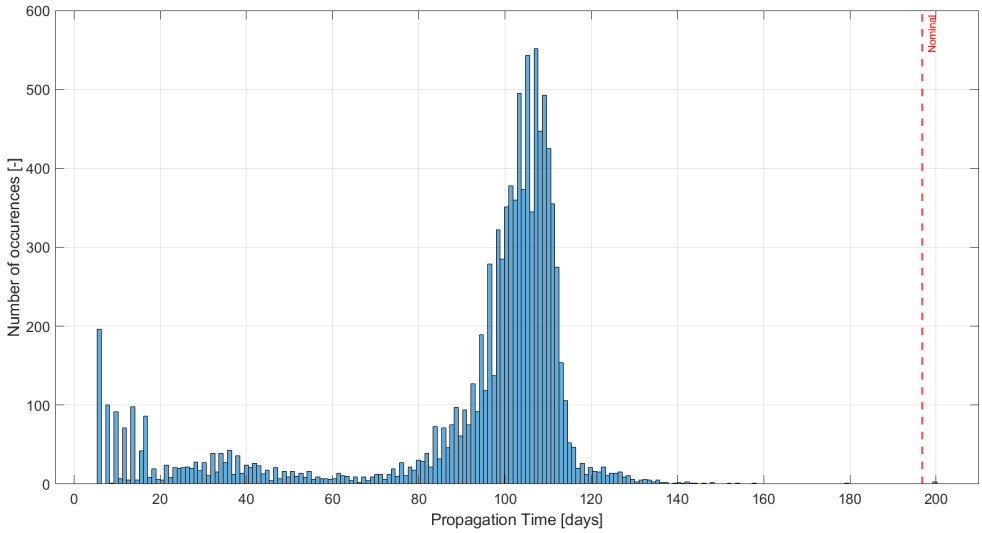

Figure 9.31: Combination of all uncertainties for point 1 in the exterior ring, with halved uncertainties in the initial velocity components of the cubesat.

The number of runs lasting for at least 60 days raises to 85.3 %, showing once again that the driving requirement for such a mission is the initial velocity uncertainties for better safety margins.

9.3.2. Point 2

The second point in the exterior ring corresponds to the one in Section 8.3.2. As a reminder, it corresponds to a pseudo-periodic orbit found in the exterior ring, which might trigger expectations.

SRP Uncertainties

The results regarding the introduced uncertainties in the solar radiation factor can be seen in Figure 9.32.

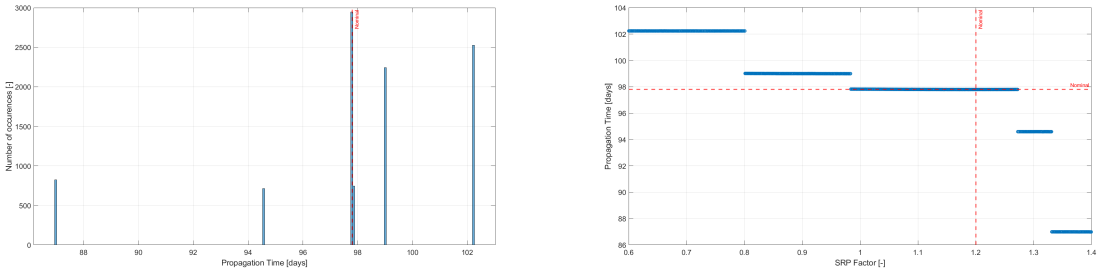

(a) Distribution of occurrences with regard to propagation time.

(b) Propagation time as a function of SRP factor.

Figure 9.32: Sensitivity analysis w.r.t the solar radiation factor, for point 2 in the exterior ring.

This pseudo-periodic orbits seems to perform well under SRP uncertainties, with again a clear visualization of the orbital period of the cubesat. Such plots seem characteristic of the pseudo-periodic family of candidates, at least in our thesis.

Gravitational Parameter Uncertainties

The effects of gravitational parameter uncertainties for both Alpha and Beta are presented in Figure 9.33 and Figure 9.34 respectively.

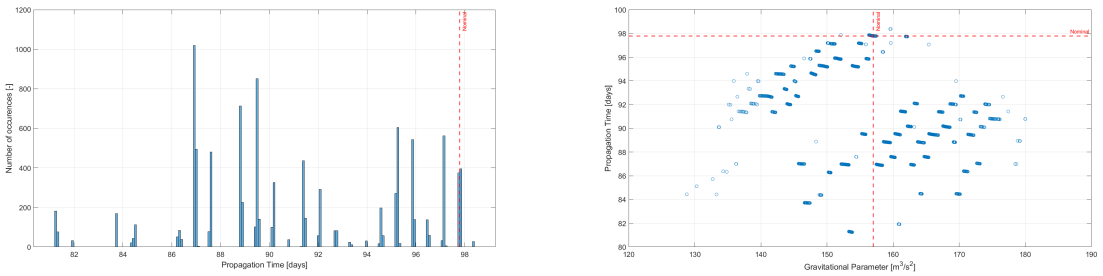

(a) Distribution of occurrences with regard to propagation time.

(b) Propagation time as a function of the gravitational parameter of Alpha.

Figure 9.33: Sensitivity analysis for the spherical harmonic coefficients of Alpha, for point 2 in the exterior ring.

While the gravitational parameter of Alpha seems to have a relatively low impact, Beta is on the contrary impactful in that sense, with early impacts into Beta appearing below 30 days when the gravitational parameter of Beta is too small as highlighted in Figure 9.34b. It is believed that the pseudo-periodic orbits in the exterior ring are disappearing in that particular case, leading to highly perturbed orbits that rapidly reach the 400 m termination condition w.r.t. Beta, which is the one ending all the runs.

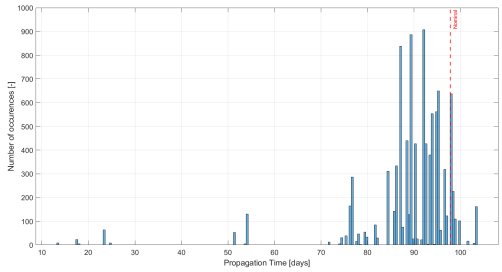

(a) Distribution of occurrences with regard to propagation time.

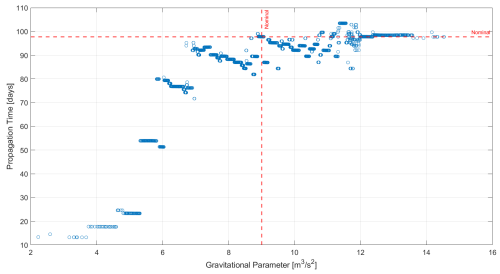

(b) Propagation time as a function of the gravitational parameter of Beta.

Figure 9.34: Sensitivity analysis for the spherical harmonic coefficients of Beta, for point 2 in the exterior ring.

Spherical Harmonics Uncertainties

The analysis on the spherical harmonics of both Alpha and Beta is shown in Figure 9.35.

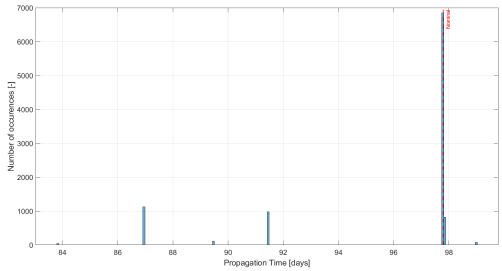

(a) Sensitivity analysis for the spherical harmonic coefficients of Alpha.

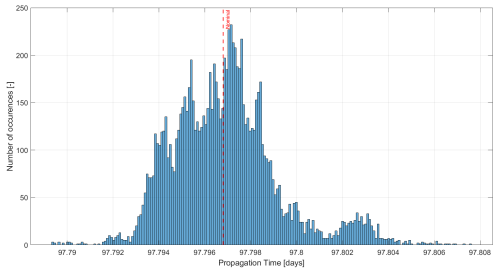

(b) Sensitivity analysis for the spherical harmonic coefficients of Beta.

Figure 9.35: Sensitivity analysis for the spherical harmonic coefficients of Alpha and Beta, for point 2 in the exterior ring.

The impact of the SH of Beta is minimal, while the ones for Alpha can lead to a few days difference, but it is deemed acceptable.

State Uncertainties

The analysis regarding the introduction of uncertainties in the initial position and velocity components of the cubesat can be seen in Figure 9.36.

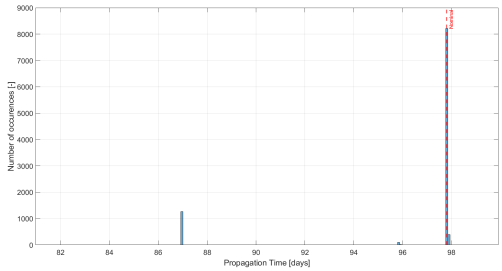

(a) Sensitivity analysis for the initial position of the cubesatg.

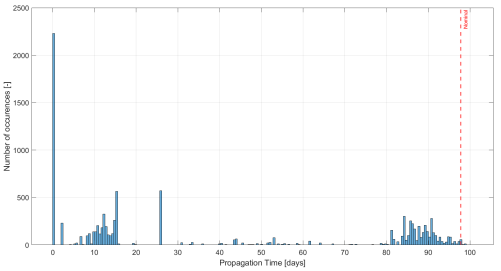

(b) Sensitivity analysis for the initial velocity of the cubesat.

Figure 9.36: Sensitivity analysis for the initial state of the cubesat, for point 2 in the exterior ring.

Again, uncertainties in the initial position are not the most problematic in comparison to the ones in the initial velocity of the cubesat. They can lead to very early impact into Beta in that particular case.

Combination of All Uncertainties

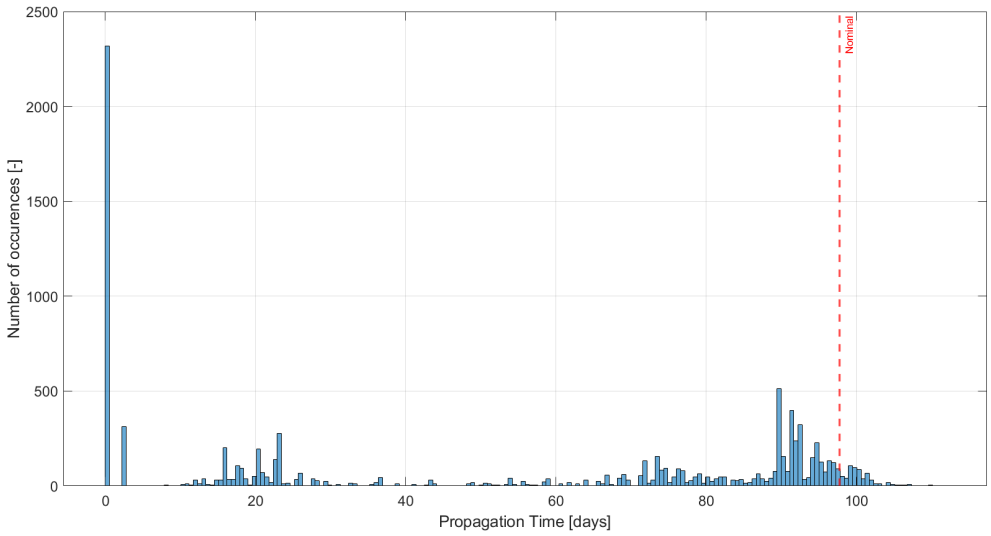

Figure 9.37: Combination of all uncertainties for point 2 in the exterior ring.

All the runs in this simulation end with the termination condition w.r.t. Beta. The initial position of the cubesat is close to this condition, leading to an important number of occurrences that are lasting for less than a day. If an uncontrolled pseudo-periodic orbit in the exterior ring is still deemed relevant for a mission team, it would be advised to revise the risk acceptability by lowering the termination condition w.r.t. Beta, or manage to be more constraining on the injection mechanism in order to introduce smaller velocity uncertainties. This could indeed redefine the level of accessibility for a given orbit, as highlighted in Figure 9.38 where the velocity uncertainties are halved compared to the previous plot.

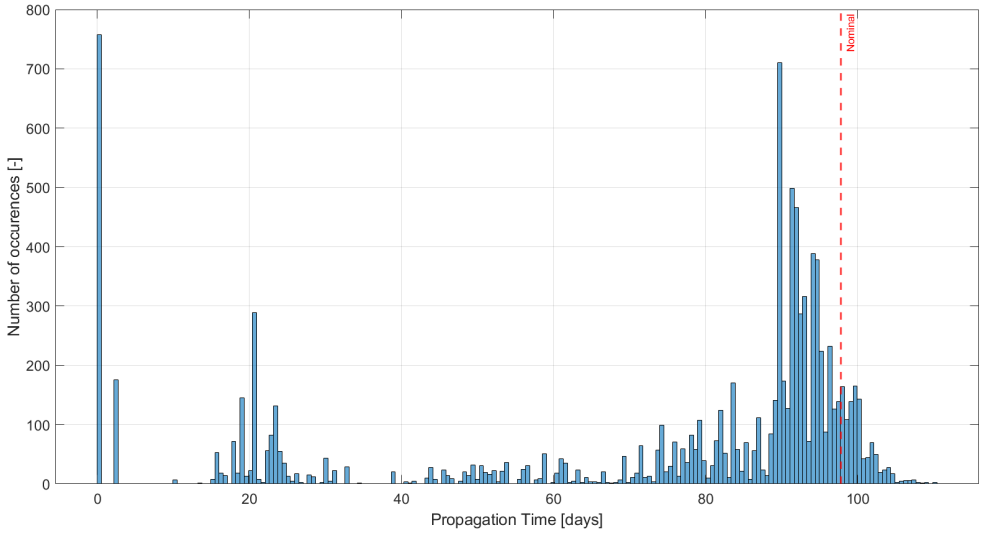

Figure 9.38: Combination of all uncertainties for point 2 in the exterior ring, for halved uncertainties in the initial velocity components of the cubesat.

9.3.3. Point 3

The third point in the exterior ring corresponds to the one in Section 8.3.3. Point 1 in the exterior ring highlighted the fact that runs lasting for almost 200 days are only residual isolated points that do not withstand the introduction of uncertainties. It was seen that the region around point 1 led to simulations that were more around 100 days, which is approximately the propagation time for point 3 in the exterior ring.

SRP Uncertainties

The sensitivity analysis w.r.t. the solar radiation factor is shown in Figure 9.39.

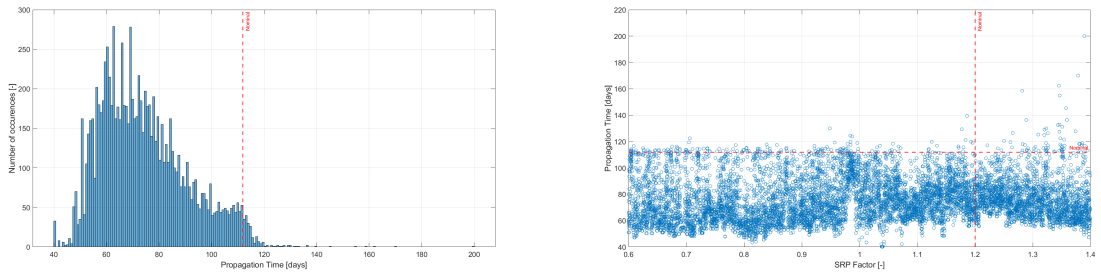

(a) Distribution of occurrences with regard to propagation time.

(b) Propagation time as a function of SRP factor.

Figure 9.39: Sensitivity analysis w.r.t the solar radiation factor, for point 3 in the exterior ring.

It can be seen that all runs are widely distributed between 40 and 120 days which is not a promising result, although most runs last for longer than 60 days.

Gravitational Parameter Uncertainties

The introduction of uncertainties in the gravitational parameter of Alpha and Beta can be seen in Figure 9.40 and Figure 9.41 respectively.

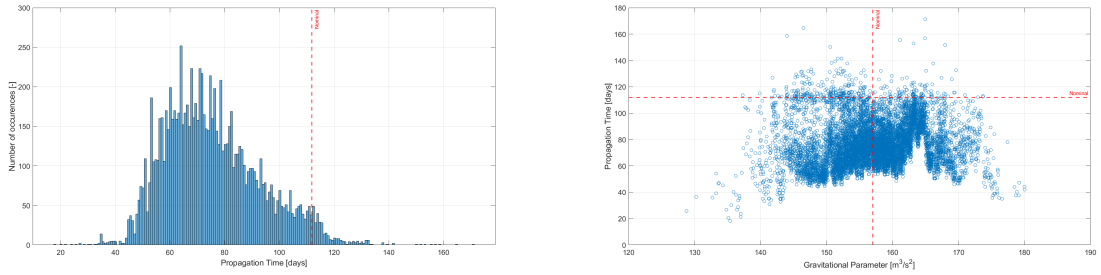

(a) Distribution of occurrences with regard to propagation time.

(b) Propagation time as a function of the gravitational parameter of Alpha.

Figure 9.40: Sensitivity analysis for the spherical harmonic coefficients of Alpha, for point 3 in the exterior ring.

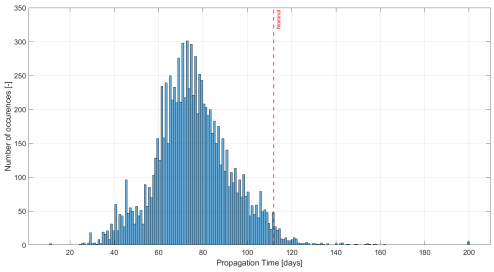

(a) Distribution of occurrences with regard to propagation time.

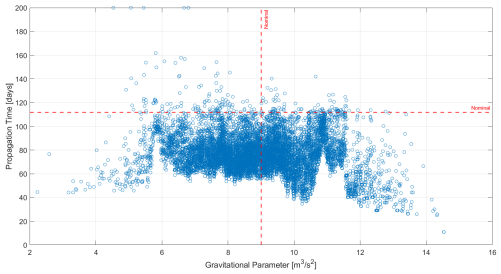

(b) Propagation time as a function of the gravitational parameter of Beta.

Figure 9.41: Sensitivity analysis for the spherical harmonic coefficients of Beta, for point 3 in the exterior ring.

Bad combinations of low/high gravitational parameter of either Alpha or Beta lead to reduced simulations times below 60 days, reaching 20 days sometimes. The majority of the runs last for more than 60 days which is what matters for a run in the exterior ring, but still point 3 seems too risky for a mission even at this point.

Spherical Harmonics Uncertainties

Spherical harmonics uncertainties for both Alpha and Beta led to the results in Figure 9.42.

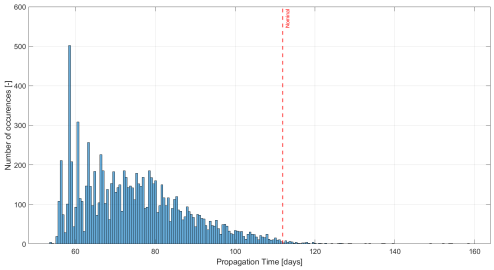

(a) Sensitivity analysis for the spherical harmonic coefficients of Alpha.

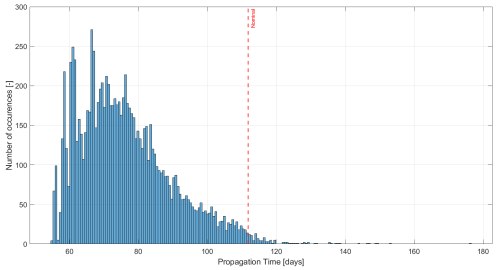

(b) Sensitivity analysis for the spherical harmonic coefficients of Beta.

Figure 9.42: Sensitivity analysis for the spherical harmonic coefficients of Alpha and Beta, for point 3 in the exterior ring.

The runs again drift from the nominal propagation time, but are always longer than 60 days which is what can be ensured by the integrator/propagator settings in the exterior ring anyway.

State Uncertainties

Results of the analysis regarding the introduction of uncertainties in the initial position and velocity components of the cubesat can be seen in Figure 9.43.

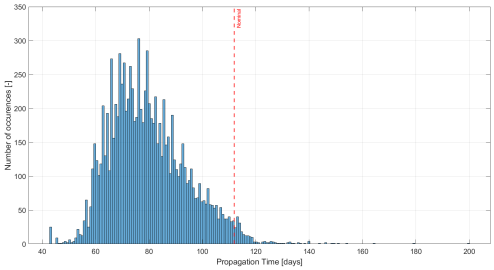

(a) Sensitivity analysis for the initial position of the cubesat.

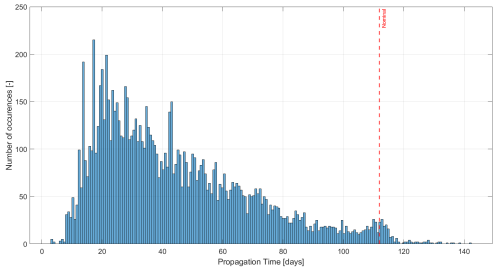

(b) Sensitivity analysis for the initial velocity of the cubesat.

Figure 9.43: Sensitivity analysis for the initial state of the cubesat, for point 3 in the exterior ring.

It can be observed that the results are too spread for the velocity uncertainties, showing that particularly bad runs can be found in the exterior ring.

Combination of All Uncertainties

Introducing all the above uncertainties in one simulation led Figure 9.44.

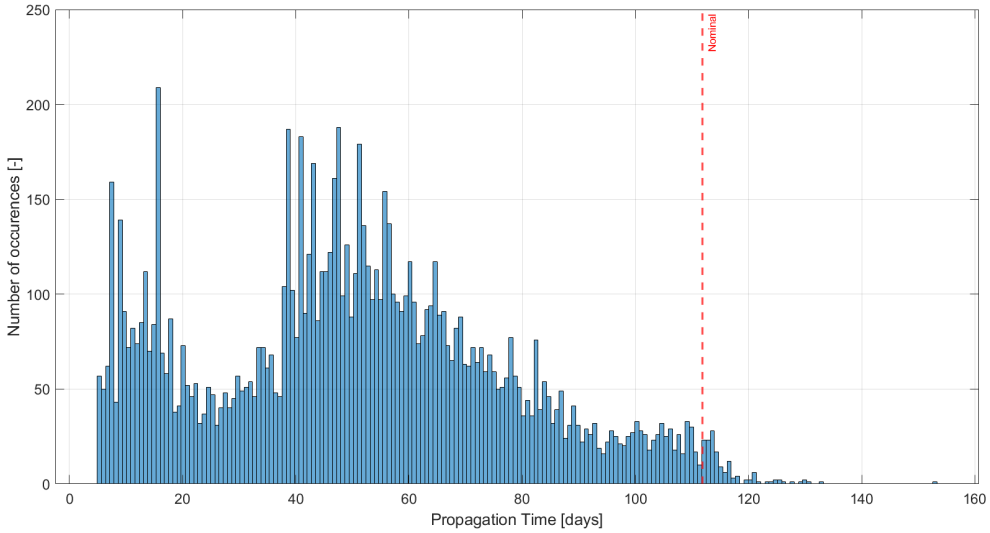

Figure 9.44: Combination of all uncertainties for point 3 in the exterior ring.

As expected, the runs are too widely spread to even consider this point for a mission. The 60 days mark cannot even be ensured under the introduction of uncertainties, which is an indication of the fact that most runs in the exterior ring are too sensitive in essence, and should in general be avoided for an orbit control-free mission.

9.4. Conclusions

This chapter was all about assessing whether the points found in the interior and exterior ring of the binary asteroid in Chapter 8 are still promising for an orbit control-free mission, recognizing the fact that the environment is not perfectly modelled.

After investigation, it seems that points in the exterior ring are too sensitive to the introduction of uncertainties and thus deemed too high a risk to investigate with this concept, even when trying to target a pseudo-periodic orbit in the exterior ring. Lowering the uncertainties in the initial velocity of the cubesat can however help to mitigate this observation.

Promising orbits are however found in the interior ring, such as point 1 which is still a very good one after introduction of uncertainties. The inherent stability of the pseudo-periodic orbit enables to ensure an orbit lasting for at least 100 days around Alpha. Although one could think that any point in the yellow region of Figure 8.2 could be chosen in that sense, it seems that some initial conditions can lead to an early impact on either Alpha or Beta. This is however due to the very constraining 400 m termination condition on both Alpha and Beta which was chosen for the purpose of having a stable and reliable orbit integration. It is most likely that such points are also performing well if the termination condition was to be lowered, but it comes at the expense of a higher risk acceptance w.r.t. the results.

Targeting pseudo-periodic orbit seems overall the best strategy to adopt for an orbit control-free mission, in comparison to more perturbed orbits that are not as reliable.

10 Validation

This chapter presents the validation process of this thesis, to ensure that results are reliable, representative and have a physical meaning. It is emphasized that all coding-related aspects of this thesis are made using TUDAT which is a very trustworthy software with a continuous support and added features. It is for this reason that many parts in this thesis are already assumed validated because they are already implemented in TUDAT. It is for example the case for the implementation of all perturbing forces. It is also the case for all built-in integration and propagation methods which will not be reviewed when used.

The only validation process worthy to be pursued regards the implementation of the environment model itself, to ensure that it correctly represents the binary asteroid system.

10.1. Ephemeris Validation

The ephemeris for Alpha is retrieved directly from the JPL Small-Body Database as explained in Subsection 6.2.2 so no validation process is needed on that end. The ephemeris for Beta however is computed by propagating Beta around Alpha for 200 days using a high-fidelity acceleration model and initial conditions from the nominal parameters in [Ostro and al., 2006]. These parameters are fitted to the system motion under Keplerian assumptions using a least-squares estimation procedure from an Earth flyby in May 2001. Both [Fahnestock and Scheeres, 2008] and [Compère and Lemaître, 2014] however tested their models using two different and simpler test cases corresponding to a so-called relaxed system configuration, and an excited one. The orbital elements from those two configurations differ in essence from the nominal ones in [Ostro and al., 2006], this is why no comparison can be made directly between them.

The ephemeris used for Beta in this thesis relies entirely on the nominal model in [Ostro and al., 2006], but the two relaxed and excited test configurations can be implemented for the full purpose of validating our implementation. All simulations in this validation process are performed using a Cowell propagator with a Runge-Kutta 7(8) integrator with tolerances 10^{-15}.

10.1.1. Relaxed and Excited Models

The relaxed test configuration is supposed to model the situation of an Earth flyby while the excited configuration should represent a perihelion passage of the binary asteroid 1999 KW4. Given that the current perihelion passage of the binary system is as close as 0.2 AU, an hypothesis is that this is actually the main mechanism for the system's excitation. These two configurations assume a two-body problem with no third-body influences.

The orbital elements of Beta around Alpha using these two configurations are plotted in Figure 10.1 using our own model, for a total of 200 hours to approach the results of both [Compère and Lemaître, 2014] and [Fahnestock and Scheeres, 2008].

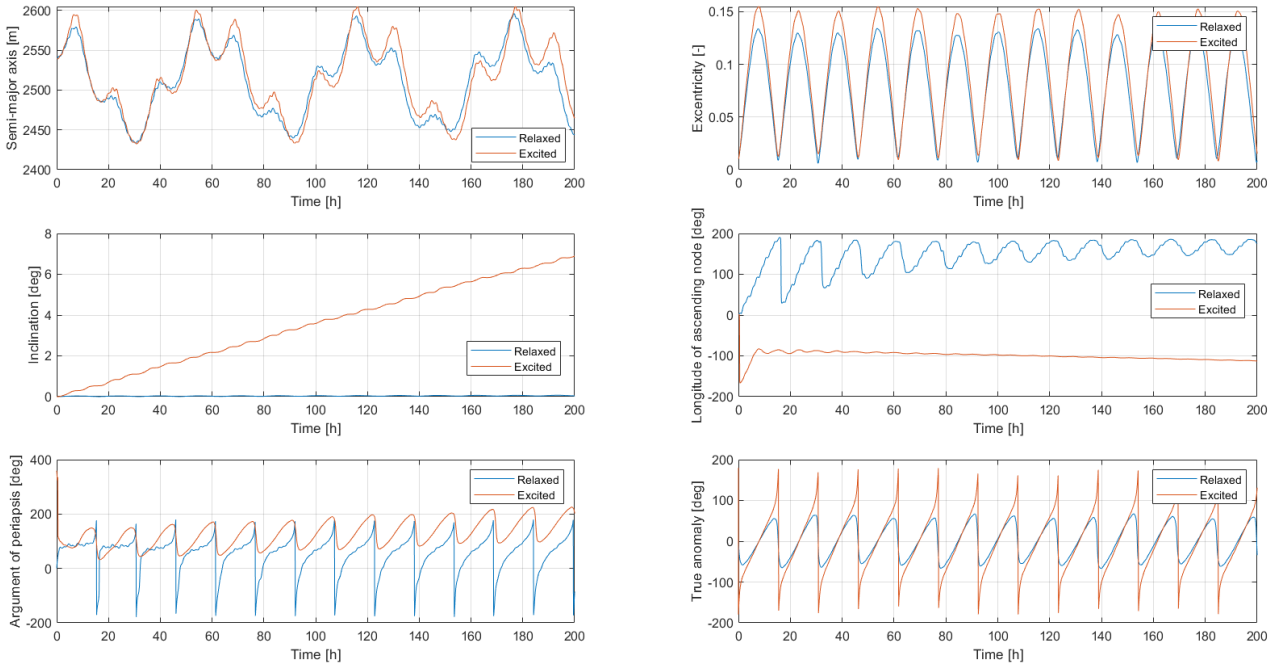

Figure 10.1: Orbital elements for the relative orbit of Beta around Alpha, computed using the relaxed and excited configurations in [Compère and Lemaître, 2014] from [Fahnestock and Scheeres, 2008].

The results are similar to the ones in [Compère and Lemaître, 2014], who proved to obtain the same results as [Fahnestock and Scheeres, 2008] who used a different orientation frame for their simulations, linked to the total angular momentum vector at the initial time. The results obtained by these two papers are given for convenience in Appendix A for comparison purposes.

The evolution of Beta's orbital elements enable to identify three system modes with different periods. The first one (and the fastest), can faintly be seen and matches Alpha's spin period of about 2.76 hours like in [Compère and Lemaître, 2014] and [Fahnestock and Scheeres, 2008]. The second one corresponds to the orbital period of Beta of 17.45 hours, which is the same as its rotation period, which can also be seen in [Compère and Lemaître, 2014] and [Fahnestock and Scheeres, 2008]. The last one has a period of approximately 60 hours, and appears to be specific to our model. It is due to the fact that the acceleration model used for Beta in our simulations uses a so-called third-body mutual spherical harmonic perturbation, meaning that Beta can be perturbed back by its own impact on Alpha. It is usually only used for detailed propagation of planetary systems, but it was chosen to include it for the generation of the ephemeris of Beta. The only difference with only considering the spherical harmonic perturbation of Alpha on Beta is that this third system mode disappears.

The main difference between our model and results from literature comes with the semi-major axis whose oscillations are larger in our model with less differences between the relaxed and excited case. This could be seen as a worst scenario for our own simulations, thus it is not detrimental for our model. Another noticeable difference is with the eccentricity which has a lower amplitude in the excited case in our model than in the two papers. This is again not a big issue as the nominal model used in this thesis and presented in Section 10.1.2 is based on observations from an Earth flyby and should thus be closer to the relaxed scenario.

All these differences should come from the differences in the model used itself, our rotational model is for instance a simpler one with no libration. The similarities are however clear to validate our own model.

10.1.2. Nominal Model

This is the model from [Ostro and al., 2006] which is used in this thesis as it is based on real observations from an Earth flyby of 1999 KW4 in May 2001. Although no direct comparison can be made in literature between our model and this nominal one for validation purposes, it is however possible to identify some interesting behaviours from the generated ephemeris of Beta in this thesis, that enable to validate its proper implementation. The orbital elements of Beta orbiting Alpha are plotted in Figure 10.2 for a total of 200 hours using the nominal model, again to approach the results of both [Compère and Lemaître, 2014] and [Fahnestock and Scheeres, 2008].

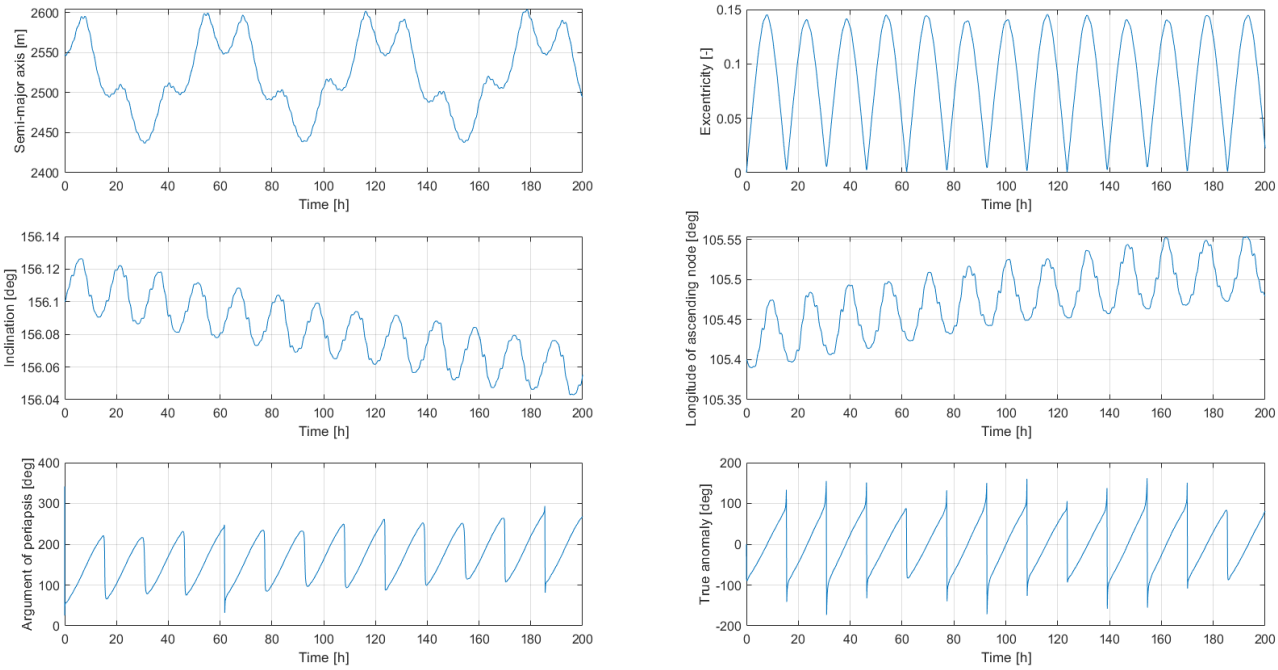

Figure 10.2: Orbital elements for the relative orbit of Beta around Alpha for our own model, using the nominal configuration in [Ostro and al., 2006].

It is again possible to identify three system's modes in Figure 10.2, with the two fastest ones being linked to Alpha and Beta's spin rates respectively, which can be seen also in both [Compère and Lemaître, 2014] and [Fahnestock and Scheeres, 2008] (see Appendix A).

In view of the proper implementation of the two relaxed and excited test configurations as seen in Subsection 10.1.1, it can be fairly assumed that the nominal model is also validated.

11

Conclusions and Recommendations

11.1. Conclusions

This thesis focused on the uncontrolled orbit behaviour of a cubesat in a binary asteroid environment, highlighting the example of the representative Near-Earth Asteroid (66391) 1999 KW4, using the TU Delft Astrodynamics Tool (TUDAT) for numerical computations.

It was found that the tuning of the integrator/propagator settings in such a perturbed environment is not an easy task, and required many iterations. The tuning was performed on the best found runs in the interior and exterior ring of the binary w.r.t. propagation time after an extensive 3D search, for better representation of all possible applications. Multiple termination conditions were implemented to individually end the simulations, comprising impact or escape scenarios as well as a so-called BIBO termination condition on the semi-major axis of the cubesat to avoid highly perturbed and sensitive orbits in the exterior zone. It was indeed found that flybys closer than 400 meters to either Alpha or Beta could introduce sufficient sensitivity for a large build-up of integration error differences between different integrators/propagators, so a choice was made to make the impact scenarios occurring when the cubesat approaches the surfaces of either Alpha or Beta closer than this distance. The introduction of these hard requirements for the distance of the cubesat w.r.t. Alpha and Beta enabled to find smoother differences between various integration/propagation methods while also finding orbits that are less likely to be affected by close flybys. This came at the expense of filtering orbits that could be found close to the bodies, but it was deemed necessary to ensure the reliability of the results in both the interior and exterior ring. An extensive tuning of the integration and propagation method led to the conclusion that a requirement in accuracy of 10 meters for the cubesat's position can be reached for more than a hundred days targeting pseudo-periodic orbits in the interior ring. This value drops to 60 days for orbits in the exterior ring, showing that they are much more sensitive. The combinaison of the DOPRI8(7) integrator with tolerances 10^{-10} with the usm6 propagator was selected as the best choice in terms of low cpu time and reaching the requirement above.

The next parts of this work thus focused on whether such lifetimes could at least be ensured depending on the injection location, and whether they would withstand the introduction of uncertainties in the model.

In order to prove the feasibility of an orbit control-free mission around a binary asteroid, it was chosen to investigate whether stable regions exist in the system, the notion of stability being understood in the numerical sense of termination-conditions stability. The rationale for this is that an orbit whose initial conditions start in a stable region is more likely to withstand the introduction of various uncertainties, compared to an isolated point (with a potential better lifetime estimate).

Regarding our research question:

- Can we identify attractive trajectories around binary asteroids that can be used by cubesat missions without any means of orbit control?

The best orbits found in the interior ring of the binary are all located in planes that are very close to the orbital plane of Beta, which suggests that this is the best option for an uncontrolld mission in the interior zone.

Such orbits are furthermore pseudo-periodic in a stable band around Alpha for initial semi-major axes of the cubesat approximately ranging between 1200 and 1500 meters, and propagation times of more than 100 days w.r.t. our termination conditions. Targeting such specific orbits seems to be the most interesting application compared to more perturbed and sensitive orbits around Alpha.

The best orbits found in the exterior ring can sometimes reach propagation times of almost 200 days, even though only 60 days can be ensured in the exterior zone due to the build-up of integration errors in this more sensitive area. Most of the best runs in the exterior ring follow a sort of precession motion around the whole system, but a region corresponding to pseudo-periodic orbits was also found in the exterior ring of the system and could be promising.

Regarding our research subquestions:

- What is their relevance? What is their level of stability?

Such orbits are overall relevant for the study of Near-Earth asteroids. They also provide reasonable lifetimes for an uncontrolled cubesat mission, and the absence of a propulsion system could represent a saving in the mass budget for the benefit of more science instrumentation. The addition of requirements from a mission perspective could further help to highlight their relevance.
Regarding the level of stability of the promising orbits, a sensitivity analysis was performed on all nominal results w.r.t. uncertainties in the solar radiation pressure coefficient, the gravitational parameters of Alpha/Beta, their spherical harmonic coefficients, the initial position and velocity of the cubesat, and finally all of the above combined. Pseudo-periodic orbits that withstand uncertainties for more than 100 days days were found, which proves that an uncontrolled cubesat mission is in theory feasible in the interior ring targeting such orbits and for this timespan at least. Another conclusion that was made is that not all pseudo-periodic orbits behave the same w.r.t. our termination conditions, depending on their initial conditions. Some early terminations are indeed seen, always due to an early impact into either Alpha or Beta with the 400 meters criteria above their respective surfaces. One could suggest that this requirement is a bit too constraining, but it has however been chosen as a safety margin for more trustworthy results. Orbits in the exterior ring generally do not withstand uncertainties, again due to early impacts with our requirements. A clear outcome of this thesis is that the velocity uncertainties in the initial state of the cubesat are the driving aspect in terms of sensitivity analysis. It was seen that being able to halve those uncertainties to 5 mm/s using a 1-σ normal distribution could shift a seemingly too risky run into an acceptable one w.r.t. our criteria, especially in the interior ring, but some improvements were seen in the exterior ring as well.

11.2. Recommendations

For an uncontrolled cubesat mission around a binary asteroid, it is recommended to focus first on pseudo-periodic orbits around the primary, which can orbit for at least 100 days according to our results. Orbits in the exterior are much more sensitive, but some of them could be considered for a mission of at least 60 days orbiting the whole system with much higher risks. It is however advised to focus on lowering the velocity uncertainties in that particular case for a higher chance of success, but it could be a general advise as well. Mention is made on the fact that orbits around Beta were not considered in this thesis, but could be of particular interest. Pseudo-periodic orbits around Beta could maybe be found, but at a lower distance to the secondary. This thesis work being seen as a first proof of concept, one could also be interested in building such a cubesat mission, focusing on the relevance of an uncontrolled mission in retrieving scientific data. Such a cubesat mission could very well last for longer time spans than the ones coming from our results, but a clear distinction would have to be made by the mission team after the nominal phase, where the position of the cubesat is much more unpredictable. It could however be seen as an end-of-life scenario and still bring a large amount of scientific insight.

As a final note, the use of the unified state model propagators is recommended as they showed very efficient, especially in combination to the Dormand-Prince category of integrators, considering accuracy and cpu time for our particular problem. Further development of the dynamics model could consider tidal interaction as well as the YORP effect for high accuracy. The environment model could be further developed using a more advanced rotational model for the asteroids using precession.

A

Appendix A - Validation

A.1. Environment Model Validation

The orbital elements of Beta orbiting Alpha are plotted in Figure A.1, directly taken from the work of [Compère and Lemaître, 2014]. The validation process of the environment model in Chapter 10 refers to this figure. The inertial frame used by the authors has its X-axis from the center of Alpha to the initial position of Beta, the Z-axis perpendicular to the initial orbital plane and the Y-axis mutually orthogonal to the two others.

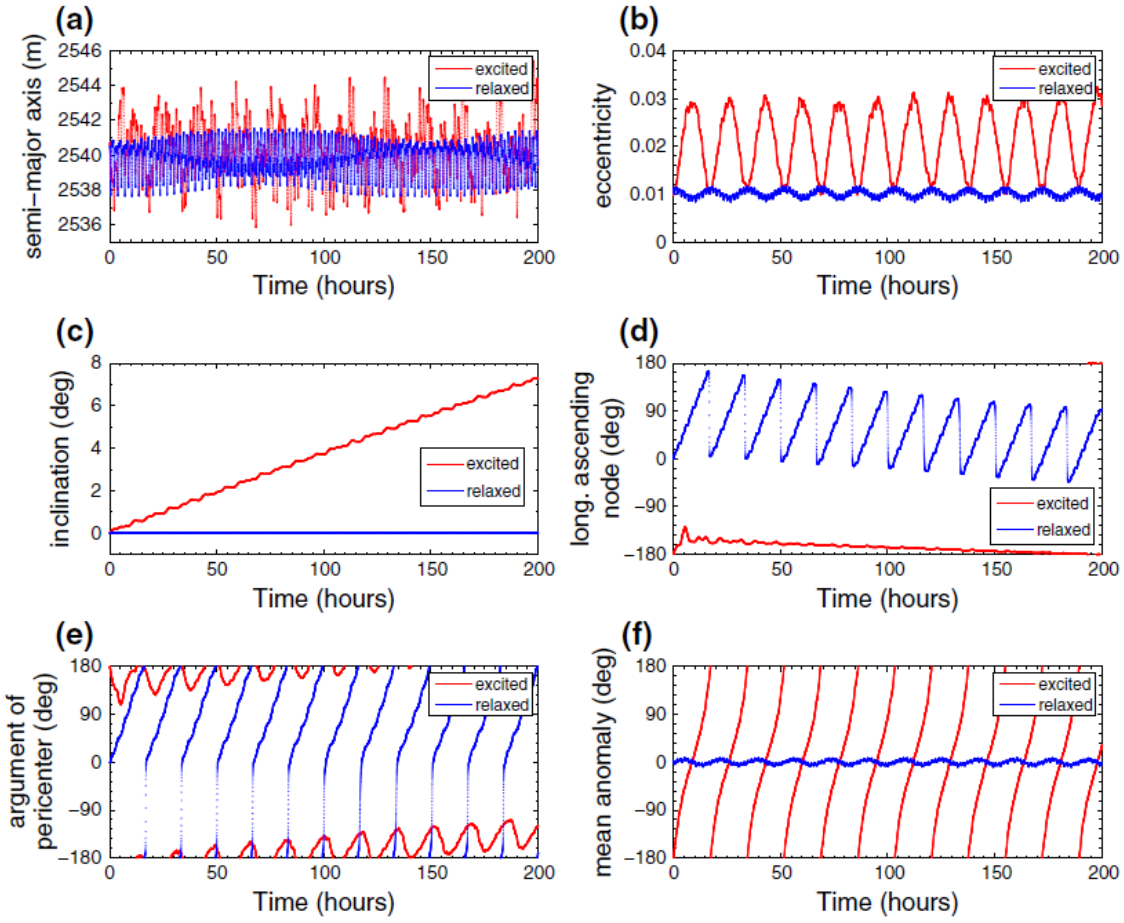

Figure A.1: Orbital elements of Beta around Alpha for a duration of 200 h, represented in the inertial frame for the relaxed and excited configurations in [Compère and Lemaître, 2014].

In their work, [Fahnestock and Scheeres, 2008] used a different orientation frame, linked this time to the total angular momentum vector at the initial time. While the two frames are similar for the relaxed case, it is no longer the case for the excited configuration. [Compère and Lemaître, 2014] proved that their results were very similar to the ones in [Fahnestock and Scheeres, 2008] by performing a change in their own orientation frame and obtaining the results in [Fahnestock and Scheeres, 2008]. For this reason, the sole comparison of our own results with [Compère and Lemaître, 2014] is sufficient in this thesis. For comparison purposes, results from [Fahnestock and Scheeres, 2008] are directly plotted in Figure A.2.

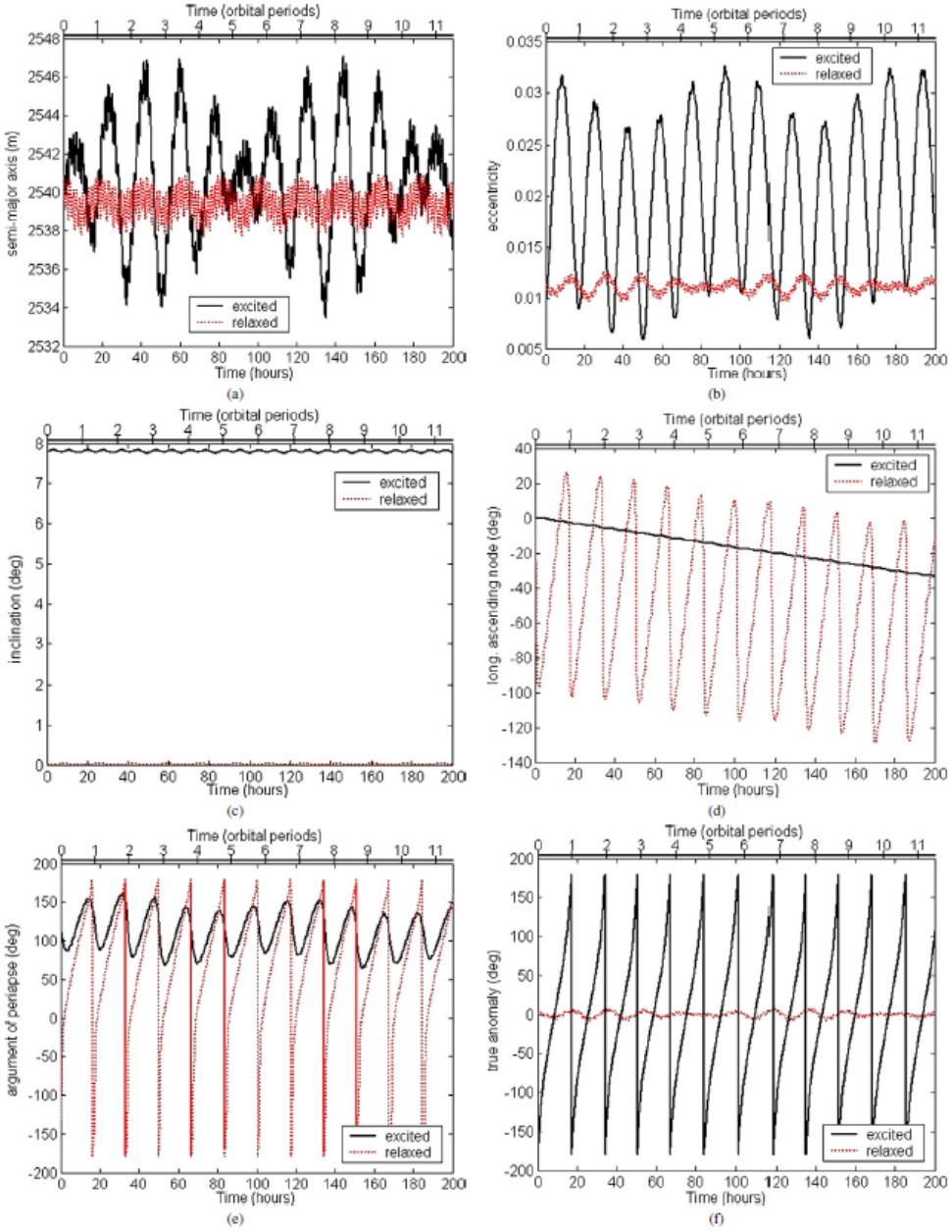

Figure A.2: Orbital elements of Beta around Alpha for a duration of 200 h in the inertial represented in the inertial frame aligned with the total angular momentum vector at the initial time, for the relaxed and excited configurations in [Fahnestock and Scheeres, 2008].

B

Appendix B - Sensitivity to Flybys

Figure B.1 highlights the sensitivity to flybys around Beta for different integrator/propagator settings as mentioned in Section 7.1, for the best run found in the interior ring during preliminary simulations.

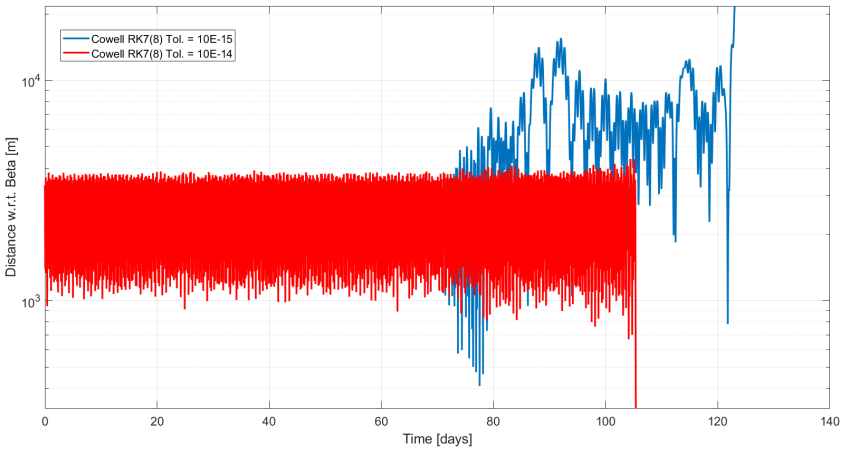

(a) Change of integrator tolerances from 10^{-15} to 10^{-14}.

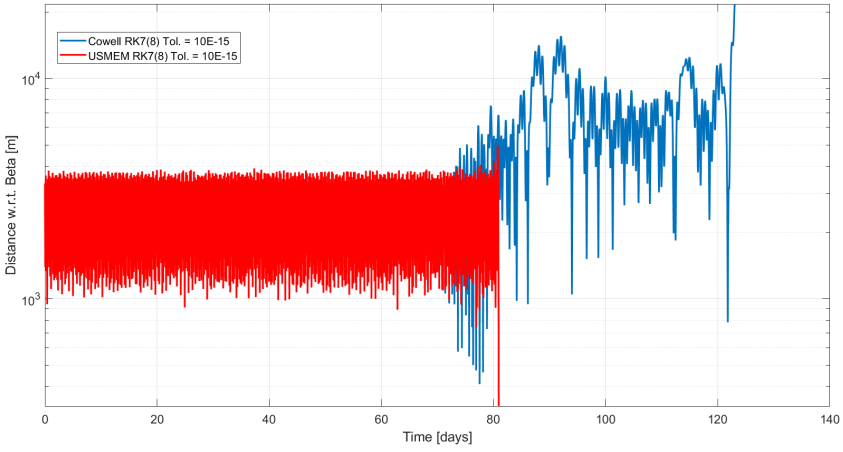

(b) Change of propagator with same tolerances from Cowell to USMEM.

Figure B.1: Best found run in the interior ring during preliminary simulations (using a Cowell propagator with an RK7(8) integrator with tolerances 10^{-15}), and its sensitivity to integrator/propagator settings due to a close flyby around Beta.

It can be seen in both figures Figure B.1a and Figure B.1b that the Cowell propagator combined with an RK7(8) with tolerances 10^{-15} slowly builds up differences w.r.t. the same simulation but with a change of integrator tolerances, or with a change of propagator to USMEM. These differences become so important that the cubesat comes as close as 400 m of Beta in one case, but manages to pursue afterwards a highly perturbed orbit that exits the interior ring. This kind or orbit is deemed unreliable because it is too sensitive to integrator/propagator settings, and this is why close flybys are seen detrimental for our concept. The same kind of behaviour was also observed regarding flybys around Alpha, although for distances of about 800 m to its surface. For the sake of simplicity, it was chosen to make the distance termination conditions w.r.t. the two asteroids to 400 m above their respective surface, so that close flybys are filtered out in our grid search analysis.

Bibliography

R. A. N. Araujo, O. C. Winter, and A. F. B. A. Prado. Stable retrograde orbits around the triple system 2001 SN263. *Monthly Notices of the Royal Astronomical Society, 449*, 2015. pp. 4404–4414.

A. Compère and A. Lemaître. The two-body interaction potential in the STF tensor formalism: An application to binary asteroids. *Celestial Mechanics and Dynamical Astronomy*, 2014. doi: 10.1007/s10569-014-9568-1. 119(3-4):313-330.

F. Damme, H. Hussmann, and J. Oberst. Spacecraft orbit lifetime within two binary near-Earth asteroid systems. *Planetary and Space Science, 146:1-9*, 2017.

L. A. Darriba, N. P. Maffione, P. M. Cincotta, and C. M. Giordano. Comparative study of variational chaos indicators and ODEs' numerical integrators. *International Journal of Bifurcation and Chaos, 22*, 2012. pp. 105-112.

Dominik Dirkx and Erwin Mooij. AE4866 - Propagation and Optimization - Numerical Integration - Lecture. *Astrodynamics and Space Missions, Delft University of Technology*, 2018.

Dominik Dirkx and Erwin Mooij. AE4866 - Propagation and Optimization - Formulations of Equations of Motion - Lecture. *Astrodynamics and Space Missions, Delft University of Technology*, 2019.

Eugene G. Fahnestock and Daniel J. Scheeres. Simulation and analysis of the dynamics of binary near-Earth Asteroid (66391) 1999 KW4. *Icarus Volume 194, Issue 2, 410-435*, 2008. doi: https://doi.org/10.1016/j.icarus.2007.11.007.

J. Feng. Orbital dynamics in the vicinity of contact binary asteroid systems. *Delft University of Technology, Doctoral Thesis*, 2016. URL `https://doi.org/10.4233/uuid:d8d5d083-5027-4468-9cb2-21a691dcdc72`.

M. Fouchard, E. Lega, Ch. Froeschlé, and Cl. Froeschlé. On the relationship between fast Lyapunov indicator and periodic orbits for continuous flows. *Celestial Mechanics and Dynamical Astronomy, 83*, 2002. pp. 205-222.

C. Froeschlé, E. Lega, and R. Gonczi. The fast Lyapunov indicator: a simple tool to detect weak chaos. Application to the structure of the main asteroidal belt. *Celestial Mechanics and Dynamical Astronomy, 67*, 1997. pp. 41-62.

W. Hu and D. J. Scheeres. Numerical determination of stability regions for orbital motion in uniformly rotating second degree and order gravity fields. *Planetary and Space Science, 52*, 2004. pp. 685–692.

R.E. Kalman. A new approach to linear filtering and prediction problems. *Transactions of the ASME (Series D) Journal of Basic Engineering*, 1960. Vol. 82, pp. 35-45.

Wiley J. Larson and James R. Wertz. *Space Mission Analysis and Design, Third Edition*. Space Technology Library, Vol. 8, 2005.

William D. MacMillan. *The Theory Of The Potential*. Dover Publications Inc, 1958.

R. Lasagni Manghi and al. Preliminary orbital analysis for a CubeSat mission to the Didymos binary asteroid system. *Advances in Space Research*, 2017. doi: https://doi.org/10.1016/j.asr.2017.12.014. 62(8).

S. Mast. Stable Orbits in the Small-Body Problem: An Application to the Psyche Mission. *Delft University of Technology*, 2018. http://resolver.tudelft.nl/uuid:499b354e-7159-4043-a003-41dcc64cd1ae.

O. Montenbruck and E. Gill. *Satellite Orbits: Models, Methods, and Applications*. Springer Science & Business Media, 2012.

E. Mooij. *AE4870B - Re-entry Systems - Lecture Notes*. Astrodynamics and Space Missions, Delft University of Technology, 2017-2018.

A. Morbidelli. *Modern Celestial Mechanics: Aspects of Solar System Dynamics*. Taylor & Francis Ltd, 2002.

S. J. Ostro and al. Radar Imaging of Binary Near-Earth Asteroid (66391) 1999 KW4. *Science 314, 1276-1280*, 2006. doi: 10.1126/science.1133622.

P. Pravec, P. Scheirich, P. Kušnirák, L. Šarounová, S. Mottola, G. Hahn, P. Brown, G. Esquerdo, N. Kaiser, Z. Krzeminski, D. P. Pray, B. D. Warner, A. W. Harris, M. C. Nolan, E. S. Howell, L. A. M. Benner, J. L. Margot, A. Galádaj, and G. Koberaj. Photometric survey of binary near-Earth asteroids. *Icarus 181, 63–93*, 2009. doi: https://doi.org/10.1016/j.icarus.2005.10.014.

H.M. Sanders, J.M. Boscher, A.T. Hogedoorn, J.L.P.A. Moerel, B.T.C. Zandbergen, and M.C. Louwerse. System analysis and development of a cool gas generator based micropropulsion system. *TNO, Delft University of Technology, University of Twente*, 2007. included in the conference proceedings of the 6th ESA Round Table on Micro & Nano Technologies for Space Applications held in October 2007.

D. J. Scheeres and al. Dynamical Configuration of Binary Near-Earth Asteroid (66391) 1999 KW4. *Science 314, 1280-1283*, 2006. doi: 10.1126/science.1133599.

Daniel J. Scheeres. *Orbital Motion In Strongly Perturbed Environment: Applications to Asteroid, Comet and Planetary Satellite Orbiters*. Springer Praxis, 2012.

J. Schoolcraft, A. Klesh, and T. Werne. MarCO: Interplanetary Mission Development on a CubeSat Scale. *American Institute of Aeronautics and Astronautics*, 2016.

W.J. Ubbels, A.R. Bonnema, E.D. van Breukelen, J.H. Doorn, R. van den Eikhoff, E. Van der Linden, G.T. Aalbers, J. Rotteveel, R.J. Hamann, and C.J.M Verhoeven. Delfi-C3: a Student Nanosatellite as a Test-bed for Thin Film Solar Cells and Wireless Onboard Communication. *Proceedings of 2nd International Conference on Recent Advances in Space Technologies, 2005. RAST 2005.*, 2005.

E.D. van Breukelen, A.R.Bonnema, W.J. Ubbels, and R.J. Hamann. Delfi C3: Delft University of Technology's Nanosatellite. *Proceedings of the 4S Symposium: Small Satellites, Systems and Services 25-29 September 2006, Chia Laguna, Sardinia, Italy (ESA SP-625, November 2006)*, 2006.

B. F. Villac and J. J. Aiello. Mapping long-term stability regions using the fast Lyapunov indicator. *In 15th AAS/AIAA Spaceflight Mechanics Meeting, Copper Mountain, CO, USA*, 2005. Pasadena, CA: Jet Propulsion Laboratory, National Aeronautics and Space Administration.

V. Vittaldev, E. Mooij, and M. C. Naeije. Unified State Model theory and applications in Astrodynamics. *Celestial Mechanics and Dynamical Astronomy, 112(3)*, 2012. pp. 253-282.

Karel F. Wakker. *Fundamentals of Astrodynamics. Lecture Notes*. 2015. URL `http://resolver.tudelft.nl/uuid:3fc91471-8e47-4215-af43-718740e6694e`.

R.A. Werner. The gravitational potential of a homogeneous polyhedron or don't cut corners. *Celestial Mechanics and Dynamical Astronomy, 59*, 1994. pp. 253-278.

R.A. Werner. Sperical harmonic coefficients for the potential of a constant-density polyhedron. *Computers and Geosciences, 23*, 1997. pp. 1071-1077.

James R. Wertz, David F. Everett, and Jeffery J. Puschell. *Space Mission Engineering: The New SMAD*. Space Technology Library, Vol 28., 2011.

Marco Zannoni, Giacomo Tommei, Dario Modenini, Paolo Tortora, Ruaraidh Mackenzie, Mehdi Scoubeau, Ulrich Herfort, and Ian Carnelli. Radio Science Investigations with the Asteroid impact mission. *Advances in Space Research 62(8)*, 2017. doi: 10.1016/j.asr.2017.12.003.